國 立 交 通 大 學

應 用 數 學 系

博 士 論 文

耦合網路的同步研究

The Study of Synchronization in Coupled Networks

研究生： 梁育豪

指導教授： 莊重 教授

中 華 民 國 一 百 年 九 月

耦合網路的同步研究

The Study of Synchronization in Coupled Networks

研究生：梁育豪　　Student: Yu-Hao Liang

指導教授：莊重　　Advisor: Jonq Juang

國 立 交 通 大 學

應 用 數 學 系

博 士 論 文

A Dissertation
Submitted to Department of Applied Mathematics
College of Science
National Chiao Tung University
in Partial Fulfillment of Requirements
for the Degree of
Doctor of Philosophy
in
Applied Mathematics

September 2011

Hsinchu, Taiwan, Republic of China

中 華 民 國 一 百 年 九 月

耦合網路的同步研究

研究生: 梁育豪　　指導教授: 莊　重 教授

國立交通大學

應用數學系

摘　要

本篇論文的目的是為研究一些常見耦合網路的同步化現象。對於混沌耦合網路，基於矩陣測度的概念，我們發展出一些同步化平面的全域穩定性判別定理。對比於其他研究，本篇論文所建立的方法是較容易做驗證的：我們僅需確認單一未耦合系統的向量場結構，便能辨別出耦合系統是否得能達成同步。此外，此處所考慮的耦合網路涵蓋相當的廣泛，包含了時變的耦合網路。特別地，為了顯示我們發展出的定理其可用性以及其和生物模型的相關性，我們將拿 Hindmarsh-Rose 神經元的耦合系統作為一同步化的探討例子（在這裡，我們也將顯示一些神經元達成同步化時會出現的一些有趣動態行為）。

對於耦合映像晶格系統(CMLs)，我們考慮同步化平面的鄰域穩定性問題。我們將給出此穩定性的充分必要條件，並且提供了一個簡單

的建構*同步化曲線*演算法。利用此同步化曲線，我們可以容易地解釋波長分歧與系統大小相依性的問題。進一步地，我們考慮小波變換方法對 CMLs 所造成的影響。我們將在數值上以及理論上顯示出此變換方法在 CMLs 模型中是可以提高同步化現象的發生。

The Study of Synchronization in Coupled Networks

Student: Yu-Hao Liang Advisor: Prof. Jonq Juang

Department of Applied Mathematics
National Chiao Tung University

Abstract

The purpose of this thesis is to study the onset of synchronization in some common models. For the coupled chaotic systems, based on the concept of matrix measure, we derive some criteria for the global stability of the synchronous manifold. Comparing with other developed criteria, our criteria are easy to apply. By merely checking the structure of the vector field of the single oscillator, we shall be able to determine if the coupled system could acquire synchrony. Moreover, the considered coupled networks could be quite general including the time-varying networks. Specifically, to illustrate the applicability of our developed criteria and to be much relative to the real phenomena, the coupled Hindmarsh-Rose neurons are considered. Some interesting phenomena under synchronization are showed. For the coupled map lattices (CMLs), ones consider the local stability problem. We shall give the necessary and sufficient conditions for the local stability of the synchronous manifold for the arbitrary coupled networks. Also, a simple algorithm for the construction the so-called *synchronization curve* is given. Using it, one can simply explain the phenomena of the wavelength bifurcation and the size dependence problem. In addition, the effect of the wavelet transform method developed by Wei and et al is considered for the CMLs. We shall show that both numerically and theoretically, it enhances the onset of the synchronization.

誌　謝

首先感謝我的指導教授 莊重老師，在我六年的交大學生生涯中不論是在研究、課業、生活上的種種幫助。在研究有困難時，感謝老師您對我的鼓勵；感謝老師您經常鼓勵我去參加國內外的研討會，讓我更能看清研究本質、培養國際觀。另外，在與老師相處的這些年中，老師的研究態度深深的影響著我。相信這對於我未來的研究是會有很大得助益的。真的很感謝老師您這些年來的照顧。另外，也感謝口試委員 林文偉教授、郭忠勝教授、李明佳教授以及陳國璋教授，在論文口試時給我的寶貴意見，使論文更甄完善。而這些建議更提供我作為未來研究生涯中的一個研究方向。

在六年的交大應數系學習中，深深得發覺交大老師們對於學生有著濃濃得關懷。感謝許元春老師、賴明治老師經常地鼓勵我應該到國外看看別人的研究，也願意提供給我一些出國的管道。雖然最後我還是待在交大應數系裡，但是老師們對我的關心，真的是由衷的感謝。感謝陳秋媛老師，常常地問候我的研究情況，也常常的給予我鼓勵，這些都讓我覺得十分的窩心，讓我覺得應數就像是個大家庭一樣。感謝石至文老師，您教授的常微分方程、生物系統等課程，讓我對動態系統的領域充滿了研究興趣。因為有了您的教導，我才會選擇這塊研究領域。感謝林文偉老師，您在論文研究上給予我的許多寶貴方向、意見，以及其他許多在學習、研究方面的幫助。另外，感謝李明佳老師、林琦琨老師、李榮耀老師、梁耀文老師、鄧清政老師、陳宗麟老師，感謝您們曾經給過我的指導與幫助。也感謝系辦的張麗君、陳盈吟、張慧珊、宋雅鈴小姐們，感謝您們給予的許多幫忙，有很多地方都麻煩您們了。

在這博士班四年的學習中，感謝許多朋友、同學、學長、學姊、學弟、學妹：李金龍、張郁泉、張靖尉、黃俊銘、陳怡樺、洪千茹、周芳竹、鄧仁益、魏士傑、黃仕翰、黃韋強、陳冠羽、邱鈺傑、廖康伶、呂明杰、林光暉、蔡佳穎、林信佑（未來Google全球CEO =.=|||）、

蔡宗憲、葉淑娟、李芷萱、陳玉雯、方怡中、連威翔的互相提攜鼓勵，感謝您們使得我這段求學過程充滿了樂趣、更加的多采多姿。其中，特別感謝同學黃俊銘、魏士傑、黃仕翰，你們在我有困難時，對我的幫助。另外，我也想特別感謝周芳竹學妹以及林信佑學弟(未來Google全球CEO =.=|||)，那段一起在研究小間的日子總是那麼令人難忘，而你們畢業後還一直常來看我、陪我聊天、給我加油打氣。真的謝謝你們，我會想念你們的。

最後，我要感謝我親愛的父母（梁有忠、王瓊珠）、姊姊（梁翠洺）、弟弟（梁育瑋）、外婆（王吳秀桃）、阿姨、姨丈、舅舅、舅媽、表弟、表妹們，謝謝你們的一路相挺、始終支持著我。另外，也要感謝我已過世的奶奶（梁蘇灼），謝謝你從小到大一直疼愛著我。

最後，我想要感謝老天，謝謝您賜給我的一切，這一切的一切使我的生命是這麼的美好。

梁育豪 2011/9/9 於交大

Contents

Chapter 1

Introduction

1.1 Synchronization in lattices of coupled systems

Synchronization is a common, significant phenomenon occurring in the natural world no matter from the micro view or the macro view. It depicts a group of different individuals displaying the same behaviors at the same time under certain interactions. The purpose of it is to get them to solve problems cooperatively. For instance, in the human brain, there are about 10^{10} neurons. To integrate separately processing information in the brain, they have to synchronize their activity [14,31]. In the nights of the South-East Asia, such as Thailand, Malaysia or Borneo, male fireflies accumulate along the river banks flashing on and off simultaneously [13] in order to attract the female fireflies cooperatively.

Correspondingly, in the technology field, synchronization now and then is designed to occur in the experiment for some purpose, especially in the design of the electronic circuit system. In engineering, it is studied as a tool for transmitting information by using chaotic signals and monitoring dynamical systems [36].

So as an interesting, important topic, synchronization has drawn a great deal of attention and is intensively studied in many fields, including neuron science, biology, physics, engineering, and other fields of science [1,16,24,26,32–34,48,58,59,62,69, 71,73,77,84,90,94,96,99]. Consequently, several elegant theories and articles concerning synchronization have been rapidly constructed and published in the past few decades. The general approaches involved for driving the synchronization criteria are roughly the

Lyapunov function method (global results) and the master-stability function method (local results), the analysis of the transversal Lyapunov exponents calculated from the linearized equations for the perturbations transversal to the synchronous manifold.

Since in the real world the number of coupled units is usually large, the increasing interest in synchronization phenomena has led many researchers to consider synchronization in large networks of coupled systems with different coupling configurations [1,2,27,48,66,74,85,86,97,100]. As a result, one of the most important questions in synchronization phenomena is that how the coupling strengths and coupling configurations of the network influence the stability of the synchronous state. Furthermore, one may ask the following controlling problem: Can one slightly modify the coupling configuration of coupled systems to dramatically reduce the coupling strength needed to acquire synchrony [51,52,98]? In this thesis, we shall focus on these issues by considering various models that are frequently used to explain these phenomena.

1.2 Modeling

Based on the disparate individuals, the dynamics of interesting qualities, like movement, velocity, energy, potential, and so modeling are in the various fashions. Similarly, connection and commutation between themselves have several types. Depending upon the different models considered, there are different explanations as to why the units in the coupled systems synchronize. In this context, we will introduce three different kinds of models (Model I $\sim$ Model III) that are often used to describe the real collective networks, and synchronization within. Specifically, the first two models (Model I $\sim$ Model II) are to be extensively studied. By it, in this section, we start with the introduction of the models.

1.2.1 Model I: Coupled Chaotic Systems

The model under consideration in this subsection is of continuous time with continuous state coupling. Specifically, we consider a unit with the interesting dynamics governed by a set of ordinary differential equations, saying $\frac{d\boldsymbol{x}}{dt} = \boldsymbol{f}(\boldsymbol{x}, t)$. Here, $\boldsymbol{x} \in \mathbb{R}^n$, and $\boldsymbol{f}$ is a

vector-valued function from $\mathbb{R}^n \times \mathbb{R}$ to $\mathbb{R}^n$ denoted by $\boldsymbol{f}(\boldsymbol{x}, t) = (f_1(\boldsymbol{x}, t), \cdots, f_n(\boldsymbol{x}, t))^T$. Moreover, when there are connections/commutations between a group of such m units, the induced whole dynamics under interaction is then described by

$$\frac{d\boldsymbol{x}_i}{dt} = \boldsymbol{f}(\boldsymbol{x}_i, t) + d \cdot \sum_{j=1}^{m} g_{ij}(t)\, \boldsymbol{D}\boldsymbol{x}_j, \quad i = 1, 2, \ldots, m, \tag{1.1a}$$

where $\boldsymbol{x}_i = (x_{i1}, x_{i2}, \ldots, x_{in})^T \in \mathbb{R}^n$, d is the coupling strength, $\boldsymbol{D} = (d_{ij}) \in \mathbb{R}^{n\times n}$ is the inner coupling matrix, and the quantity $g_{ij}(t)$ describes the coupling weight from the unit j to the unit i. Let $\boldsymbol{x} = (\boldsymbol{x}_1, \boldsymbol{x}_2 \ldots, \boldsymbol{x}_m)^T$, and $\boldsymbol{G}(t) = (g_{ij}(t)) \in \mathbb{R}^{m\times m}$. Then $\boldsymbol{G}(t)$ represents the (outer) coupling configuration of the network at time t. Equivalently, (1.1a) becomes

$$\dot{\boldsymbol{x}} = \begin{pmatrix} \boldsymbol{f}(\boldsymbol{x}_1, t) \\ \vdots \\ \boldsymbol{f}(\boldsymbol{x}_m, t) \end{pmatrix} + d(\boldsymbol{G}(t) \otimes \boldsymbol{D})\boldsymbol{x} =: \boldsymbol{F}(\boldsymbol{x}, t) + d(\boldsymbol{G}(t) \otimes \boldsymbol{D})\boldsymbol{x}, \tag{1.1b}$$

where $\otimes$ denotes the Kronecker product.

Such type of model can been seen in some nervous systems or designs of the electronic circuit systems [99]. For this model, general approaches to deal with the local stability of the synchronization state, include the master stability function-based criteria [1,72,74,75,81] and the matrix measure criteria [17,18]. For the global stability, the developing method includes the Lyapunov function-based criteria [2–4,8,78,100–104] and the matrix measure approach [17,18], and et. al. Among the Lyapunov function-based criteria, the connection graph approach proposed by Belykh [2–4,8] is sui generis since the proposed criteria combine some graph theories to avoid the *direct* computation of the eigenvalues of the coupling matrix $\boldsymbol{G}(t)$. (Not surprisingly, quantities related to the eigenvalues of matrix $\boldsymbol{G}(t)$ should play the decisive roles in the synchronization phenomena realistically and theoretically.) What involved term to replace the role of eigenvalues of $\boldsymbol{G}(t)$ is the total length of all paths passing through an edge in the network connection graph inducing from $\boldsymbol{G}(t)$. Nevertheless, the method is limited to the networks with cooperative couplings, i.e., $g_{ij}(t) \geq 0$, $\forall i \neq j$. As well, despite

the fact that the criterion based on the analysis of Lyapunov function guarantees the onset of synchronization, it is not a general method since there is no procedure for constructing the Lyapunov function for an arbitrary system. Similar problem occurs in the matrix measure approach. Furthermore, such criteria may not hold when the number of the coupled systems is large.

In the thesis, we shall present some criteria for the onset of synchronization in this model. Instead of constructing the Lyapunov function, the developed criteria are based on the completely different version of the matrix measure approach as proposed in [17,18]. The approach can overcome the drawbacks mentioned above.

1.2.2 Model II: Coupled Map Lattices

The model considered in this subsection is essentially similar to that given in Model I, except that the dynamics of units and the intersection ways are governed by some maps. It implies the equations of the motion then read:

$$\boldsymbol{x}_i(k+1) = \boldsymbol{f}(\boldsymbol{x}_i(k)) + d \cdot \sum_{j=1}^{m} g_{ij} \boldsymbol{f}(\boldsymbol{x}_j(k)), \quad i = 1, \ldots, m. \tag{1.2a}$$

Here $\boldsymbol{x} \in \mathbb{R}^n$ and $\boldsymbol{f}$ is a vector-valued function from $\mathbb{R}^n \times \mathbb{R}$ to $\mathbb{R}^n$. Based on the structure of the modeling, ones usually call (1.2a) as the *coupled map lattices* (CMLs). Set $\boldsymbol{G} = (g_{ij})$. Then in the vector-matrix form, (1.2a) becomes

$$\boldsymbol{x}(k+1) = \boldsymbol{F}(\boldsymbol{x}(k)) + d(\boldsymbol{G} \otimes \boldsymbol{I})\boldsymbol{F}(\boldsymbol{x}(k)), \tag{1.2b}$$

where $\boldsymbol{x}(k) = (\boldsymbol{x}_1(k), \ldots, \boldsymbol{x}_m(k))^T$, and $\boldsymbol{F}(\boldsymbol{x}(k)) = (\boldsymbol{f}(\boldsymbol{x}_1(k)), \ldots, \boldsymbol{f}(\boldsymbol{x}_m(k)))^T$.

This model, first introduced in 1980's [20,56,93], has been the subject of much recent research. It is studied in the populations, chemical reactions, information processing, and biological networks and et. al [57]. Many dynamical behaviors have been observed, including spatiotemporal chaos and synchronization. In this thesis, we shall specifically focus on the issue of the synchronization.

The method developed to deal with the local stability problem for the synchronization state is based on the master-stability function criteria [1,19,28–30,42,106].

For the global stability problem, the methods include constructing the Lyapunov function [64,65], applying the matrix measure criteria [61] and et. al. Nevertheless, comparing with Model I (1.1a), these methods are more limited. More precisely, the criteria limit to the special forms of the coupling matrix $\boldsymbol{G}$.

In the thesis, we shall consider the local stability problem for the synchronization state in the model with coupling matrix $\boldsymbol{G}$ arbitrary given and study some corresponding problems.

1.2.3 Model III: Pulse Coupled Systems

The model introduced in this section is to explain the flashing synchrony in the fireflies [13,69], and the rhythmic activity of cells of the heart pacemaker [47,68,76,89], of cells of the pancreas [82] and of neural networks [12,13,25,76,80,88]. The most difference between this model and Models I, II is the interaction fashion. Interaction in Models I, II is "continuous in time", while that in this model is "fleeting and intermittent in time". Moreover, the reset mechanism occurs herein. Such a coupling fashion is called to be *pulse-coupled*, and the model is called the *integrate-and-fire model*. We start with introducing the Peskin's model [76].

Let m be the number of the units in the coupled system, and the individual state be denoted by x_i $(i = 1, 2, \cdots, m)$, where x_i are subject to the dynamics

$$\frac{dx_i}{dt} = -r_i x_i + I_i, \quad 0 \le x_i \le 1, \tag{1.3}$$

with $I_i > r_i \ge 0$. As time progresses, suppose $t-$ [1] is the first time that some ith unit reaches the threshold 1, i.e., $x_i(t-) = 1$ (one also says such unit *fires*). Then x_i is *reset*, i.e.

$$x_i(t-) = 1 \to x_i(t+) = 0, \tag{1.4a}$$

and the firing effect from i to j $(j \ne i)$ yields immediately:

$$x_j(t-) \to \begin{cases} x_j(t-) + g_{ji} & \text{if } x_j(t-) + g_{ji} < 1, \\ 1 & \text{if } x_j(t-) + g_{ji} \ge 1. \end{cases} \tag{1.4b}$$

[1] We use symbols $t-$ and $t+$ to represent the time instantly before and after the time t , respectively.

Suppose in this instant, the kth unit fires, i.e., $x_k(t-) + g_{ki} \geq 1$, then similar process like (1.4) occurs again at once. This process at time t is lasted until all effects of the firing units are evaluated. In addition, the whole evolution dynamics shall repeat above process once and once again. For the onset of synchronization in the integrate-and-fire model, it means that all units fire simultaneously after some fixed time T.

This model was later generalized by Mirollo and Strogatz [69]. It is assumed that the state variable x_i evolves according to $x_i = f_i(\phi_i)$, where $f_i : [0,1] \to [0,1]$ is smooth, strictly increasing, and satisfies $f_i(0) = 0$ and $f_i(1) = 1$, and the dynamics of phase ϕ_i is governed by

$$\frac{d\phi_i}{dt} = \frac{1}{T_i}, \quad 0 \leq \phi_i \leq 1. \tag{1.5}$$

Moreover, as time progresses, suppose $t-$ is the first time that $\phi_i(t-) = 1$ (correspondingly, $x_i(t-) = 1$) for some i (one also says such unit *fires*). Then let $E_j(t-) = f(\frac{T_i}{T_j}(1 - \phi_i(t-)) + \phi_j(t-))$, $j = 1, 2, \cdots, m$, and undergo the process of the reset and firing effects as given in (1.4) for $E_j(t-)$, $j = 1, 2, \cdots, m$ to get $E_j(t+)$. Then the phase ϕ_i at time $t+$ is defined as $\phi_i(t+) = g(E_j(t+))$. Here g is the inverse function of f. In addition, the whole evolution dynamics shall repeat above process once and once again.

As follows, we define some terminologies in the model. We say $\boldsymbol{\phi} = (\phi_1, \cdots, \phi_m)$ is in the *firing state* if $\phi_i = 0$ for some i. For a given initial phase $\boldsymbol{\phi}(0)$, we say $< t_i >$ is its *firing time series* if it is the increasing sequence that records the successive time when phase $\boldsymbol{\phi}(t_i) =: \boldsymbol{\phi}^{(i)}$ is in the firing state. Let r be the map defined in the set of firing states by $r(\boldsymbol{\phi}^{(i)}) = \boldsymbol{\phi}^{(i+1)}$ (Such definition is well-defined). Then synchronization in the model is defined to satisfy that for any $\boldsymbol{\phi}$ in the firing state, there is $N \in \mathbb{N}$ such that $r^n(\boldsymbol{\phi}) = (0, \cdots, 0)$, $\forall n \geq N$.

Note that the Peskin's model is one of the special model proposed by Mirollo and Strogatz with

$$f_i(\phi) = \frac{I_i}{r_i}(1 - e^{-r_i T_i \phi}).$$

and

$$T = \frac{\ln(\frac{I_i}{I_i - r_i})}{r}.$$

In the article [76], Peskin conjectured that, first, for identical units, the coupled system approaches synchronization for almost all initial conditions, and second, this remains true even when the units are not quite identical. Herein, "*identical*" means $f_i \equiv f$, $T_i \equiv T$, and $g_{ij} \equiv g > 0$. For the first conjecture, Mirollo and Strogatz [69] give a rigorous proof for the case that $f_i'' < 0$. The second part of Peskin's conjecture was verified by Urbanczik and Senu [91] with flat units, i.e., $f_i'' \equiv 0$. However, Bottani [11] numerically showed that even concave-upward units, i.e., $f_i'' > 0$, can synchronize, provided that the concavity is not too large. In the article [15], Chang and Juang show that if the *stability condition* holds (see, Eq. (2.9) therein), then the nonidentical coupled system with $f_i'' < 0$ will achieve synchrony for almost all initial conditions; if both the *stability condition* (see, Eq. (2.9) therein) and *absorption condition* (see, Eq. (3.19) and (3.20) therein) hold, then the coupled system with $f_i'' > 0$ will achieve synchrony for almost all initial conditions. The holding of the stability condition implies a group of units reaching the threshold at the same time will remain coordinated in the future, while the holding of the absorption condition implies the number of firing units grows larger and larger and ultimately all units fire simultaneously. We comment that the stability condition requires that $g_{ij} > 0$.

1.3 Organization and results of the thesis

The organization of the thesis is as follows. In Chapter 2, we study the global synchronization in Model I (1.1), including the cases that coupling matrix $\boldsymbol{G}(t)$ therein is time independence and time dependence. Some criteria for the onset of synchronization are given. In Chapter 3, we take the coupled Lorenz equations, coupled Duffing equations, and Hindmarsh-Rose neurons as examples to see the applications of the given criteria. Specifically, we study furthermore the dynamics of the coupled Hindmarsh-Rose neurons under synchronization. The developing method for these criteria includes roughly the concepts of *matrix measure*, and *coordinate transformation*. In Chapter 4, we study the local synchronization in Model II with coupling matrix $\boldsymbol{G}$ generally given. Some criteria for the local stability of the synchronization state are given. In addition, the

phenomenon of *wavelength bifurcations*, as the terminology using in [37], and the application of *wavelet transform method* in Model II are discussed. Here, the wavelet transform method is an approach which is first given out concerning about Model I (see, e.g., [51,52,83,98]) in order to bring the synchronization easier to happen. It will be shown that this method also applies well in the CMLs (1.2). In Chapter 5, we summarize the results in this thesis and give some directions of the future work. We remark that most results in the thesis are adopted from [49,50,53–55].

Chapter 2

Synchronization in Model I

Before going into details of the derivation of synchronization for Model I, we first give some needed preliminaries.

2.1 Preliminaries

First, we introduce the concept of matrix measures. The following definitions and properties of matrix measures can be referenced to the book by M. Vidyasagar [92].

Definition 2.1.1. *([92]) Let $||\cdot||_i$ be an induced matrix norm on $\mathbb{R}^{n\times n}$. The matrix measure of matrix $\boldsymbol{K}$ on $\mathbb{R}^{n\times n}$ is defined to be $\mu_i(\boldsymbol{K}) = \lim_{\epsilon\to 0^+} \frac{||I+\epsilon\boldsymbol{K}||_i - 1}{\epsilon}$.*

Lemma 2.1.1. *([92]) Let $||\cdot||_k$ be an induced k-norm on $\mathbb{R}^{n\times n}$, where $k = 1, 2, \infty$. Then each of matrix measure $\mu_k(\boldsymbol{K})$, $k = 1, 2, \infty$, of matrix $\boldsymbol{K} = (k_{ij})$ on $\mathbb{R}^{n\times n}$ is, respectively,*

$$\mu_\infty(\boldsymbol{K}) = \max_i\{k_{ii} + \sum_{j\neq i} |k_{ij}|\},$$

$$\mu_1(\boldsymbol{K}) = \max_j\{k_{jj} + \sum_{i\neq j} |k_{ij}|\},$$

and

$$\mu_2(\boldsymbol{K}) = \lambda_{\max}(\boldsymbol{K}^T + \boldsymbol{K})/2.$$

Here $\lambda_{\max}(\boldsymbol{K})$ is the maximum eigenvalue of $\boldsymbol{K}$.

Theorem 2.1.1. *([92]) (i)* $\mu_i(\alpha \boldsymbol{A}) = \alpha\mu_i(\boldsymbol{A})$, $\forall\ \alpha \geq 0$ *(ii)* $\mu_i(\boldsymbol{A}+\boldsymbol{B}) \leq \mu_i(\boldsymbol{A}) + \mu_i(\boldsymbol{B})$. *(iii) If* λ *is an eigenvalue of* $\boldsymbol{A}$, *then* $Re\lambda \leq \mu(\boldsymbol{A})$. *(iv) Consider the differential equation* $\dot{\boldsymbol{x}}(t) = \boldsymbol{K}(t)\boldsymbol{x}(t)+\boldsymbol{v}(t)$, $t \geq 0$, *where* $\boldsymbol{x}(t) \in \mathbb{R}^n$, $\boldsymbol{K}(t) \in \mathbb{R}^{n\times n}$, *and* $\boldsymbol{K}(t), \boldsymbol{v}(t)$ *are piecewise-continuous. Let* $||\cdot||_i$ *be a norm on* $\mathbb{R}^n$, *and* $||\cdot||_i$, μ_i *denote, respectively, the corresponding induced norm and matrix measure on* $\mathbb{R}^{n\times n}$. *Then whenever* $t \geq t_0 \geq 0$, *we have*

$$||\boldsymbol{x}(t)||_i \leq ||\boldsymbol{x}(t_0)||_i \exp\left\{\int_{t_0}^{t} \mu_i(\boldsymbol{K}(s))ds\right\} + \int_{t_0}^{t} \exp\left\{\int_{s}^{t} \mu_i(\boldsymbol{K}(\tau))d\tau\right\} ||\boldsymbol{v}(s)||_i\, ds. \tag{2.1}$$

Next, we introduce a function being of type K, which generates a monotone dynamics of the system of linear differential equations. For completeness and ease of the references, we also recall the definitions of the above described concepts and their properties [41,92].

Let $\mathbb{R}^n_+ = \{\boldsymbol{x} = (x_1, x_2, \ldots, x_n)^T \in \mathbb{R}^n : x_i \geq 0, i = 1, \ldots, n\}$ be the nonnegative cone. Let $\boldsymbol{a}, \boldsymbol{b} \in \mathbb{R}^n$. We write $\boldsymbol{a} \leq \boldsymbol{b}$ if $\boldsymbol{b} - \boldsymbol{a} \in \mathbb{R}^n_+$.

Definition 2.1.2. *We say that a function* $\boldsymbol{f} = (f_1, \ldots, f_n) : D \subset \mathbb{R}^n \to \mathbb{R}^n$ *is of type K on* D *if, for each* i, $f_i(\boldsymbol{a}) \leq f_i(\boldsymbol{b})$ *whenever* $\boldsymbol{a} = (a_1, \ldots, a_n)$ *and* $\boldsymbol{b} = (b_1, \ldots, b_n)$ *are in* D *with* $\boldsymbol{a} \leq \boldsymbol{b}$ *and* $a_i = b_i$.

The following theorem amounts to saying that a vector field being of type K is a sufficient condition to generate a monotone dynamics.

Theorem 2.1.2. *([41]) Let* $\boldsymbol{f}(t, \boldsymbol{x})$ *be of type K on* $\mathbb{R}^n$ *for each fixed* t *and let* $\boldsymbol{x}(t)$ *be a solution of* $\dot{\boldsymbol{x}}(t) = \boldsymbol{f}(t, \boldsymbol{x})$ *on* $[a, b]$. *Let* $\boldsymbol{z}(t)$ *be continuous on* $[a, b]$ *and satisfy* $D_l\boldsymbol{z}(t) \leq \boldsymbol{f}(t, \boldsymbol{z})$. *Here* $D_l\boldsymbol{x}(t) = \lim_{h\to 0^-} \frac{\boldsymbol{x}(t+h)-\boldsymbol{x}(t)}{h}$. *Then* $\boldsymbol{z}(t) \leq \boldsymbol{x}(t)$ *for* $a \leq t \leq b$ *provided that* $\boldsymbol{z}(a) \leq \boldsymbol{x}(a)$.

Consider linear system of differential equations in the homogeneous case

$$\boldsymbol{y}' = \boldsymbol{A}(t)\boldsymbol{y}. \tag{2.2}$$

Here $\boldsymbol{A}(t)$ is an $n \times n$ matrix. Then clearly if $\overline{\lim_{t\to\infty}} \frac{\int_0^t \mu_2(\boldsymbol{A}(s))ds}{t} \leq -r$ for some $r > 0$. Then $\boldsymbol{y}(t)$ converges to zero exponentially. The following propositions play one of the critical steps in obtaining our main results.

Proposition 2.1.1. *Suppose $\xi(t)$, $\eta(t)$ and $\zeta(t)$ are nonnegative functions on $[0,\infty)$ satisfying the following inequalities*

$$D_l\xi(t) \le a_1(t)\xi(t) + a_4(t)\eta(t) + a_5(t)\zeta(t), \tag{2.3a}$$

$$D_l\eta(t) \le a_6(t)\xi(t) + a_2(t)\eta(t) + a_7(t)\zeta(t), \tag{2.3b}$$

$$D_l\zeta(t) \le a_8(t)\xi(t) + a_9(t)\eta(t) + a_3(t)\zeta(t). \tag{2.3c}$$

Here $a_i(t)$, $i = 4, 5, \ldots, 9$, are nonnegative functions on $[0,\infty)$. Then $\xi(t)$, $\eta(t)$, and $\zeta(t)$ converge to zero exponentially provided that $\overline{\lim_{t\to\infty}} \frac{\int_0^t \mu_2(\boldsymbol{A}(s))ds}{t} \le -r$, for some $r > 0$, where

$$\boldsymbol{A}(t) = \begin{pmatrix} a_1(t) & a_4(t) & a_5(t) \\ a_6(t) & a_2(t) & a_7(t) \\ a_8(t) & a_9(t) & a_3(t) \end{pmatrix}, \tag{2.4}$$

(ii) Suppose, in addition, that, $a_i(t)$, $i = 1, \ldots, 9$, are constants. Then $\xi(t)$, $\eta(t)$, and $\zeta(t)$ converge to zero exponentially provided that all eigenvalues of $\boldsymbol{A}$ are negative.

Proof. Let $\overline{\xi}(t)$, $\overline{\eta}(t)$ and $\overline{\zeta}(t)$ satisfy the following equation.

$$\begin{aligned}
\dot{\overline{\xi}} &= a_1(t)\overline{\xi} + a_4(t)\overline{\eta} + a_5(t)\overline{\zeta}, \quad \overline{\xi}(0) = \xi(0), \\
\dot{\overline{\eta}} &= a_6(t)\overline{\xi} + a_2(t)\overline{\eta} + a_7(t)\overline{\zeta}, \quad \overline{\eta}(0) = \eta(0), \\
\dot{\overline{\zeta}} &= a_8(t)\overline{\xi} + a_9(t)\overline{\eta} + a_3(t)\overline{\zeta}, \quad \overline{\zeta}(0) = \zeta(0).
\end{aligned}$$

It is easily checked that the above system is of type K. Following from Theorem 2.1.2 that $\overline{\xi}(t) \ge \xi(t)$, $\overline{\eta}(t) \ge \eta(t)$, and $\overline{\zeta}(t) \ge \zeta(t)$, for all $t \ge 0$, we see that the first statement of the proposition holds as claimed. The second assertion of the proposition is obvious. □

Proposition 2.1.2. *Let $\dot{\boldsymbol{x}} = \boldsymbol{A}(t)\boldsymbol{x}$. Here $\boldsymbol{A}(t)$ is an $n\times n$ matrix. Suppose $\lim_{t\to\infty} \boldsymbol{A}(t) = \overline{\boldsymbol{A}}$. Then $\boldsymbol{x}(t)$ converges to the origin exponentially provided that all real parts of eigenvalues of $\overline{\boldsymbol{A}}$ are negative.*

Proof. For any $\epsilon > 0$, there is a $\boldsymbol{P}_\epsilon$ such that $\overline{\boldsymbol{A}}$ can be decomposed into a Jordan form of the form (see e.g., P.128 of [40]):

$$\boldsymbol{P}_\epsilon \overline{\boldsymbol{A}} \boldsymbol{P}_\epsilon^{-1} = \boldsymbol{D} + \epsilon \boldsymbol{Q},$$

where $\boldsymbol{D}$ is a diagonal matrix with the diagonal entries being all the eigenvalues of $\overline{\boldsymbol{A}}$, and $\boldsymbol{Q}$ is a matrix with its entries being either 0 or 1. Then $\boldsymbol{P}_\epsilon \boldsymbol{A}(t) \boldsymbol{P}_\epsilon^{-1} = \boldsymbol{P}_\epsilon (\boldsymbol{A}(t) - \overline{\boldsymbol{A}}) \boldsymbol{P}_\epsilon^{-1} + \epsilon \boldsymbol{Q} + \boldsymbol{D}$. It follows $\mu_2(\boldsymbol{P}_\epsilon \boldsymbol{A}(t) \boldsymbol{P}_\epsilon^{-1}) \leq \mu_2(\boldsymbol{P}_\epsilon (\boldsymbol{A}(t) - \overline{\boldsymbol{A}}) \boldsymbol{P}_\epsilon^{-1}) + \epsilon \mu_2(\boldsymbol{Q}) + \mu_2(\boldsymbol{D}) \leq \mu_2(\boldsymbol{P}_\epsilon (\boldsymbol{A}(t) - \overline{\boldsymbol{A}}) \boldsymbol{P}_\epsilon^{-1}) + \epsilon n + \mu_2(\boldsymbol{D})$. Since $\lim_{t \to \infty} \boldsymbol{A}(t) = \overline{\boldsymbol{A}}$, we get

$$\mu_2(\boldsymbol{P}_\epsilon \boldsymbol{A}(t) \boldsymbol{P}_\epsilon^{-1}) \leq (n+1)\epsilon + \mu_2(\boldsymbol{D}),$$

whenever $t \geq t_\epsilon$ for some $t_\epsilon > 0$. Hence,

$$\overline{\lim_{t \to \infty}} \frac{\int_0^t \mu_2(\boldsymbol{P}_\epsilon \boldsymbol{A}(t) \boldsymbol{P}_\epsilon^{-1}) ds}{t} \leq (n+1)\epsilon + \mu_2(\boldsymbol{D}).$$

By the arbitrariness of ϵ, take $\epsilon = \frac{-\mu_2(\boldsymbol{D})}{2(n+1)}$. Then, we have

$$\overline{\lim_{t \to \infty}} \frac{\int_0^t \mu_2(\boldsymbol{P}_\epsilon \boldsymbol{A}(t) \boldsymbol{P}_\epsilon^{-1}) ds}{t} \leq \frac{\mu_2(\boldsymbol{D})}{2}$$

Thus, all solutions of $\dot{\boldsymbol{y}} = (\boldsymbol{P}_\epsilon \boldsymbol{A}(t) \boldsymbol{P}_\epsilon^{-1}) \boldsymbol{y}$ converges to the origin, and so are those of $\dot{\boldsymbol{x}} = \boldsymbol{A}(t) \boldsymbol{x}$. □

Proposition 2.1.3. *Let $\boldsymbol{A}$ and $\boldsymbol{G}$ be matrices of dimension $m \times m$ and $n \times n$, respectively, and $\boldsymbol{I}_p$ be the $p \times p$ identity matrix. Let λ_i, $i = 1, \cdots, k$, be all the eigenvalues of $\boldsymbol{G}$. Then the real parts of the eigenvalues of*

$$(\boldsymbol{A} \otimes \boldsymbol{I}_n) + \left(\begin{pmatrix} \boldsymbol{I}_1 & \boldsymbol{0} \\ \boldsymbol{0} & \boldsymbol{0} \end{pmatrix} \otimes \boldsymbol{G} \right)$$

are negative provided that all real parts of the eigenvalues of matrices

$$\boldsymbol{M}_i := \boldsymbol{A} + \lambda_i \begin{pmatrix} \boldsymbol{I}_1 & \boldsymbol{0} \\ \boldsymbol{0} & \boldsymbol{0} \end{pmatrix}$$

are negative.

Proof. For any $\epsilon > 0$, there is $\boldsymbol{P}_\epsilon$ such that

$$\boldsymbol{P}_\epsilon \boldsymbol{G} \boldsymbol{P}_\epsilon^{-1} = \boldsymbol{D} + \epsilon \boldsymbol{Q},$$

where $\boldsymbol{D}$ is a diagonal matrix with the diagonal entries being all the eigenvalues of $\boldsymbol{G}$, and $\boldsymbol{Q}$ is a matrix with its entries being either 0 or 1. Then

$$(\boldsymbol{I}_m \otimes \boldsymbol{P}_\epsilon)\left[(\boldsymbol{A}\otimes\boldsymbol{I}_n)+\left(\begin{pmatrix}\boldsymbol{I}_1 & \boldsymbol{0}\\ \boldsymbol{0} & \boldsymbol{0}\end{pmatrix}\otimes\boldsymbol{G}\right)\right](\boldsymbol{I}_m\otimes\boldsymbol{P}_\epsilon^{-1})$$
$$=\left\{(\boldsymbol{A}\otimes\boldsymbol{I}_n)+\begin{pmatrix}\boldsymbol{I}_1 & \boldsymbol{0}\\ \boldsymbol{0} & \boldsymbol{0}\end{pmatrix}\otimes\boldsymbol{D}\right\}+\epsilon\begin{pmatrix}\boldsymbol{I}_1 & \boldsymbol{0}\\ \boldsymbol{0} & \boldsymbol{0}\end{pmatrix}\otimes\boldsymbol{Q}$$

By taking ϵ sufficiently small, we get real parts of the eigenvalues of

$$(\boldsymbol{A}\otimes\boldsymbol{I}_n)+\left(\begin{pmatrix}\boldsymbol{I}_1 & \boldsymbol{0}\\ \boldsymbol{0} & \boldsymbol{0}\end{pmatrix}\otimes\boldsymbol{G}\right)$$

are negative iff those of

$$(\boldsymbol{A}\otimes\boldsymbol{I}_n)+\begin{pmatrix}\boldsymbol{I}_1 & \boldsymbol{0}\\ \boldsymbol{0} & \boldsymbol{0}\end{pmatrix}\otimes\boldsymbol{D} \tag{2.5}$$

are negative. Then, the proof is completed by noting that after some permutation, matrix in (2.5) becomes $\mathrm{diag}(\boldsymbol{W}_1,\cdots,\boldsymbol{W}_n)$, where $\boldsymbol{W}_i=\boldsymbol{M}_j$, for some $j=1\ldots,k$. □

2.2 Global synchronization with time-invariant coupling

In this section, we first consider synchronization of (1.1) with the time-invariant coupling. It means we consider the synchronization in the following system.

$$\frac{d\boldsymbol{x}_i}{dt}=\boldsymbol{f}(\boldsymbol{x}_i,t)+d\cdot\sum_{j=1}^{m}g_{ij}\boldsymbol{D}\boldsymbol{x}_j,\quad i=1,2,\ldots,m, \tag{2.6a}$$

where $\boldsymbol{x}_i=(x_{i1},x_{i2},\ldots,x_{in})^T\in\mathbb{R}^n$, and $\boldsymbol{f}$ is a vector-valued function from $\mathbb{R}^n\times\mathbb{R}$ to $\mathbb{R}^n$ denoted by $\boldsymbol{f}(\boldsymbol{x},t)=(f_1(\boldsymbol{x},t),\cdots,f_n(\boldsymbol{x},t))^T$. Or equivalently,

$$\dot{\boldsymbol{x}}=\begin{pmatrix}\boldsymbol{f}(\boldsymbol{x}_1,t)\\ \vdots\\ \boldsymbol{f}(\boldsymbol{x}_m,t)\end{pmatrix}+d(\boldsymbol{G}\otimes\boldsymbol{D})\boldsymbol{x}=:\boldsymbol{F}(\boldsymbol{x},t)+d(\boldsymbol{G}\otimes\boldsymbol{D})\boldsymbol{x}, \tag{2.6b}$$

where $\boldsymbol{x}=(\boldsymbol{x}_1,\boldsymbol{x}_2\ldots,\boldsymbol{x}_m)^T$, and $\boldsymbol{G}=(g_{ij})$.

As one usually concerns, synchronization is the phenomenon that units in a group have their dynamical behaviors get closer and closer as time progresses, and eventually they tend to be identical. So, mathematically, we define synchronization in the same sense. Mention that such definitions are also set for the time-varying coupling.

Definition 2.2.1. *(i) The synchronous manifold* $\mathfrak{M}$ *of Model I* (1.1) *is defined as the set* $\mathfrak{M} = \{\boldsymbol{x} = (\boldsymbol{x}_1, \cdots, \boldsymbol{x}_m)^T : \boldsymbol{x}_i = \boldsymbol{x}_j,\ 1 \le i, j \le m\}$. *(ii) Model I* (1.1) *is said to be locally synchronized if the synchronous manifold* $\mathfrak{M}$ *is asymptotically stable under the given coupling strength* d.

Definition 2.2.2. *Model I* (1.1) *is said to be globally synchronized if, under the given coupling strength* d, *for all initial conditions* $\boldsymbol{x}_i(t_0)$ $(i = 1, 2, \ldots, m)$ *in* $\mathbb{R}^n$,

$$\lim_{t\to\infty} \|\boldsymbol{x}_i(t) - \boldsymbol{x}_j(t)\| = 0, \quad \forall 1 \le i, j \le m.$$

We next give the definition of the bounded dissipation of a system.

Definition 2.2.3. *Model I* (1.1) *is called to be* bounded dissipative *(with respect to* α*) if there is a bounded region* $B_{mn}(\alpha) =: \{\boldsymbol{x} : \|\boldsymbol{x}\| \le \alpha\}$ *such that for each parameter* $d > 0$, *and each initial value* $\boldsymbol{x}(0)$, *there is a time* t_0, *such that* $\boldsymbol{x}(t)$ *lies in* $B_{mn}(\alpha)$ *whenever* $t \ge t_0$.

To prove global synchronization of coupled chaotic systems, one needs to assume bounded dissipation, which plays the role of an a priori estimate. Without such an a priori estimate, as in the case of the Rössler system, global synchronization is much more difficult to obtain. Only local synchronization was reported numerically in literature (see e.g., [75]). An interesting question in this direction is how bounded dissipation of the coupled system is related to the uncoupled dynamics and its connectivity topology. Not much general theorems have been provided so far. In just the case that $\boldsymbol{G}(t)$ and $\boldsymbol{D}$ are specially given, it was shown in [7] that bounded dissipation of the single oscillator implies that of the coupled oscillators. Moreover, the absorbing domain of the coupled system is a topological product of the absorbing domain of each individual system.

Now, we impose the conditions on coupling matrices $\boldsymbol{G}$ and $\boldsymbol{D}$. We assume, throughout the section, that

$$\begin{aligned} &\text{(i)}\lambda = 0 \text{ is a simple eigenvalue of } \boldsymbol{G} \text{ and} \\ &\quad \boldsymbol{e} = \tfrac{1}{\sqrt{m}}(1, 1, \ldots, 1)^T_{1\times m} \text{ is its corresponding eigenvector;} && \text{(2.7a)} \\ &\text{(ii) All nonzero eigenvalues of } \boldsymbol{G} \text{ have negative real part.} && \text{(2.7b)} \end{aligned}$$

Such assumption above is to ensure the invariant property of the synchronous manifold $\mathfrak{M}$ and make the dynamics of each unit under synchronization be the same as that without coupling. We further assume that coupling matrix $\boldsymbol{D}$ is, without loss of generality, of the form

$$\boldsymbol{D} = \begin{pmatrix} \boldsymbol{I}_k & \boldsymbol{0} \\ \boldsymbol{0} & \boldsymbol{0} \end{pmatrix}_{n\times n.} \tag{2.7c}$$

The index k, $1 \leq k \leq n$, means that the first k components of the individual system are coupled. If $k \neq n$, then the system is said to be partial-state coupled. Otherwise, it is said to be full-state coupled.

To study synchronization of equation (2.6), we permute the state variables in the following way:

$$\tilde{\boldsymbol{x}}_i = \begin{pmatrix} x_{1i} \\ \vdots \\ x_{mi} \end{pmatrix}, \text{ and } \tilde{\boldsymbol{x}} = \begin{pmatrix} \tilde{\boldsymbol{x}}_1 \\ \vdots \\ \tilde{\boldsymbol{x}}_n \end{pmatrix}. \tag{2.8}$$

Then (2.6b) can be written equivalently as

$$\dot{\tilde{\boldsymbol{x}}} = \begin{pmatrix} \tilde{\boldsymbol{f}}_1(\tilde{\boldsymbol{x}}, t) \\ \vdots \\ \tilde{\boldsymbol{f}}_n(\tilde{\boldsymbol{x}}, t) \end{pmatrix} + d(\boldsymbol{D} \otimes \boldsymbol{G})\tilde{\boldsymbol{x}} =: \tilde{\boldsymbol{F}}(\tilde{\boldsymbol{x}}, t) + d(\boldsymbol{D} \otimes \boldsymbol{G})\tilde{\boldsymbol{x}}, \tag{2.9a}$$

where

$$\tilde{\boldsymbol{f}}_i(\tilde{\boldsymbol{x}}, t) = \begin{pmatrix} f_i(\boldsymbol{x}_1, t) \\ \vdots \\ f_i(\boldsymbol{x}_m, t) \end{pmatrix}. \tag{2.9b}$$

The purpose of such a reformulation is two-fold. First, a transformation of coordinates of $\tilde{\boldsymbol{x}}$ is to be applied to (2.9a) so as to isolate the synchronous manifold. Second, once the synchronous manifold is isolated, proving synchronization of (2.6), is then equivalent to showing that the origin is asymptotically stable with respect to reduced system (2.12). To do this, we first make a coordinate change to decompose the synchronous subspace. Let $\boldsymbol{A}$ be an $m \times m$ matrix of the form

$$\boldsymbol{A} = \begin{pmatrix} 1 & -1 & 0 & \cdots & 0 \\ 0 & \ddots & \ddots & \ddots & \vdots \\ \vdots & \ddots & \ddots & \ddots & 0 \\ 0 & \cdots & 0 & 1 & -1 \\ \frac{1}{\sqrt{m}} & \cdots & \cdots & \frac{1}{\sqrt{m}} & \frac{1}{\sqrt{m}} \end{pmatrix}_{m\times m} =: \begin{pmatrix} \boldsymbol{E} \\ \boldsymbol{e}^T \end{pmatrix}, \tag{2.10a}$$

where $\boldsymbol{e}$ is given as in (2.7a). It is then easy to see that $\boldsymbol{E}\boldsymbol{E}^T$ is invertible and that

$$\boldsymbol{A}^{-1} = \big(\boldsymbol{E}^T(\boldsymbol{E}\boldsymbol{E}^T)^{-1}, \boldsymbol{e}\big). \tag{2.10b}$$

Setting

$$\widehat{\boldsymbol{A}} = \boldsymbol{I}_n \otimes \boldsymbol{A}, \tag{2.10c}$$

we see that

$$\begin{aligned} \widehat{\boldsymbol{A}}(\boldsymbol{D}\otimes\boldsymbol{G})\widehat{\boldsymbol{A}}^{-1} &= (\boldsymbol{I}_n\otimes\boldsymbol{A})(\boldsymbol{D}\otimes\boldsymbol{G})(\boldsymbol{I}_n\otimes\boldsymbol{A}^{-1}) \\ &= \boldsymbol{D}\otimes\boldsymbol{A}\boldsymbol{G}\boldsymbol{A}^{-1} = \boldsymbol{D}\otimes\begin{pmatrix} \boldsymbol{E}\boldsymbol{G}\boldsymbol{E}^T(\boldsymbol{E}\boldsymbol{E}^T)^{-1} & \boldsymbol{0} \\ \boldsymbol{e}^T\boldsymbol{G}\boldsymbol{E}^T(\boldsymbol{E}\boldsymbol{E}^T)^{-1} & 0 \end{pmatrix} \\ &=: \boldsymbol{D}\otimes\begin{pmatrix} \bar{\boldsymbol{G}} & \boldsymbol{0} \\ \boldsymbol{h}^T & 0 \end{pmatrix}. \end{aligned} \tag{2.10d}$$

We remark, via (2.10d), that $\sigma(\bar{\boldsymbol{G}}) = \sigma(\boldsymbol{G}) - \{0\}$, where $\sigma(\cdot)$ takes the spectrum of a matrix. Multiplying $\widehat{\boldsymbol{A}}$ to the both side of equation (2.9a), we get

$$\begin{aligned} \dot{\tilde{\boldsymbol{y}}} =: \widehat{\boldsymbol{A}}\dot{\tilde{\boldsymbol{x}}} &= \widehat{\boldsymbol{A}}\tilde{\boldsymbol{F}}(\tilde{\boldsymbol{x}},t) + d\widehat{\boldsymbol{A}}(\boldsymbol{D}\otimes\boldsymbol{G})\widehat{\boldsymbol{A}}^{-1}\tilde{\boldsymbol{y}} \\ &= \widehat{\boldsymbol{A}}\tilde{\boldsymbol{F}}(\widehat{\boldsymbol{A}}^{-1}\tilde{\boldsymbol{y}},t) + d(\,\boldsymbol{D}\otimes\begin{pmatrix} \bar{\boldsymbol{G}} & \boldsymbol{0} \\ \boldsymbol{h}^T & 0 \end{pmatrix})\tilde{\boldsymbol{y}}. \end{aligned} \tag{2.11}$$

Let $\tilde{\boldsymbol{y}} = \begin{pmatrix} \tilde{\boldsymbol{y}}_1 \\ \vdots \\ \tilde{\boldsymbol{y}}_n \end{pmatrix}$. Then $\tilde{\boldsymbol{y}}_i = \begin{pmatrix} x_{1,i} - x_{2,i} \\ \vdots \\ x_{m-1,i} - x_{m,i} \\ \frac{1}{\sqrt{m}}\sum_{j=1}^{m} x_{j,i} \end{pmatrix}$. Setting $\tilde{\boldsymbol{y}}_i = \begin{pmatrix} \bar{\boldsymbol{y}}_i \\ \frac{1}{\sqrt{m}}\sum_{j=1}^{m} x_{j,i} \end{pmatrix}$, and $\bar{\boldsymbol{y}} = \begin{pmatrix} \bar{\boldsymbol{y}}_1 \\ \vdots \\ \bar{\boldsymbol{y}}_n \end{pmatrix}$, we have that the dynamics of $\bar{\boldsymbol{y}}$ is satisfied by following equation

$$\dot{\bar{\boldsymbol{y}}} = d(\boldsymbol{D}\otimes\bar{\boldsymbol{G}})\bar{\boldsymbol{y}} + \bar{\boldsymbol{F}}(\bar{\boldsymbol{y}},t). \tag{2.12}$$

Here $\bar{\boldsymbol{F}}$ is obtained from $\widehat{\boldsymbol{A}}\tilde{\boldsymbol{F}}(\widehat{\boldsymbol{A}}^{-1}\tilde{\boldsymbol{y}}, t)$ accordingly.

The task of obtaining global synchronization of system (2.6) is now reduced to showing that the origin is globally and asymptotically stable with respect to system (2.12). To this end, the space $\bar{\boldsymbol{y}}$ is broken into two parts $\bar{\boldsymbol{y}}_c$, the coupled space, and $\bar{\boldsymbol{y}}_u$, the uncoupled space.

$$\bar{\boldsymbol{y}} = \begin{pmatrix} \bar{\boldsymbol{y}}_c \\ \bar{\boldsymbol{y}}_u \end{pmatrix}, \text{ and } \bar{\boldsymbol{F}}(\bar{\boldsymbol{y}}, t) = \begin{pmatrix} \bar{\boldsymbol{F}}_c(\bar{\boldsymbol{y}}, t) \\ \bar{\boldsymbol{F}}_u(\bar{\boldsymbol{y}}, t) \end{pmatrix}, \text{ respectively.} \tag{2.13}$$

Here $\bar{\boldsymbol{y}}_c = \begin{pmatrix} \bar{\boldsymbol{y}}_1 \\ \vdots \\ \bar{\boldsymbol{y}}_k \end{pmatrix}$, and $\bar{\boldsymbol{y}}_u = \begin{pmatrix} \bar{\boldsymbol{y}}_{k+1} \\ \vdots \\ \bar{\boldsymbol{y}}_n \end{pmatrix}$. The dynamics on the coupled space with respect to the linear part is under the influence of $\bar{\boldsymbol{G}}$, which is asymptotically stable. The dynamics of the nonlinear part on coupled space can then be controlled by choosing large coupling strength. As a matter of fact, it is easier to obtain synchronization of coupled chaotic systems with a larger coupled space. On the other hand, the uncoupled space has no stable matrix $\bar{\boldsymbol{G}}$ to play with. Thus, its corresponding vector field $\bar{\boldsymbol{F}}_u(\bar{\boldsymbol{y}}, t)$ must have a certain structure to make the trajectory stay closer to the origin as time progresses. As we shall explain latter.

Now, assume that $\bar{\boldsymbol{F}}_c(\bar{\boldsymbol{y}}, t)$ satisfies a uniformly Lipschitz condition with a uniformly Lipschitz constant b_1. That is,

$$\|\bar{\boldsymbol{F}}_c(\bar{\boldsymbol{y}}, t)\| \leq b_1 \|\bar{\boldsymbol{y}}\| \tag{2.14a}$$

whenever $\bar{\boldsymbol{y}}$ in the ball $B_{(m-1)n}(\alpha)$, and for all time t. Since the estimate in the right-hand side of (2.14a) depends on the whole space $\bar{\boldsymbol{y}}$, condition (2.14a) is a mild assumption provided that the coupled system is bounded dissipative. Write $\bar{\boldsymbol{F}}_u(\bar{\boldsymbol{y}}, t)$ as

$$\begin{aligned} \bar{\boldsymbol{F}}_u(\bar{\boldsymbol{y}}, t) &= \boldsymbol{U}(t)\bar{\boldsymbol{y}}_u + (\bar{\boldsymbol{F}}_u(\bar{\boldsymbol{y}}, t) - \boldsymbol{U}(t)\bar{\boldsymbol{y}}_u) \\ &=: \boldsymbol{U}(t)\bar{\boldsymbol{y}}_u + \bar{\boldsymbol{R}}_u(\bar{\boldsymbol{y}}, t). \end{aligned} \tag{2.14b}$$

We assume further that the followings hold.

(i) $\boldsymbol{U}(t)$ is a block diagonal matrix of the form $\boldsymbol{U}(t) = \text{diag}(\boldsymbol{U}_1(t), \cdots, \boldsymbol{U}_l(t))$ where each $\boldsymbol{U}_j(t)$, $j = 1, \ldots, l$, are matrices of size $(m-1)k_j \times (m-1)k_j$. Here $\sum_{j=1}^{l} k_j = n - k$, and $k_j \in \mathbb{N}$. Assume that there exists a constant $\gamma > 0$ such that matrix measures $\mu_i(\boldsymbol{U}_j(t)) \leq -\gamma$, for all t and all j. (2.14c)

(ii) Let $\bar{\boldsymbol{R}}_u(\bar{\boldsymbol{y}}, t) = \begin{pmatrix} \boldsymbol{R}_{u1}(\bar{\boldsymbol{y}}, t) \\ \vdots \\ \boldsymbol{R}_{ul}(\bar{\boldsymbol{y}}, t) \end{pmatrix}$. Here l is the number given in (i). Then $\boldsymbol{R}_{uj}(\bar{\boldsymbol{y}}, t)$, $j = 1, \ldots, l$, satisfy a strong uniformly Lipschitz condition with a strong uniformly Lipschitz constant b_2. Specifically, let $\bar{\boldsymbol{y}}_u = \begin{pmatrix} \bar{\boldsymbol{y}}_{u1} \\ \vdots \\ \bar{\boldsymbol{y}}_{ul} \end{pmatrix}$, written in accordance with the block structure of $\boldsymbol{U}(t)$. Then we assume that

$$\|\boldsymbol{R}_{uj}(\bar{\boldsymbol{y}}, t)\| \leq b_2 \| \begin{pmatrix} \bar{\boldsymbol{y}}_e \\ \bar{\boldsymbol{y}}_{u1} \\ \vdots \\ \bar{\boldsymbol{y}}_{u\,j-1} \end{pmatrix} \| \tag{2.14d}$$

whenever $\bar{\boldsymbol{y}}$ in the ball $B_{(m-1)n}(\alpha)$, and for all $j = 1, \ldots, l$ and all time t.

Specifically, we break the vector field $\bar{\boldsymbol{F}}_u$ into (time dependent) linear part $\boldsymbol{U}(t)\bar{\boldsymbol{y}}_u$ and nonlinear part $\bar{\boldsymbol{R}}_u(\bar{\boldsymbol{y}}, t)$. We will further break $\boldsymbol{U}(t)$ into certain block diagonal form if necessary. Note that form (2.14b) can always be achieved since the remainder term $\bar{\boldsymbol{R}}_u$ still depends on the whole space $\bar{\boldsymbol{y}}$. To take control of the dynamics on the linear part, we assume that the matrix measure of each diagonal block $\boldsymbol{U}_j(t)$ is negative. As to contain corresponding dynamics on the nonlinear part, we assume that (2.14d) holds. Note that though the nonlinear terms $\boldsymbol{R}_{uj}(\bar{\boldsymbol{y}}, t)$ could possibly depend on the whole space, their norm estimates are required to depend only on the coupled space and uncoupled subspaces with their indices proceeding j. In this set up, the nonlinear dynamics on uncoupled space can be iteratively controlled by choosing large

coupling strength. We also remark that if (2.14c) and (2.14d) are satisfied for l, the number of diagonal blocks, being one, then we do not need to further break $\boldsymbol{U}(t)$. Such further breaking is needed only if (2.14c) and (2.14d) are not satisfied. The proof in the following theorem gives exactly how the above strategy can be realized.

Theorem 2.2.1. *Let $\boldsymbol{G}$ and $\boldsymbol{D}$ be given as in* (2.7). *Assume that $\bar{\boldsymbol{F}}$ satisfies* (2.14), *and system* (2.12) *is bounded dissipative with respect to α. Let $\lambda_1 = \max\{\lambda_j | \lambda_j \in Re(\sigma(\bar{\boldsymbol{G}}))\}$. If*

$$d > \frac{cb_1}{-\lambda_1 - \epsilon}\left(1 + (\frac{b_2}{\gamma})^2\right)^{\frac{l}{2}} =: d_{\min}, \tag{2.15}$$

where $\epsilon \geq 0$ and c is some constant depending on $\boldsymbol{G}$ and ϵ, then $\lim_{t\to\infty} \bar{\boldsymbol{y}}(t) = 0$.

Proof. Since system (2.12) is bounded dissipative with respect to α, without loss of generality, we may assume that $\|\bar{\boldsymbol{y}}(t)\| \leq \alpha$ for all time $t \geq t_0$. Using (2.14b), we write (2.12) as

$$\begin{pmatrix} \dot{\bar{\boldsymbol{y}}}_c \\ \dot{\bar{\boldsymbol{y}}}_u \end{pmatrix} = \begin{pmatrix} d(\boldsymbol{I}_k \otimes \bar{\boldsymbol{G}}) & \boldsymbol{0} \\ \boldsymbol{0} & \boldsymbol{U}(t) \end{pmatrix} \begin{pmatrix} \bar{\boldsymbol{y}}_c \\ \bar{\boldsymbol{y}}_u \end{pmatrix} + \begin{pmatrix} \bar{\boldsymbol{F}}_c(\bar{\boldsymbol{y}}, t) \\ \bar{\boldsymbol{R}}_u(\bar{\boldsymbol{y}}, t) \end{pmatrix}. \tag{2.16a}$$

Applying the variation of constant formula to (2.16a) on $\bar{\boldsymbol{y}}_c$, we get

$$\bar{\boldsymbol{y}}_c(t) = e^{(t-t_0)d(\boldsymbol{I}_k \otimes \bar{\boldsymbol{G}})}\bar{\boldsymbol{y}}_c(t_0) + \int_{t_0}^{t} e^{(t-s)d(\boldsymbol{I}_k \otimes \bar{\boldsymbol{G}})}\bar{\boldsymbol{F}}_c(\bar{\boldsymbol{y}}(s), s)ds. \tag{2.16b}$$

Let $\lambda_1 = \max\{\, \lambda_j | \lambda_j \in Re(\, \sigma(\boldsymbol{G}) - \{0\}\,)\,\}$. Then

$$\|e^{td(\boldsymbol{I}_k \otimes \bar{\boldsymbol{G}})}\| \leq ce^{td\nu} \tag{2.16c}$$

for $\nu = \lambda_1 + \epsilon$ and some constant c. Here $0 < \epsilon < -\lambda_1$. Thus,

$$\begin{aligned} \|\bar{\boldsymbol{y}}_c(t)\| &\leq ce^{(t-t_0)d\nu}\|\bar{\boldsymbol{y}}_c(t_0)\| + cb_1\int_{t_0}^{t} e^{d(t-s)\nu}\|\bar{\boldsymbol{y}}(s)\|ds \\ &\leq ce^{(t-t_0)d\nu}\alpha + \frac{\alpha}{d}\frac{cb_1}{|\nu|} =: ce^{(t-t_0)d\nu}\alpha + \frac{\alpha}{d}c_0. \end{aligned} \tag{2.16d}$$

Let $\delta > 1$, we see that

$$\|\bar{\boldsymbol{y}}_c(t)\| \leq \frac{\alpha}{d}c_0\delta, \tag{2.17a}$$

whenever $t \geq t_{0,1}$ for some $t_{0,1} > 0$. We then apply Theorem 2.1.1 on $\bar{\boldsymbol{y}}_{u1}$ and the resulting inequality is

$$\|\bar{\boldsymbol{y}}_{u1}(t)\| \leq \|\bar{\boldsymbol{y}}_{u1}(t_{0,1})\| \exp\left\{\int_{t_{0,1}}^{t} \mu_i(\boldsymbol{U}_1(s))ds\right\} + \int_{t_{0,1}}^{t} \exp\left\{\int_{s}^{t} \mu_i(\boldsymbol{U}_1(\tau))d\tau\right\} \|\boldsymbol{R}_{u1}(\bar{\boldsymbol{y}}(s), s)\|ds.$$

It then follows from (2.14c), (2.14d), and (2.17a) that

$$\|\bar{\boldsymbol{y}}_{u1}(t)\| \leq \alpha e^{-\gamma(t-t_{0,1})} + \frac{\alpha}{d}\frac{b_2}{\gamma}c_0\delta \leq \frac{\alpha}{d}\frac{b_2}{\gamma}c_0\delta^2 =: \frac{\alpha}{d}c_1\delta^2, \tag{2.17b}$$

whenever $t \geq t_{1,1}$ for some $t_{1,1} \geq t_{0,1}$. Inductively, we get

$$\|\bar{\boldsymbol{y}}_{uj}(t)\| \leq \frac{\alpha}{d}\left(\frac{b_2}{\gamma}\sqrt{\sum_{i=0}^{j-1} c_i^2}\right)\delta^{j+1} =: \frac{\alpha}{d}c_j\delta^{j+1}, \quad j = 2, \ldots, l, \tag{2.17c}$$

whenever $t \geq t_{j,1} (\geq t_{j-1,1})$. Letting $t_{l,1} = t_1$ and summing up (2.17a)-(2.17c), we get

$$\|\bar{\boldsymbol{y}}(t)\| = \sqrt{\sum_{j=1}^{l} \|\bar{\boldsymbol{y}}_{uj}(t)\|^2 + \|\bar{\boldsymbol{y}}_c(t)\|^2} \leq \frac{\alpha}{d}\left(1 + (\frac{b_2}{\gamma})^2\right)^{\frac{l}{2}} \frac{cb_1}{|\nu|}\delta^{l+1} =: h\alpha,$$

whenever $t \geq t_1$. Choosing $d > \left(1 + (\frac{b_2}{\gamma})^2\right)^{\frac{l}{2}} \frac{cb_1}{|\nu|}\delta^{l+1}$, we see that the contraction factor h is strictly less than 1, and $\|\bar{\boldsymbol{y}}(t)\|$ contracts as time progresses. To complete the proof of the theorem, we note that $\delta > 1$ can be made arbitrary close to 1. Consequently, if $d > \left(1 + (\frac{b_2}{\gamma})^2\right)^{\frac{l}{2}} \frac{cb_1}{|\nu|}$, then h can still be made to be less than 1. □

Remark 2.2.1. *(i) In case that $\bar{\boldsymbol{G}}$ is symmetric, then c and ϵ can be chosen to be 1 and 0, respectively. (ii) b_1 and b_2 could possibly depend on α.*

Corollary 2.2.1. *Suppose $\bar{\boldsymbol{F}}$ and $\boldsymbol{G}$ are given as in Theorem 2.2.1. Let*

$$\boldsymbol{D} = \begin{pmatrix} \tilde{\boldsymbol{D}}_{k\times k} & \boldsymbol{0} \\ \boldsymbol{0} & \boldsymbol{0} \end{pmatrix}_{n\times n,} \quad \text{where } Re(\,\sigma(\tilde{\boldsymbol{D}})\,) > 0. \tag{2.18}$$

Assume, in addition, that either $\sigma(\boldsymbol{G})$ or $\sigma(\tilde{\boldsymbol{D}})$ has no complex eigenvalue. Then assertions in Theorem 2.2.1 still hold true, except $d_{\min}$ needs to be replaced by

$$d_{\min} = \frac{c\,b_1}{(-\lambda_1 - \epsilon)\cdot \min\{Re(\,\sigma(\tilde{\boldsymbol{D}})\,)\}}\left(1 + (\frac{b_2}{\gamma})^2\right)^{\frac{l}{2}}. \tag{2.19}$$

Proof. Assumption on $\boldsymbol{D}$ is to ensure that (2.16c) is still valid. Other parts of the proof are similar to those in Theorem 2.2.1 and are thus omitted. □

We next turn our attention to finding conditions on the nonlinearities $f_i(\boldsymbol{u}, t)$, $i = 1, \ldots, n$, $\boldsymbol{u} \in \mathbb{R}^n$, so that assumptions (2.14) are satisfied. To this end, we need the following notations. Let $\tilde{\boldsymbol{x}}_i$ and $\tilde{\boldsymbol{x}}$ be given as in (2.8). Define

$$[\tilde{\boldsymbol{x}}_i]^- = \begin{pmatrix} x_{1,i} \\ \vdots \\ x_{m-1,i} \end{pmatrix}, \text{ and } [\tilde{\boldsymbol{x}}]^- = \begin{pmatrix} [\tilde{\boldsymbol{x}}_1]^- \\ \vdots \\ [\tilde{\boldsymbol{x}}_n]^- \end{pmatrix}. \tag{2.20}$$

We then break $\tilde{\boldsymbol{F}}$ as given in (2.9a) into two parts so that the breaking is in consistent with $\bar{\boldsymbol{y}}$ in (2.13). Specifically, we shall write

$$\tilde{\boldsymbol{F}}(\tilde{\boldsymbol{x}}, t) = \begin{pmatrix} \tilde{\boldsymbol{F}}_c(\tilde{\boldsymbol{x}}, t) \\ \tilde{\boldsymbol{F}}_u(\tilde{\boldsymbol{x}}, t) \end{pmatrix}. \tag{2.21}$$

We are now in the position to state the following propositions.

Proposition 2.2.1. *Suppose that $f_i(\boldsymbol{x}, t)$, $i = 1, 2, \ldots, k$ satisfy a Lipschitz condition in $B_n(\frac{\alpha}{2})$ with a Lipschitz constant b_1. That is*

$$|f_i(\boldsymbol{u}, t) - f_i(\boldsymbol{v}, t)| \leq \frac{b_1}{k} \|\boldsymbol{u} - \boldsymbol{v}\|, \; i = 1, 2, \ldots, k, \tag{2.22}$$

for all $\boldsymbol{u}$, $\boldsymbol{v}$ in $B_n(\frac{\alpha}{2})$ and all time t. Then (2.14a) *holds true.*

Proof. Note that $\widehat{\boldsymbol{A}}\tilde{\boldsymbol{F}}(\tilde{\boldsymbol{x}}, t) = \begin{pmatrix} \boldsymbol{A}\tilde{\boldsymbol{f}}_1(\tilde{\boldsymbol{x}}, t) \\ \vdots \\ \boldsymbol{A}\tilde{\boldsymbol{f}}_n(\tilde{\boldsymbol{x}}, t) \end{pmatrix}$ where $\boldsymbol{A}$ is given as in (2.10a), and so

$$[\boldsymbol{A}\tilde{\boldsymbol{f}}_i(\tilde{\boldsymbol{x}}, t)]^- = \begin{pmatrix} f_i(\boldsymbol{x}_1, t) - f_i(\boldsymbol{x}_2, t) \\ \vdots \\ f_i(\boldsymbol{x}_{m-1}, t) - f_i(\boldsymbol{x}_m, t) \end{pmatrix}, \quad i = 1, 2, \ldots, n. \tag{2.23}$$

Since

$$\bar{\boldsymbol{F}}_c(\bar{\boldsymbol{y}}, t) = \begin{pmatrix} [\boldsymbol{A}\tilde{\boldsymbol{f}}_1(\tilde{\boldsymbol{x}}, t)]^- \\ \vdots \\ [\boldsymbol{A}\tilde{\boldsymbol{f}}_k(\tilde{\boldsymbol{x}}, t)]^- \end{pmatrix},$$

we conclude that (2.14a) holds. □

From the above proposition, we see that the nonlinearities on the corresponding coupled space are only assumed to be Lipchitz. The following proposition is very useful in the sense that by checking how each component f_i of the nonlinearity $\boldsymbol{f}$ is formed, one would then be able to conclude whether (2.14c) and (2.14d) are satisfied.

Proposition 2.2.2. *Let $\boldsymbol{u} = (u_1, \ldots, u_n)^T$ and $\boldsymbol{v} = (v_1, \ldots, v_n)^T$ be vectors in $B_n(\frac{\alpha}{2})$. Let $w_p = \sum_{i=0}^{p} k_i$, $p = 1, \ldots, l$, where $k_0 = k$, the dimension of coupled space, and $k_1, \ldots, k_l$ and l are given as in (2.14c). Write $f_{w_{p-1}+i}(\boldsymbol{u}, t) - f_{w_{p-1}+i}(\boldsymbol{v}, t)$, $i = 1, \ldots, k_p$, as*

$$\begin{aligned} & f_{w_{p-1}+i}(\boldsymbol{u}, t) - f_{w_{p-1}+i}(\boldsymbol{v}, t) \\ & \qquad = \sum_{j=1}^{k_p} q_{w_{p-1}+i, w_{p-1}+j}(\boldsymbol{u}, \boldsymbol{v}, t)(u_{w_{p-1}+j} - v_{w_{p-1}+j}) + r_{w_{p-1}+i}(\boldsymbol{u}, \boldsymbol{v}, t). \end{aligned} \tag{2.24a}$$

We further assume that the followings are true.

(i) For $p = 1, \ldots, l$, let $\boldsymbol{Q}_{\boldsymbol{u},\boldsymbol{v},p} = (q_{w_{p-1}+i, w_{p-1}+j}(\boldsymbol{u}, \boldsymbol{v}, t))$, where $1 \le i, j \le k_p$. Then $\mu_*(\boldsymbol{V}_p) < -\gamma$ for all p, $\boldsymbol{u}, \boldsymbol{v}$ in $B_n(\frac{\alpha}{2})$ and all time t, where $* = 1, 2, \infty$.

(2.24b)

(ii) Let $\boldsymbol{r}_p = \left(r_{w_{p-1}+1}(\boldsymbol{u}, \boldsymbol{v}, t), \ldots, r_{w_p}(\boldsymbol{u}, \boldsymbol{v}, t)\right)^T$. We have that

$$\|\boldsymbol{r}_p\| \le b_2 \left\| \begin{pmatrix} u_1 - v_1 \\ \vdots \\ u_{w_{p-1}} - v_{w_{p-1}} \end{pmatrix} \right\| \tag{2.24c}$$

for all p, $\boldsymbol{u}, \boldsymbol{v}$ in $B_n(\frac{\alpha}{2})$ and all time t.

Then (2.14c) *and* (2.14d) *hold true for $* = 1, 2, \infty$.*

Proof. Since $r_i(\boldsymbol{u}, \boldsymbol{v}, t)$ depend on the whole space, $f_i(\boldsymbol{u}, t) - f_i(\boldsymbol{v}, t)$ can always be written as the form in (2.24a). Using (2.24a) and (2.23), we have that the matrices $\boldsymbol{U}_p(t)$ in the linear part of $\bar{\boldsymbol{F}}_u(\bar{\boldsymbol{y}}, t)$ take the form

$$\boldsymbol{U}_p(t) = \sum_{w=1}^{m-1} \boldsymbol{Q}_{\boldsymbol{x}_w, \boldsymbol{x}_{w+1}, p}(t) \otimes \boldsymbol{D}_w, \tag{2.25}$$

where $\boldsymbol{x}_w$ are given as in (2.6a), and

$$(\boldsymbol{D}_w)_{ij} = \begin{cases} 1 & i = j = w, \\ 0 & otherwise, \end{cases} \quad 1 \leq i, j \leq m-1.$$

It then follows from Lemma 2.1.1, and (2.25) that $\mu_*(\boldsymbol{U}_p(t)) < -\gamma$ for $* = 1$ or ∞. For $* = 2$, we have that

$$\begin{aligned} &\bigcup_{w=1}^{m-1} \sigma\{\boldsymbol{Q}_{\boldsymbol{x}_w,\boldsymbol{x}_{w+1},p}(t) + \left(\boldsymbol{Q}_{\boldsymbol{x}_w,\boldsymbol{x}_{w+1},p}(t)\right)^T\} \\ &\qquad = \sigma\left\{\sum_{w=1}^{m-1}\left(\boldsymbol{Q}_{\boldsymbol{x}_w,\boldsymbol{x}_{w+1},p}(t) \otimes \boldsymbol{D}_w + \left(\boldsymbol{Q}_{\boldsymbol{x}_w,\boldsymbol{x}_{w+1},p}(t)\right)^T \otimes \boldsymbol{D}_w\right)\right\} \\ &\qquad = \sigma\left(\boldsymbol{U}_p(t) + \boldsymbol{U}_p^T(t)\right), \end{aligned}$$

where $\sigma(\boldsymbol{A})$ is the spectrum of $\boldsymbol{A}$. We remark that the first equality above can be verified by the definition of eigenvalues due to the structure of $\boldsymbol{U}_p(t)$. It then follows from Lemma 2.1.1 that $\mu_2(\boldsymbol{U}_p(t)) < -\gamma$. The remainder of the proof is similar to that of Proposition 2.2.1, and is thus omitted. □

Remark 2.2.2. *The upshot of Proposition 2.2.2 is that by only checking the "structure" of the vector field $\boldsymbol{f}$ of the single oscillator, one should be able to determine if our main result can be applied. To be precise, we begin with saving notations by setting $\boldsymbol{f}$ as $\boldsymbol{f} = \boldsymbol{f}(\boldsymbol{x}, t) = (f_1(\boldsymbol{x}, t), \ldots, f_n(\boldsymbol{x}, t))^T$. We then check the form of the difference of "uncoupled" part of dynamics. That is, we write $f_i(\boldsymbol{u}, t) - f_i(\boldsymbol{v}, t)$ in the form of* (2.24a) *with $i = k+1, \ldots, n$. If* (2.24b)-(2.24c) *can be satisfied, then $l = 1$ gets the job done. Otherwise, we further break the uncoupled states into a set of smaller pieces to see if the resulting* (2.24b)-(2.24c) *are satisfied.*

We are now ready to state the main theorems of the paper.

Theorem 2.2.2. *Assume that system* (2.6) *is bounded dissipative. Let coupling matrices $\boldsymbol{G}$ and $\boldsymbol{D}$ satisfy* (2.7) *and the nonlinearities $f_i(\boldsymbol{x}, t)$, $i = 1, 2, \ldots, n$, satisfy* (2.22) *and* (2.24). *Suppose d is greater than $d_{\min}$, as given in* (2.15). *Then system* (2.6) *is globally synchronized.*

Proof. The proof is direct consequences of Propositions 2.2.1 and 2.2.2, and Theorem 2.2.1. □

Theorem 2.2.3. *Coupled system* (2.6) *with* $\boldsymbol{D}$ *given as in Corollary 2.2.1, is globally synchronized provided that the coupled system is bounded dissipative, the nonlinearities* $f_i(\boldsymbol{x}, t)$, $i = 1, 2, \ldots, n$, *satisfy* (2.22) *and* (2.24), *and* d *is greater than* $d_{\min}$. *Here* $d_{\min}$ *is given in* (2.19).

The actual way to apply the above Theorem 2.2.1, 2.2.2 to the real question is postponed to the Chapter 3.

2.3 Global synchronization with time-varying coupling

In this section, we consider the synchronization of Model (1.1). As given in (2.9a), we can write the coupled system equivalently as

$$\dot{\tilde{\boldsymbol{x}}} = \begin{pmatrix} \tilde{\boldsymbol{f}}_1(\tilde{\boldsymbol{x}}, t) \\ \vdots \\ \tilde{\boldsymbol{f}}_n(\tilde{\boldsymbol{x}}, t) \end{pmatrix} + d(\boldsymbol{D} \otimes \boldsymbol{G}(t))\tilde{\boldsymbol{x}} =: \tilde{\boldsymbol{F}}(\tilde{\boldsymbol{x}}, t) + d(\boldsymbol{D} \otimes \boldsymbol{G}(t))\tilde{\boldsymbol{x}}, \tag{2.26}$$

where $\tilde{\boldsymbol{x}}_i$, $\tilde{\boldsymbol{x}}$ and $\tilde{\boldsymbol{f}}_i(\tilde{\boldsymbol{x}}, t)$ are defined as in (2.8), (2.9b). Our basic strategy to get the criteria of synchronization such as Theorem 2.2.2 is similar to that gotten there. What makes the most difference is that in this case Eq. (2.16b) does not hold again. To deal with it, we will apply Theorem 2.1.1. Nevertheless, in Theorem 2.1.1, what is concerned is the matrix measure of a matrix not the eigenvalue of a matrix. Thus, one needs to deal with the corresponding problem carefully. To do so, we make the usage of the concept of "*coordinate transformation*".

First, instead of defining $\boldsymbol{E}$ as in (2.10a), herein we let $\boldsymbol{E}$ be an $(m-1) \times m$ full-rank matrix with all its row sums being zero. Such a matrix is to be termed a *coordinate transformation*. Define

$$\boldsymbol{A} = \begin{pmatrix} \boldsymbol{E} \\ \boldsymbol{e}^T \end{pmatrix}. \tag{2.27a}$$

Then $\boldsymbol{A}^{-1} = \left(\boldsymbol{E}^T(\boldsymbol{E}\boldsymbol{E}^T)^{-1}, \boldsymbol{e}\right)$ and

$$\boldsymbol{A}\boldsymbol{G}(t)\boldsymbol{A}^{-1} = \begin{pmatrix} \boldsymbol{E}\boldsymbol{G}(t)\boldsymbol{E}^T(\boldsymbol{E}\boldsymbol{E}^T)^{-1} & \boldsymbol{0} \\ \boldsymbol{e}^T\boldsymbol{G}(t)\boldsymbol{E}^T(\boldsymbol{E}\boldsymbol{E}^T)^{-1} & 0 \end{pmatrix} =: \begin{pmatrix} \bar{\boldsymbol{G}}_{\boldsymbol{E}}(t) & \boldsymbol{0} \\ \boldsymbol{h}(t)^T & 0 \end{pmatrix}. \tag{2.27b}$$

Let $\widehat{\boldsymbol{A}} = \boldsymbol{I}_n \otimes \boldsymbol{A}$ and $\tilde{\boldsymbol{y}} = \widehat{\boldsymbol{A}}\tilde{\boldsymbol{x}}$. Multiplying $\widehat{\boldsymbol{A}}$ to both sides of Equation (2.26), we get

$$\dot{\tilde{\boldsymbol{y}}} = \widehat{\boldsymbol{A}}\tilde{\boldsymbol{F}}(\widehat{\boldsymbol{A}}^{-1}\tilde{\boldsymbol{y}}, t) + d\left(\boldsymbol{D} \otimes \begin{pmatrix} \bar{\boldsymbol{G}}_{\boldsymbol{E}}(t) & \boldsymbol{0} \\ \boldsymbol{h}(t)^T & 0 \end{pmatrix}\right)\tilde{\boldsymbol{y}}.$$

Let $\tilde{\boldsymbol{y}} = (\tilde{\boldsymbol{y}}_1, \ldots, \tilde{\boldsymbol{y}}_n)^T$. Then

$$\tilde{\boldsymbol{y}}_i = \begin{pmatrix} \boldsymbol{E}\tilde{\boldsymbol{x}}_i \\ \sum_{j=1}^m x_{ji}/\sqrt{m} \end{pmatrix} =: \begin{pmatrix} \bar{\boldsymbol{y}}_i \\ \boldsymbol{e}_i \end{pmatrix}. \tag{2.28}$$

Setting $\bar{\boldsymbol{y}} = (\bar{\boldsymbol{y}}_1, \ldots, \bar{\boldsymbol{y}}_n)^T$, we have that the dynamics of $\bar{\boldsymbol{y}}$ is now satisfied by the following equation

$$\dot{\bar{\boldsymbol{y}}} = d(\boldsymbol{D} \otimes \bar{\boldsymbol{G}}_{\boldsymbol{E}}(t))\bar{\boldsymbol{y}} + \bar{\boldsymbol{F}}(\bar{\boldsymbol{y}}, t), \tag{2.29a}$$

where

$$\bar{\boldsymbol{F}}(\bar{\boldsymbol{y}}, t) = (\boldsymbol{I}_n \otimes \boldsymbol{E}) \cdot \tilde{\boldsymbol{F}}(\widehat{\boldsymbol{A}}^{-1}\tilde{\boldsymbol{y}}, t). \tag{2.29b}$$

Since the rank and the row sums of $\boldsymbol{E}$ are $m-1$ and 0, respectively, we conclude that the task of obtaining global synchronization of system (1.1) is now reduced to showing that the origin is globally and asymptotically stable with respect to system (2.29a). The choice of a coordination transformation will greatly influence how negative the matrix measure of $\bar{\boldsymbol{G}}_{\boldsymbol{E}}(t)$ could be, which plays the important role, among others, to determine the global stability of (2.29a) with respect to the origin.

2.3.1 Matrices of the Coordinate Transformation

In what follows we shall address the question of how to choose a matrix $\boldsymbol{E}$ of the coordinate transformation, and its corresponding properties. To make the origin an asymptotically stable equilibrium of system (2.29a), one would like to have the matrix measure of $\bar{\boldsymbol{G}}_{\boldsymbol{E}}(t)$ as smaller a negative number as possible. In fact, such an optimal choice $\boldsymbol{E}$ can be achieved provided that the outer coupling matrix $\boldsymbol{G}(t)$ is symmetric, nonpositive definite.

Definition 2.3.1. *Denote by* $\mathfrak{C}$ *the set of* $(m-1)\times m$ *coordinate transformations, i.e.,*

$$\mathfrak{C} = \{\boldsymbol{E} \in \mathbb{R}^{(m-1)\times m} : \boldsymbol{E} \text{ is full-rank, and all its row sums are zero}\}.$$

Let $\mathfrak{O} \subseteq \mathfrak{C}$ *be such that*

$$\mathfrak{O} = \{\boldsymbol{E} \in \mathfrak{C} : \boldsymbol{E} \text{ such that matrix } \boldsymbol{A} = (\boldsymbol{E}^T, \boldsymbol{e})^T \text{ is orthogonal}\}.$$

Theorem 2.3.1. *Assume that all eigenvalues of outer coupling matrix* $\boldsymbol{G}(t)$ *have nonpositive real parts. Then* $\inf_{\boldsymbol{E}\in\mathfrak{C}} \mu_2(\bar{\boldsymbol{G}}_{\boldsymbol{E}}(t)) \geq Re\,\lambda_2(\boldsymbol{G}(t))$. *Here* $Re\,\lambda_2(\boldsymbol{G}(t))$ *is the second largest real part of eigenvalues of* $\boldsymbol{G}(t)$. *If, in addition,* $\boldsymbol{G}(t)$ *is symmetric for all* t, *then the above equality can be achieved by choosing any* $\boldsymbol{E}$ *in* $\mathfrak{O}$.

Proof. It follows from (2.27b) that the spectrum $\sigma(\bar{\boldsymbol{G}}_{\boldsymbol{E}}(t))$ of $\bar{\boldsymbol{G}}_{\boldsymbol{E}}(t)$ is equal to $\sigma(\boldsymbol{G}(t))-\{0\}$. Using the fact that $\mathrm{Re}\,\lambda(\boldsymbol{K}) \leq \lambda_{\max}(\frac{\boldsymbol{K}+\boldsymbol{K}^T}{2})$ for any real matrix $\boldsymbol{K}$, we have, via Lemma 2.1.1, that $\mu_2(\bar{\boldsymbol{G}}_{\boldsymbol{E}}(t)) \geq \mathrm{Re}\,\lambda_2(\boldsymbol{G}(t))$. In particular, if $\boldsymbol{E} \in \mathfrak{O}$ and $\boldsymbol{G}(t)$ is symmetric, then $\bar{\boldsymbol{G}}_{\boldsymbol{E}}(t)$ $\left(= \boldsymbol{E}\boldsymbol{G}(t)\boldsymbol{E}^T\right)$ is symmetric and $\boldsymbol{h}(t) = \boldsymbol{0}$. Here $\boldsymbol{h}(t)$ is given as in (2.27b). Therefore, $\mu_2(\bar{\boldsymbol{G}}_{\boldsymbol{E}}(t)) = \lambda_2(\boldsymbol{G}(t))$. We have just completed the proof of the theorem. □

The theorem above amounts to saying that if $\boldsymbol{G}(t)$ is symmetric, nonpositive definite, then any choice of $\boldsymbol{E}$ in $\mathfrak{O}$ yields the smallest possible matrix measure of $\bar{\boldsymbol{G}}_{\boldsymbol{E}}(t)$. This, in turn, gives one the best possible position to study the stability of equation (2.29a) with respect to the origin.

Remark 2.3.1. *In those earlier papers (see, e.g., [17,53,104]), the choice of the coordinate transformations is either*

$$\boldsymbol{E}_1 = \begin{pmatrix} 1 & -1 & 0 & \cdots & 0 \\ 1 & 0 & -1 & \ddots & \vdots \\ \vdots & \vdots & \ddots & \ddots & 0 \\ 1 & 0 & \cdots & 0 & -1 \end{pmatrix} \text{ or } \boldsymbol{E}_2 = \begin{pmatrix} 1 & -1 & 0 & \cdots & 0 \\ 0 & 1 & -1 & \ddots & \vdots \\ \vdots & \ddots & \ddots & \ddots & 0 \\ 0 & \cdots & 0 & 1 & -1 \end{pmatrix}. \tag{2.30}$$

The drawback for such a choice of $\boldsymbol{E}$ *is that even if* $\boldsymbol{G}(t)\,(\equiv \boldsymbol{G})$ *is the diffusive matrix*

with periodic boundary conditions, i.e.,

$$\boldsymbol{G}(t) \equiv \begin{pmatrix} -2 & 1 & 0 & \cdots & 0 & 1 \\ 1 & -2 & 1 & 0 & \cdots & 0 \\ 0 & \ddots & \ddots & \ddots & \ddots & \vdots \\ \vdots & \ddots & \ddots & \ddots & \ddots & 0 \\ 0 & \cdots & 0 & 1 & -2 & 1 \\ 1 & 0 & \cdots & 0 & 1 & -2 \end{pmatrix}_{m\times m}, \tag{2.31}$$

the corresponding matrix measure of $\bar{\boldsymbol{G}}_{\boldsymbol{E}_i}$, $i = 1, 2$ *is positive whenever* $m > 7$ *(see Table 2.1), while* $\mu_2(\bar{\boldsymbol{G}}_{\boldsymbol{E}}) = \lambda_2(\boldsymbol{G}) < 0$ *for all* $\boldsymbol{E} \in \mathfrak{O}$ *regardless the size of* $\boldsymbol{G}$.

m	4	5	6	7	8	9
$\boldsymbol{E}_1$	-1.78	-1	-0.51	-0.19	0.05	0.23
$\boldsymbol{E}_2$	-1.78	-1	-0.51	-0.19	0.05	0.23

Table 2.1: The table gives the matrix measures of $\bar{\boldsymbol{G}}_{\boldsymbol{E}_i}$, $i = 1, 2$, with various size of $\boldsymbol{G}$, which is given in (2.31). Since $\boldsymbol{G}$ is a circular matrix, the matrix measures of $\bar{\boldsymbol{G}}$ with respect to $\boldsymbol{E}_1$ and $\boldsymbol{E}_2$ are equal. Note that the matrix measure of $\bar{\boldsymbol{G}}_{\boldsymbol{E}}$ is $\lambda_2(\boldsymbol{G})$, $\forall \boldsymbol{E} \in \mathfrak{O}$, which is negative regardless the size of $\boldsymbol{G}$.

Theorem 2.3.2. *For any outer coupling matrix* $\boldsymbol{G}(t)$*, and any coordinate transformations* $\boldsymbol{E}_p$, $\boldsymbol{E}_q$ *in* $\mathfrak{O}$, $\mu_2(\bar{\boldsymbol{G}}_{\boldsymbol{E}_p}(t)) = \mu_2(\bar{\boldsymbol{G}}_{\boldsymbol{E}_q}(t))$.

Proof. Since for any $\boldsymbol{x} \in \mathbb{R}^{m-1}$, there is $\boldsymbol{z} = \boldsymbol{E}_q\boldsymbol{E}_p^T\boldsymbol{x}$ such that

$$\boldsymbol{x}^T\boldsymbol{E}_p(\boldsymbol{G}(t) + \boldsymbol{G}(t)^T)\boldsymbol{E}_p^T\boldsymbol{x} = \boldsymbol{z}^T\boldsymbol{E}_q(\boldsymbol{G}(t) + \boldsymbol{G}(t)^T)\boldsymbol{E}_q^T\boldsymbol{z}.$$

By the definition of matrix measure, we have that $\mu_2(\bar{\boldsymbol{G}}_{\boldsymbol{E}_p}(t)) = \mu_2(\bar{\boldsymbol{G}}_{\boldsymbol{E}_q}(t))$. □

In this section, matrix $\boldsymbol{E}$ in Equation (2.29a) is assumed to lie in $\mathfrak{D}$ unless otherwise stated. For ease of the notations, we shall drop the subscript $\boldsymbol{E}$ of $\bar{\boldsymbol{G}}_{\boldsymbol{E}}(t)$ if $\boldsymbol{E} \in \mathfrak{O}$. The remainder of the subsection is devoted to finding the matrix measure of $\bar{\boldsymbol{G}}(t)$ where its corresponding coupling matrix $\boldsymbol{G}(t)$ appears often in many applications.

Proposition 2.3.1. *Assume that for each* t, $\boldsymbol{G}(t)$ *is a node-balancing matrix, i.e., its row sums and column sums are equal. Then*

$$\mu_2(\bar{\boldsymbol{G}}(t)) = \lambda_2(\frac{\boldsymbol{G}(t) + \boldsymbol{G}(t)^T}{2}), \tag{2.32}$$

whenever all eigenvalues of $\boldsymbol{G}(t)+\boldsymbol{G}(t)^T$ *are nonpositive.*

Proof. If $\boldsymbol{G}(t)$ is as assumed, then it follows from (2.27b) that

$$\boldsymbol{A}\boldsymbol{G}(t)\boldsymbol{A}^{-1}=\begin{pmatrix}\bar{\boldsymbol{G}}(t) & \boldsymbol{0}\\ \boldsymbol{0} & 0\end{pmatrix}.$$

Consequently, (2.32) holds as asserted. □

In what follows, some outer coupling matrices are to be provided. Their corresponding matrix measures of $\bar{\boldsymbol{G}}(t)$ and $\bar{\boldsymbol{G}}_{\boldsymbol{E}_i}(t)$, $i=1$ or 2, are to be compared.

Example 1. ([2]) Consider the regular coupled network by adding to the pristine world $\boldsymbol{G}$ (the ring of $2K$-nearest coupled oscillators) an additional global coupling such that the coupling $p(t)$, $0\le p(t)\le 1$ is placed on all free spots of the matrix $\boldsymbol{G}$ (see, e.g., [2]). Specifically, the resulting coupling matrix $\boldsymbol{G}(t)$ can be represented by a circular matrix of the form

$$\boldsymbol{G}(t)=\mathrm{circ}(-g(t),\overbrace{1,\ldots,1}^{K},\overbrace{p(t),\ldots,p(t)}^{m-2K-1},\overbrace{1,\ldots,1}^{K}), \tag{2.33}$$

where $g(t)=2K+(m-2K-1)p(t)$. Since $\boldsymbol{G}(t)$ is symmetric, we have that

$$\begin{aligned}\mu_2(\bar{\boldsymbol{G}}(t)) &= \lambda_2(\boldsymbol{G}(t))\\ &= \max_{1\le j\le m-1}\left(-g(t)+\sum_{l=1}^{K}(\omega^{lj}+\omega^{(m-l)j})+p(t)\sum_{l=K+1}^{m-K-1}\omega^{lj}\right).\end{aligned}$$

Here $\omega=\exp(2\pi i/m)$. The matrix measures $\mu_2(\bar{\boldsymbol{G}}(t))$ and $\mu_2(\bar{\boldsymbol{G}}_{\boldsymbol{E}_i}(t))$, $i=1,2$, with $m=8$, $K=2$, and $p(t)=t$, $t\in[0,1]$ are recorded in Figure 2.1.

Example 2. ([52,98]) Let $\boldsymbol{G}=\boldsymbol{G}_\beta^{(m)}$, $0\le\beta\le 1$ be the diffusive matrix of size $m\times m$ with mixed boundary conditions. That is, if $m>2$,

$$\boldsymbol{G}_\beta^{(m)}=\begin{pmatrix}-1-\beta & 1 & 0 & \cdots & 0 & \beta\\ 1 & -2 & 1 & 0 & \cdots & 0\\ 0 & \ddots & \ddots & \ddots & \ddots & \vdots\\ \vdots & \ddots & \ddots & \ddots & \ddots & 0\\ 0 & \cdots & 0 & 1 & -2 & 1\\ \beta & 0 & \cdots & 0 & 1 & -1-\beta\end{pmatrix}_{m\times m,} \tag{2.34}$$

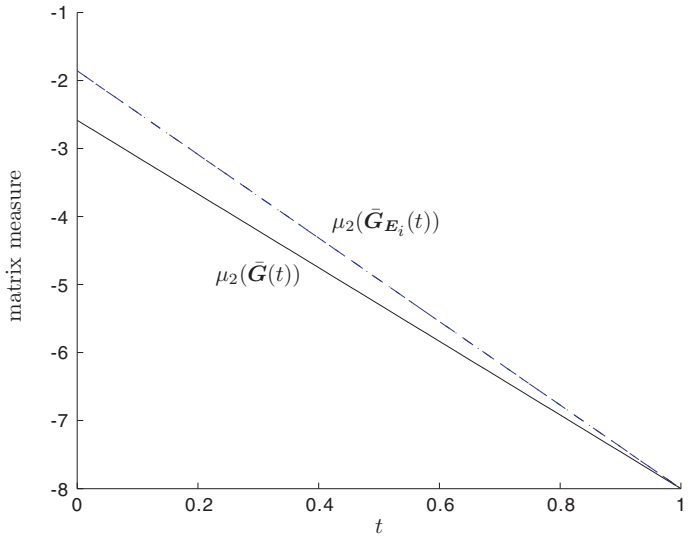

Figure 2.1: The matrix measures of $\bar{\boldsymbol{G}}(t)$ and $\bar{\boldsymbol{G}}_{\boldsymbol{E}_i}(t)$, $i = 1, 2$, with $\boldsymbol{G}$ being given in (2.33), $m = 8$, $K = 2$, and $p(t) = t$, are, respectively, represented by the solid line and the dotted lines above. Lines for $\bar{\boldsymbol{G}}_{\boldsymbol{E}_i}(t)$, $i = 1, 2$ are coincided since $\boldsymbol{G}(t)$ is circular for all t.

and if $m = 2$,

$$\boldsymbol{G}_\beta^{(2)} = \begin{pmatrix} -1-\beta & 1+\beta \\ 1+\beta & -1-\beta \end{pmatrix}.$$

For such $\boldsymbol{G}$, $\mu_2(\bar{\boldsymbol{G}}) = \lambda_2(\boldsymbol{G}) < 0$. However, $\lambda_2(\boldsymbol{G})$ would move closer to the origin as the number of nodes increases. As a result, synchronization of the network is more difficult to be realized as the number m of nodes increases. In [52,98], a wavelet transformation method is proposed to alter the connectivity topology of the network. In doing so, $\lambda_2(\boldsymbol{G}(t)) = \lambda_2(p(t))$ becomes a quantity depending on wavelet parameter $p(t)$. By choosing suitable $p(t)$, which is a wavelet transformation method [52,98] applied to the coupling matrix $\boldsymbol{G}_\beta^{(m)}$, one would expect that $\lambda_2(p(t))$ will move away from the origin regardless the number of the nodes. Under such a reconstruction, the resulting coupling matrix $\boldsymbol{G}(t)$ is of the following form

$$\boldsymbol{G}(t) = \boldsymbol{G}_\beta^{(m)} + p(t)(\boldsymbol{G}_\beta^{(\frac{m}{k})} \otimes \bar{\boldsymbol{e}}\bar{\boldsymbol{e}}^T), \tag{2.35}$$

where $\bar{\boldsymbol{e}} = (1, \ldots, 1)^T \in \mathbb{R}^k$. Here we assume $p(t) \geq 0$ and $k = 2^l$ for some $l \in \mathbb{N}$, and $m = Nk$ for some $N \in \mathbb{N} - \{1\}$. Since the reconstructed matrix $\boldsymbol{G}(t)$ is symmetric,

$\mu_2(\bar{\boldsymbol{G}}(t)) = \lambda_2(\boldsymbol{G}(t)) < 0$. The matrix measures $\mu_2(\bar{\boldsymbol{G}}(t))$ and $\mu_2(\bar{\boldsymbol{G}}_{\boldsymbol{E}_i}(t))$, $i = 1, 2$, with $m = 8$, $\beta = \frac{1}{2}$, $l = 1$, and $p(t) = t$, $t \in [0, 1]$ are recorded in Figure 2.2.

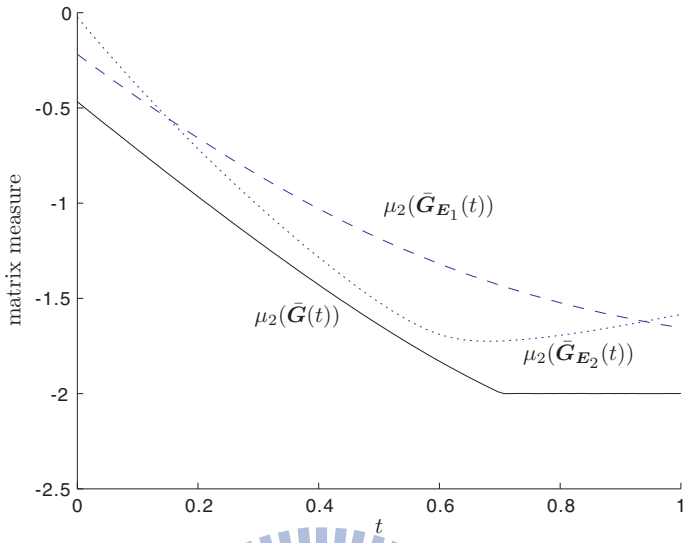

Figure 2.2: The matrix measures of $\bar{\boldsymbol{G}}(t)$ and $\bar{\boldsymbol{G}}_{\boldsymbol{E}_i}(t)$, $i = 1, 2$, with $\boldsymbol{G}$ given in (2.35), $m = 8$, $\beta = \frac{1}{2}$, $l = 1$, and $p(t) = t$, are, respectively, represented by the solid line and the dotted lines above.

Example 3. Let $\boldsymbol{G}(t) = \text{circ}(-2, 2, \overbrace{0, \ldots, 0}^{m})$, a circulant matrix. Since $\boldsymbol{G}(t)$ is a node-balancing matrix, $\mu_2(\bar{\boldsymbol{G}}(t)) = \lambda_2(\boldsymbol{G}(t)) < 0$. Note that the values of $\mu_2(\bar{\boldsymbol{G}}_{\boldsymbol{E}_i})$, $i = 1, 2$, are positive provided that $m > 5$ (see Table 2.2).

m	4	5	6	7	8	9
$\boldsymbol{E}_1$	-0.83	-0.17	0.24	0.54	0.78	0.98
$\boldsymbol{E}_2$	-0.83	-0.17	0.24	0.54	0.78	0.98

Table 2.2: The table gives the matrix measures of $\bar{\boldsymbol{G}}_{\boldsymbol{E}_i}$, $i = 1, 2$, with various size of $\boldsymbol{G}$, which is given in Example 3.

Proposition 2.3.2. *Let* $\boldsymbol{E} = (\boldsymbol{e}_1, \ldots, \boldsymbol{e}_{m-1})^T \in \mathfrak{O}$. *If, in addition,* $\{\boldsymbol{e}_i\}_{i=1}^{m-1}$ *are pairwise* $\boldsymbol{G}(t)-$*conjugate, i.e.,* $\boldsymbol{e}_i^T \boldsymbol{G}(t) \boldsymbol{e}_j = 0$, $\forall 1 \leq i \neq j \leq m-1$, *then* $\bar{\boldsymbol{G}}(t)$ *is a*

diagonal matrix. Moreover,

$$\mu_2(\bar{\boldsymbol{G}}(t)) = \lambda_2(\boldsymbol{G}(t)), \tag{2.36}$$

whenever all eigenvalues of $\boldsymbol{G}(t)$ *are nonpositive.*

Proof. Note that $\bar{\boldsymbol{G}}(t) = \boldsymbol{E}\boldsymbol{G}(t)\boldsymbol{E}^T = (\boldsymbol{e}_i^T\boldsymbol{G}(t)\boldsymbol{e}_j)$. Hence, $\bar{\boldsymbol{G}}(t)$ is a diagonal matrix. Therefore, the assertion in (2.36) holds as asserted. □

Example 4. ([17]) Let $\boldsymbol{G}(t)$ describe a star-typed coupled network of the form

$$\boldsymbol{G}(t) = \begin{pmatrix} -d_1(t) & & & d_1(t) \\ & \ddots & & \vdots \\ & & -d_1(t) & d_1(t) \\ 1 & \cdots & 1 & -(m-1) \end{pmatrix}_{m\times m.} \tag{2.37}$$

Here $d_1(t)$ is a real number. We next show that a set $\{\boldsymbol{e}_i\}_{i=1}^{m-1}$ of column vectors can be chosen so that $\boldsymbol{E} = (\boldsymbol{e}_i, \ldots, \boldsymbol{e}_{m-1}) \in \mathfrak{O}$ and that $\{\boldsymbol{e}_i\}_{i=1}^{m-1}$ are pairwise $\boldsymbol{G}(t)$-conjugate. Define $\alpha_i = (i(i+1))^{-1/2}$, $i = 1, \ldots, m-1$. Let

$$\boldsymbol{e}_i^T = (\overbrace{\alpha_i, \ldots, \alpha_i}^{i}, -i\alpha_i, \overbrace{0, \ldots, 0}^{m-i-1})$$

for all $i = 1, \ldots m-1$. Then $\boldsymbol{e}_i$, $i = 1, \ldots, m-1$ are orthonormal vectors. Moreover, they are also $\boldsymbol{G}(t)$-conjugate. To see this, we first note that $d_1(t)$ is an eigenvalue of $\boldsymbol{G}(t)$ and its associated eigenvectors are $\boldsymbol{e}_i$, $i = 1, \ldots, m-2$. Therefore, $\boldsymbol{e}_i^T\boldsymbol{G}(t)\boldsymbol{e}_j = 0$ for all $1 \le i \ne j \le m-2$. Some direct computation would yield that $\boldsymbol{e}_i^T\boldsymbol{G}(t)\boldsymbol{e}_{m-1} = 0$ for $i = 1, \ldots, m-2$ and that $\boldsymbol{e}_{m-1}^T\boldsymbol{G}(t)\boldsymbol{e}_{m-1} = -d_1(t) - (m-1)$. By Proposition 2.3.2, we have that

$$\mu_2(\bar{\boldsymbol{G}}_{\boldsymbol{E}}(t)) = \max\{-d_1(t), -d_1(t) - (m-1)\} = -d_1(t). \tag{2.38}$$

The matrix measures $\mu_2(\bar{\boldsymbol{G}}(t))$ and $\mu_2(\bar{\boldsymbol{G}}_{\boldsymbol{E}_i}(t))$, $i = 1, 2$, with $m = 8$ and $d_1(t) = t$, $t \in [0, 1]$ are demonstrated in Figure 2.3.

The remainder of the subsection is to address the system with even more complex topology.

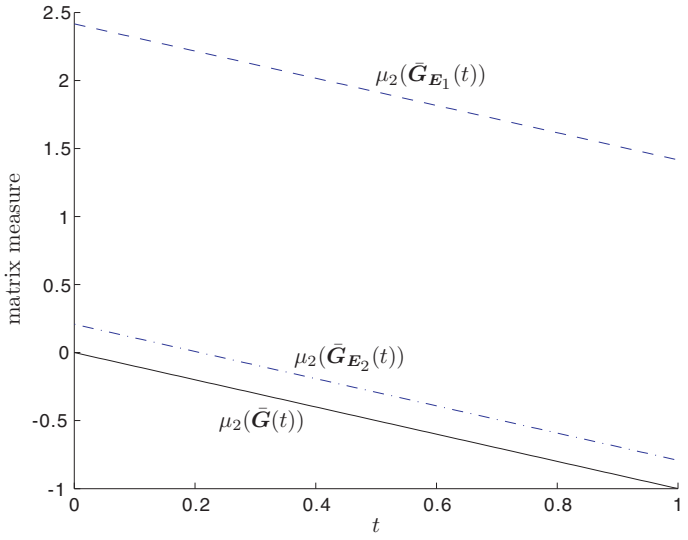

Figure 2.3: The matrix measures of $\bar{\boldsymbol{G}}(t)$ and $\bar{\boldsymbol{G}}_{\boldsymbol{E}_i}(t)$, $i = 1, 2$, with $\boldsymbol{G}$ being given in (2.37), $m = 8$, and $d_1(t) = t$, are, respectively, represented by the solid line and the dotted lines above.

Proposition 2.3.3. *Let $\boldsymbol{G}(t) = \boldsymbol{O}(t) + \boldsymbol{P}(t)$ with $\boldsymbol{O}(t)$ and $\boldsymbol{P}(t)$ having all its row sums zero. Suppose further that $\boldsymbol{P}(t)$ is node-balancing. Then*

$$\mu_2(\bar{\boldsymbol{G}}(t)) \leq \mu_2(\bar{\boldsymbol{O}}(t)) + \lambda_2\left(\frac{\boldsymbol{P}(t) + \boldsymbol{P}(t)^T}{2}\right),$$

whenever all eigenvalues of $\boldsymbol{P}(t) + \boldsymbol{P}(t)^T$ are nonpositive.

Proof. Noting that $\bar{\boldsymbol{G}}(t) = \boldsymbol{E}\boldsymbol{G}(t)\boldsymbol{E}^T = \bar{\boldsymbol{O}}(t) + \boldsymbol{E}\boldsymbol{P}(t)\boldsymbol{E}^T$, we easily conclude that the above inequality holds as asserted. □

Example 5. ([2]) Consider the outer coupling matrix $\boldsymbol{G}(t)$ to be of the random type. Specifically, $\boldsymbol{G}(t)$ is of the form:

$$\boldsymbol{G}(t) = \mathrm{circ}(-2K, \overbrace{1, \ldots, 1}^{K}, \overbrace{0, \ldots, 0}^{m-2K-1}, \overbrace{1, \ldots, 1}^{K}) + \boldsymbol{P}(t) =: \boldsymbol{O} + \boldsymbol{P}(t), \tag{2.39}$$

where $\boldsymbol{P}(t) =: (p_{ij}(t))$ is a symmetric matrix with all its row sums being zero, and satisfies $p_{ij}(t) \equiv 0$ for (i, j) with $i - j \bmod m \leq K$ or $j - i \bmod m \leq K$, and $p_{ij}(t) =$

$S_{ij}(q)$ for $(q-1)\tau \leq t < q\tau$ for all remaining pairs (i,j) with $i \neq j$. Here each of $S_{ij}(q)$ is a random variable that takes the value 1 with probability p and 0 with probability$1-p$.

The random variables $S_{ij}(q)$ are assumed to be all independent. To each realization ω of this stochastic process $S(1)$, $S(2)$, ..., where $S(q) = \{S_{ij}(q) : i-j \bmod m \leq K$ or $j-i \bmod m \leq K\}$, i.e., to each switching sequence ω, there corresponds a time-varying system described by Equation (1.1b).

Since $\boldsymbol{P}(t)$ is symmetric, by Proposition 2.3.3,

$$\mu_2(\bar{\boldsymbol{G}}(t)) \leq \mu_2(\bar{\boldsymbol{O}}) + \lambda_2(\boldsymbol{P}(t)) \leq \mu_2(\bar{\boldsymbol{O}}) = \lambda_2(\boldsymbol{O}) < 0.$$

Let $\boldsymbol{G}(t) \equiv \boldsymbol{G}$. Generally speaking, $\inf_{\bar{\boldsymbol{E}}\in\mathfrak{C}} \mu_2(\bar{\boldsymbol{G}}_{\bar{\boldsymbol{E}}}) \neq \mu_2(\bar{\boldsymbol{G}}_{\boldsymbol{E}})$ for any $\boldsymbol{E} \in \mathfrak{O}$. Nevertheless, $\mu_2(\boldsymbol{G}_{\boldsymbol{E}})$ produces a good upper bound of $\inf_{\bar{\boldsymbol{E}}\in\mathfrak{C}} \mu_2(\bar{\boldsymbol{G}}_{\bar{\boldsymbol{E}}})$.

To support the observation, we conclude this section by providing some additional network topologies where the matrix measure of its corresponding $\bar{\boldsymbol{G}}_{\boldsymbol{E}}(t)$, $\boldsymbol{E} \in \mathfrak{O}$ is smaller than that of $\bar{\boldsymbol{G}}_{\boldsymbol{E}_i}$, $i = 1, 2$. As a matter of fact, $\mu_2(\bar{\boldsymbol{G}}_{\boldsymbol{E}_i})$, $i = 1, 2$, switch signs as the number of nodes increases. In contrast, $\mu_2(\bar{\boldsymbol{G}}_{\boldsymbol{E}})$ mostly remains negative as the size of the system grows.

Example 6. Consider a *generalized wheel-typed coupled network* of the form as illustrated in Figure 2.4(a). The inner nodes have the strong all-to-all connections. The outer nodes are only directly connected with their nearest neighbors. The communications between the inner and outer nodes are through one way going from each inside node to its nearest outside node. Specifically, such a network can be written as the following.

$$\boldsymbol{G}(t) \equiv \begin{pmatrix} \boldsymbol{G}_1 & \boldsymbol{G}_2 \\ \boldsymbol{G}_3 & \boldsymbol{G}_4 \end{pmatrix}_{m\times m,} \tag{2.40}$$

where

$$\boldsymbol{G}_1 = \begin{pmatrix} -(\frac{m}{2}-1) & 1 & \cdots & 1 \\ 1 & \ddots & \ddots & \vdots \\ \vdots & \ddots & \ddots & 1 \\ 1 & \cdots & 1 & -(\frac{m}{2}-1) \end{pmatrix}_{\frac{m}{2}\times\frac{m}{2}}$$

corresponding to the all-to-all coupling, $\boldsymbol{G}_2 = \boldsymbol{0}$, $\boldsymbol{G}_3 = 0.1\boldsymbol{I}$, and $\boldsymbol{G}_4 = \boldsymbol{G}_1^{\left(\frac{m}{2}\right)} - 0.1\boldsymbol{I}$. Here $\boldsymbol{G}_1^{\left(\frac{m}{2}\right)}$ is the diffusive matrix with periodic boundary conditions and of size $\frac{m}{2}\times\frac{m}{2}$. The numerical computation suggests that the matrix measures of $\bar{\boldsymbol{G}}_{\boldsymbol{E}_i}$, $i = 1, 2$, are positive provided that $m \geq 4$ while that of $\bar{\boldsymbol{G}}_{\boldsymbol{E}}$, $\boldsymbol{E} \in \mathfrak{O}$ remains negative (see Table 2.3).

m	4	6	8	10	5000
$\boldsymbol{E}_1$	0.11	0.32	0.53	0.74	517.47
$\boldsymbol{E}_2$	0.23	0.56	0.96	1.44	34843.01
$\boldsymbol{E}$	-0.1	-0.1	-0.1	-0.1	-0.1

Table 2.3: The table gives the matrix measures of $\bar{\boldsymbol{G}}_{\boldsymbol{E}_i}$, $i = 1, 2$, and $\bar{\boldsymbol{G}}_{\boldsymbol{E}}$, $\boldsymbol{E} \in \mathfrak{O}$ with various size of $\boldsymbol{G}$, which is given in (2.40).

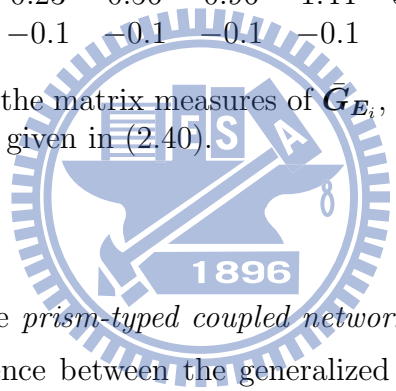

Example 7. Consider the *prism-typed coupled network* of the form as illustrated in Figure 2.4(b). The difference between the generalized wheel-typed network and the one considered here lies only on how the inner nodes communicate with each other (see Figure 2.4). Specifically, such a network can be written as the following.

$$\boldsymbol{G}(t) \equiv \begin{pmatrix} \boldsymbol{G}_1 & \boldsymbol{G}_2 \\ \boldsymbol{G}_3 & \boldsymbol{G}_4 \end{pmatrix}_{m\times m,}$$

where $\boldsymbol{G}_1 = \boldsymbol{G}_1^{\left(\frac{m}{2}\right)}$, $\boldsymbol{G}_2 = \boldsymbol{0}$, $\boldsymbol{G}_3 = 0.1\boldsymbol{I}$, and $\boldsymbol{G}_4 = \boldsymbol{G}_1^{\left(\frac{m}{2}\right)} - 0.1\boldsymbol{I}$. The numerical computation suggests (see Table 2.4) that the matrix measures of $\bar{\boldsymbol{G}}_{\boldsymbol{E}_i}$, $i = 1, 2$, are positive provided that $m \geq 4$, while that of $\bar{\boldsymbol{G}}_{\boldsymbol{E}}$, $\boldsymbol{E} \in \mathfrak{O}$ stays negative until $m = 86$. The example demonstrates that a coordinate transformation $\boldsymbol{E}$, $\boldsymbol{E} \in \mathfrak{O}$, is indeed a good candidate among all coordinate transformations.

m	4	6	8	86	88
$\boldsymbol{E}_1$	0.34	0.32	0.35	4.65	4.72
$\boldsymbol{E}_2$	0.34	0.56	0.73	4.79	4.86
$\boldsymbol{E}$	-0.1	-0.1	-0.1	-0.0006	0.0004

Table 2.4: The table gives the matrix measures of $\bar{\boldsymbol{G}}_{\boldsymbol{E}_i}$, $i = 1, 2$, and $\bar{\boldsymbol{G}}_{\boldsymbol{E}}$, $\boldsymbol{E} \in \mathfrak{D}$ with various size of $\boldsymbol{G}$, which is given in Example 7.

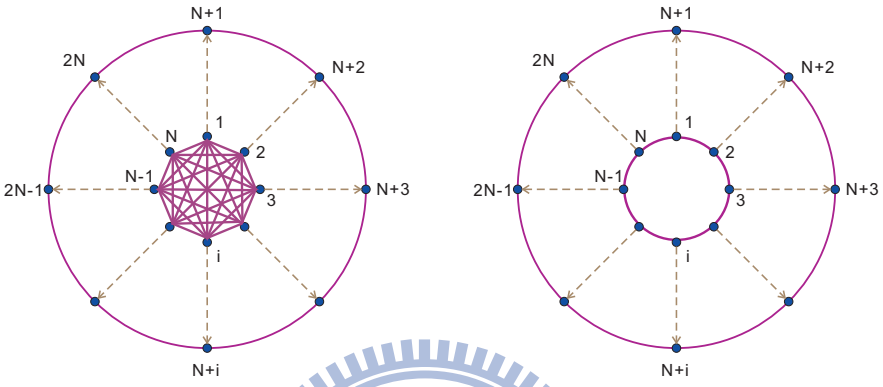

Figure 2.4: Coupling Topologies: (a) Generalized wheel-typed coupled network with $m = 2N$, and (b) Prism-typed coupled network with $m = 2N$. Networks (a) and (b) appear in Examples 6 and 7, respectively.

2.3.2 Synchronization Criteria

In the section, we turn our attention back to the dynamics of (2.29a), and analyze the stability of the origin of the system. Let $\bar{\boldsymbol{y}}$, $\bar{\boldsymbol{y}}_c$, and $\bar{\boldsymbol{y}}_u$ be defined as in (2.13). Then, like (2.16a) , Equation (2.29a) can be rewritten as in the form

$$\begin{pmatrix} \dot{\bar{\boldsymbol{y}}}_c \\ \dot{\bar{\boldsymbol{y}}}_u \end{pmatrix} = \begin{pmatrix} d(\boldsymbol{I}_k \otimes \bar{\boldsymbol{G}}(t)) & \boldsymbol{0} \\ \boldsymbol{0} & \boldsymbol{U}(t) \end{pmatrix} \begin{pmatrix} \bar{\boldsymbol{y}}_c \\ \bar{\boldsymbol{y}}_u \end{pmatrix} + \begin{pmatrix} \bar{\boldsymbol{F}}_c(\bar{\boldsymbol{y}}, t) \\ \bar{\boldsymbol{R}}_u(\bar{\boldsymbol{y}}, t) \end{pmatrix}, \tag{2.41}$$

where $\bar{\boldsymbol{R}}_u(\bar{\boldsymbol{y}}, t) =: \bar{\boldsymbol{F}}_u(\bar{\boldsymbol{y}}, t) - \boldsymbol{U}(t)\bar{\boldsymbol{y}}_u$ for some matrix $\boldsymbol{U}(t)$. Now we impose the conditions for coupling matrices $\boldsymbol{G}$ and $\boldsymbol{D}$.

(i) $\lambda = 0$ is a simple eigenvalue of $\boldsymbol{G}(t)$, $\forall\, t \geq 0$ and

$$\boldsymbol{e} = \tfrac{1}{\sqrt{m}}(1, 1, \ldots, 1)^T_{1\times m} \text{ is its corresponding eigenvector;} \tag{2.42a}$$

(ii) There is some $\lambda > 0$ such that $\mu_2(\bar{\boldsymbol{G}}(t)) \leq -\lambda, \quad \forall t \geq 0.$ (2.42b)

(iii) Coupling matrix $\boldsymbol{D}$ is of the form

$$\boldsymbol{D} = \begin{pmatrix} \boldsymbol{I}_k & \boldsymbol{0} \\ \boldsymbol{0} & \boldsymbol{0} \end{pmatrix}_{n\times n.} \tag{2.42c}$$

We are now in a position to state our first main theorem in the time-varying coupled system.

Theorem 2.3.3. *Let coupling matrices $\boldsymbol{G}(t)$ and $\boldsymbol{D}$ satisfy* (2.42). *Suppose that $\bar{\boldsymbol{F}}$, given in* (2.29a) *or* (2.41), *satisfies* (2.14a), (2.14c), *and that* (2.14d), *and system* (2.29a) *is bounded dissipative with respect to α. Then $\lim_{t\to\infty} \bar{\boldsymbol{y}}(t) = \boldsymbol{0}$ for any initial value provided that the coupling strength d satisfies the following inequality*

$$d > \frac{b_1}{\lambda}\left(1 + \frac{b_2^2}{\gamma^2}\right)^{\frac{1}{2}}. \tag{2.43}$$

Proof. For any initial condition $\bar{\boldsymbol{y}}(0)$, there is $t_0 > 0$ such that $\|\bar{\boldsymbol{y}}(t)\| \leq \alpha$ for all $t \geq t_0$. Applying the matrix measure inequality (2.1) and hypotheses (2.14a), (2.42b) on $\bar{\boldsymbol{y}}_c$, for any $t \geq t_0$, we have that

$$\begin{aligned} \|\bar{\boldsymbol{y}}_c(t)\| &\leq \|\bar{\boldsymbol{y}}_c(t_0)\| e^{-\lambda d(t-t_0)} + \frac{b_1\alpha}{\lambda d} \\ &\leq (e^{-\lambda d(t-t_0)} + \frac{b_1}{\lambda d})\alpha \\ &=: (e^{-\lambda d(t-t_0)} + c_0\frac{1}{d})\alpha. \end{aligned}$$

Let $\delta > 1$. We see that

$$\|\bar{\boldsymbol{y}}_c(t)\| \leq \frac{\alpha}{d} c_0 \delta, \tag{2.44a}$$

whenever $t \geq t_{0,1}$ for some $t_{0,1} > t_0$. Similarly, applying inequality (2.1) and hypotheses (2.14c), (2.14d) on $\bar{\boldsymbol{y}}_{u1}$,

$$\|\bar{\boldsymbol{y}}_{u1}(t)\| \leq \frac{\alpha}{d}\left(\frac{b_2}{\gamma} c_0\right)\delta^2 =: \frac{\alpha}{d} c_1 \delta^2, \tag{2.44b}$$

whenever $t \geq t_{1,1}$ for some $t_{1,1} > t_{0,1}$. Inductively, we have

$$\|\bar{\boldsymbol{y}}_{uj}(t)\| \leq \frac{\alpha}{d} c_j \delta^{j+1}, \tag{2.44c}$$

whenever $t \geq t_{j,1}$, for all $j = 2, \ldots, l$. Here $c_j = \frac{b_2}{\gamma}\sqrt{\sum_{i=0}^{j-1} c_i^2}$. Letting $t_1 = t_{l,1}$ and summing up (2.44a) to (2.44c), we get

$$\|\bar{\boldsymbol{y}}(t)\| \leq \frac{\alpha}{d}\left(1 + \frac{b_2^2}{\gamma^2}\right)^{\frac{l}{2}} \frac{b_1}{\lambda}\delta^{l+1} =: h\alpha,$$

whenever $t > t_1$. Choosing $d > \left(1 + \frac{b_2^2}{\gamma^2}\right)^{\frac{l}{2}} \frac{b_1}{\lambda}\delta^{l+1}$, we see that the contraction factor h is strictly less than 1, and $\|\bar{\boldsymbol{y}}(t)\|$ contracts to zero as time progresses. Since $\delta > 1$ can be made arbitrarily close to 1. Consequently, if d is chosen as assumed, then h can still be made to be less than 1. The assertion of the theorem now follows. □

In the following, we drive another set of hypotheses to replace that listed in Theorem 2.3.3 to get the easily checkable criteria for the synchronization in coupled system (2.26).

The following notation is needed. Let $\boldsymbol{u} = (u_1, \ldots, u_i, u_{i+1}, \ldots, u_j, \ldots, u_n)^T$. Denote by $[\boldsymbol{u}]_i^j = (u_i, u_{i+1}, \ldots, u_j)^T$.Write the difference of $\boldsymbol{f}(\cdot, t)$ at $\boldsymbol{u}$ and $\boldsymbol{v}$ in the form

$$\begin{aligned}\boldsymbol{f}(\boldsymbol{u}, t) - \boldsymbol{f}(\boldsymbol{v}, t) &= \begin{pmatrix} f_1(\boldsymbol{u}, t) - f_1(\boldsymbol{v}, t) \\ \vdots \\ f_n(\boldsymbol{u}, t) - f_n(\boldsymbol{v}, t) \end{pmatrix} =: \begin{pmatrix} \boldsymbol{f}_c(\boldsymbol{u}, t) - \boldsymbol{f}_c(\boldsymbol{v}, t) \\ \boldsymbol{f}_u(\boldsymbol{u}, t) - \boldsymbol{f}_u(\boldsymbol{v}, t) \end{pmatrix} \\ &=: \begin{pmatrix} \boldsymbol{f}_c(\boldsymbol{u}, t) - \boldsymbol{f}_c(\boldsymbol{v}, t) \\ \boldsymbol{Q}(\boldsymbol{v}, t)\,[\boldsymbol{u} - \boldsymbol{v}]_{k+1}^n + \boldsymbol{r}(\boldsymbol{u}, \boldsymbol{v}, t) \end{pmatrix}, \end{aligned} \tag{2.45}$$

where $\boldsymbol{f}_c(\cdot, t) \in \mathbb{R}^k$, $\boldsymbol{f}_u(\cdot, t) \in \mathbb{R}^{n-k}$, and matrix $\boldsymbol{Q}(\boldsymbol{v}, t)$ is of the size $(n-k) \times (n-k)$. Since $\boldsymbol{r}(\boldsymbol{u}, \boldsymbol{v}, t)$ could depend on all components of $\boldsymbol{u}$ and $\boldsymbol{v}$, such a decomposition in (2.45) can always be achieved.

Proposition 2.3.4. *Suppose $f_i(\cdot, t)$, $i = 1, \ldots, k$ are uniformly Lipschitz, i.e., there exists a positive constant $r > 0$ such that*

$$|f_i(\boldsymbol{u}, t) - f_i(\boldsymbol{v}, t)| \leq r\|\boldsymbol{u} - \boldsymbol{v}\| \tag{2.46}$$

for all $i = 1, \ldots, k$. *Then the inequality in* (2.14a) *is satisfied with* $b_1 = r\sqrt{k}cond(\boldsymbol{E}_1\boldsymbol{E}^T)$. *Here* $\boldsymbol{E}_1$ *is given as in* (2.30) *and* $cond(\boldsymbol{E}_1\boldsymbol{E}^T) = \|\boldsymbol{E}_1\boldsymbol{E}^T\|\,\|(\boldsymbol{E}_1\boldsymbol{E}^T)^{-1}\|$ *is the condition number of* $\boldsymbol{E}_1\boldsymbol{E}^T$.

Proof. Note first that $\boldsymbol{E}_1 = \boldsymbol{E}_1\boldsymbol{E}^T\boldsymbol{E}$ and $\boldsymbol{E} = (\boldsymbol{E}_1\boldsymbol{E}^T)^{-1}\boldsymbol{E}_1$. Now,

$$\begin{aligned}\|\bar{\boldsymbol{F}}_c(\bar{\boldsymbol{y}}, t)\| &= \| \begin{pmatrix} \boldsymbol{E}\tilde{\boldsymbol{f}}_1(\tilde{\boldsymbol{x}}, t) \\ \vdots \\ \boldsymbol{E}\tilde{\boldsymbol{f}}_k(\tilde{\boldsymbol{x}}, t) \end{pmatrix} \| = \|(\boldsymbol{I}_k \otimes (\boldsymbol{E}_1\boldsymbol{E}^T)^{-1}) \begin{pmatrix} \boldsymbol{E}_1\tilde{\boldsymbol{f}}_1(\tilde{\boldsymbol{x}}, t) \\ \vdots \\ \boldsymbol{E}_1\tilde{\boldsymbol{f}}_k(\tilde{\boldsymbol{x}}, t) \end{pmatrix} \| \\ &\le \|(\boldsymbol{E}_1\boldsymbol{E}^T)^{-1}\| \, \| \begin{pmatrix} \boldsymbol{E}_1\tilde{\boldsymbol{f}}_1(\tilde{\boldsymbol{x}}, t) \\ \vdots \\ \boldsymbol{E}_1\tilde{\boldsymbol{f}}_k(\tilde{\boldsymbol{x}}, t) \end{pmatrix} \|.\end{aligned}$$

Since

$$\|\boldsymbol{E}_1\tilde{\boldsymbol{f}}_i(\tilde{\boldsymbol{x}}, t)\|^2 = \| \begin{pmatrix} f_i(\boldsymbol{x}_1, t) - f_i(\boldsymbol{x}_2, t) \\ \vdots \\ f_i(\boldsymbol{x}_1, t) - f_i(\boldsymbol{x}_m, t) \end{pmatrix} \|^2 \le r^2 \| \begin{pmatrix} \boldsymbol{x}_1 - \boldsymbol{x}_2 \\ \vdots \\ \boldsymbol{x}_1 - \boldsymbol{x}_m \end{pmatrix} \|^2$$

for all $i = 1, \ldots, k$, we have that

$$\begin{aligned}\|\bar{\boldsymbol{F}}_c(\bar{\boldsymbol{y}}, t)\| &\le \sqrt{kr}\|(\boldsymbol{E}_1\boldsymbol{E}^T)^{-1}\| \, \| \begin{pmatrix} \boldsymbol{x}_1 - \boldsymbol{x}_2 \\ \vdots \\ \boldsymbol{x}_1 - \boldsymbol{x}_m \end{pmatrix} \| \\ &= \sqrt{kr}\|(\boldsymbol{E}_1\boldsymbol{E}^T)^{-1}\| \, \|(\boldsymbol{E}_1 \otimes \boldsymbol{I}_n) \begin{pmatrix} \boldsymbol{x}_1 \\ \vdots \\ \boldsymbol{x}_m \end{pmatrix} \| \\ &= \sqrt{kr}\|(\boldsymbol{E}_1\boldsymbol{E}^T)^{-1}\| \, \|(\boldsymbol{E}_1\boldsymbol{E}^T \otimes \boldsymbol{I}_n)(\boldsymbol{E} \otimes \boldsymbol{I}_n)\boldsymbol{x}\| \\ &\le \sqrt{kr}\, \mathrm{cond}(\boldsymbol{E}_1\boldsymbol{E}^T)\, \|\bar{\boldsymbol{y}}\|. \end{aligned} \tag{2.47}$$

The proof of the proposition is completed. □

We next turn our attention to the structure of the vector field of the uncoupled parts.

Proposition 2.3.5. *(i) Suppose matrix* $\boldsymbol{Q}(\boldsymbol{v}, t)$ *can be written as the block diagonal form*

$$\boldsymbol{Q}(\boldsymbol{v}, t) = diag(\boldsymbol{Q}_1(\boldsymbol{v}, t), \ldots, \boldsymbol{Q}_l(\boldsymbol{v}, t)),$$

where the size of matrices $\boldsymbol{Q}_j(\boldsymbol{v},t)$ *are* $k_j \times k_j$, $\forall j = 1,\dots l$ *and indexes* l, k_j *are given as in* (2.14c). *Moreover, there is some* $\gamma > 0$ *such that*

$$\mu_2(\boldsymbol{Q}_j(\boldsymbol{v},t)) \le -\gamma. \tag{2.48a}$$

Here γ *is independent of* $\boldsymbol{v}, t$. *Then the inequality in* (2.14c) *is fulfilled.*
(ii) Denoted by $s_1 = k$ *and* $s_j = k + \sum_{i=1}^{j-1} k_i$, $j = 2,\dots,l$, *where* k_i *and* l *are defined in* (2.14c). *Let* $\boldsymbol{E} = (e_{i,j})_{(m-1)\times m}$. *Suppose, for any* $1 \le j \le l$, *there is* $\delta > 0$ *such that*

$$\|[\boldsymbol{r}(\boldsymbol{u},\boldsymbol{v},t)]_{s_j+1}^{s_j+k_j}\| \le \delta \|[\boldsymbol{u}-\boldsymbol{v}]_1^{s_j}\|. \tag{2.48b}$$

Then the inequality in (2.14d) *is satisfied with* $b_2 = \delta\|\tilde{\boldsymbol{E}}\|\|\boldsymbol{E}_1\boldsymbol{E}^T\|$. *Here*

$$\tilde{\boldsymbol{E}} = (e_{i,j+1}) \in \mathbb{R}^{(m-1)\times(m-1)}, \quad 1 \le i,j \le m-1. \tag{2.48c}$$

Proof. Write $\bar{\boldsymbol{F}}_u(\bar{\boldsymbol{y}},t)$ as $(\boldsymbol{F}_{u1}(\bar{\boldsymbol{y}},t),\dots,\boldsymbol{F}_{ul}(\bar{\boldsymbol{y}},t))^T$, which is in consistence with the block diagonal form of $\boldsymbol{U}(t)$. Now, for $1 \le j \le l$,

$$\boldsymbol{F}_{uj}(\bar{\boldsymbol{y}},t) = \begin{pmatrix} \boldsymbol{E}\tilde{\boldsymbol{f}}_{s_j+1}(\tilde{\boldsymbol{x}},t) \\ \vdots \\ \boldsymbol{E}\tilde{\boldsymbol{f}}_{s_j+k_j}(\tilde{\boldsymbol{x}},t) \end{pmatrix} = \begin{pmatrix} \sum_{k=1}^m e_{1,k} f_{s_j+1}(\boldsymbol{x}_k,t) \\ \wr \\ \sum_{k=1}^m e_{m-1,k} f_{s_j+1}(\boldsymbol{x}_k,t) \\ \vdots \\ \sum_{k=1}^m e_{1,k} f_{s_j+k_j}(\boldsymbol{x}_k,t) \\ \wr \\ \sum_{k=1}^m e_{m-1,k} f_{s_j+k_j}(\boldsymbol{x}_k,t) \end{pmatrix}$$

$$= \boldsymbol{P} \begin{pmatrix} \sum_{k=1}^m e_{1,k} f_{s_j+1}(\boldsymbol{x}_k,t) \\ \wr \\ \sum_{k=1}^m e_{1,k} f_{s_j+k_j}(\boldsymbol{x}_k,t) \\ \vdots \\ \sum_{k=1}^m e_{m-1,k} f_{s_j+1}(\boldsymbol{x}_k,t) \\ \wr \\ \sum_{k=1}^m e_{m-1,k} f_{s_j+k_j}(\boldsymbol{x}_k,t) \end{pmatrix} =: \boldsymbol{P}\boldsymbol{h}.$$

Here $\boldsymbol{P}$ is a permutation matrix. That is, we exchange a certain rows of $\bar{\boldsymbol{F}}_{uj}(\bar{\boldsymbol{y}},t)$ to obtain $\boldsymbol{F}$. Using the fact that the row sums of $\boldsymbol{E}$ are all zeros, we have that for $1 \le i \le m-1$, $s_j + 1 \le l \le s_j + k_j$,

$$\sum_{k=1}^m e_{i,k} f_l(\boldsymbol{x}_k,t) = \sum_{k=2}^m e_{i,k}(f_l(\boldsymbol{x}_k,t) - f_l(\boldsymbol{x}_1,t)). \tag{2.49}$$

To save notations, $\forall i = 1\ldots, k_j$, we denote by $[\boldsymbol{r}_{s_j+i}(\boldsymbol{x}_l, \boldsymbol{x}_1, t)]_{l=2}^m$ the vector $(\boldsymbol{r}_{s_j+i}(\boldsymbol{x}_2, \boldsymbol{x}_1, t), \boldsymbol{r}_{s_j+i}(\boldsymbol{x}_3, \boldsymbol{x}_1, t), \ldots, \boldsymbol{r}_{s_j+i}(\boldsymbol{x}_m, \boldsymbol{x}_1, t))^T$.

Applying (2.45) and (2.48a)- (2.48c), we shall be able to rewrite $\boldsymbol{h}$ as

$$\begin{pmatrix} \sum_{k=2}^m e_{1,k}\boldsymbol{Q}_j(\boldsymbol{x}_1,t)[\boldsymbol{x}_k - \boldsymbol{x}_1]_{s_j+1}^{s_j+k_j} \\ \vdots \\ \sum_{k=2}^m e_{m-1,k}\boldsymbol{Q}_j(\boldsymbol{x}_1,t)[\boldsymbol{x}_k - \boldsymbol{x}_1]_{s_j+1}^{s_j+k_j} \end{pmatrix} + \begin{pmatrix} \sum_{k=2}^m e_{1,k}[\boldsymbol{r}(\boldsymbol{x}_k,\boldsymbol{x}_1,t)]_{s_j+1}^{s_j+k_j} \\ \vdots \\ \sum_{k=2}^m e_{m-1,k}[\boldsymbol{r}(\boldsymbol{x}_k,\boldsymbol{x}_1,t)]_{s_j+1}^{s_j+k_j} \end{pmatrix}$$

$$= \begin{pmatrix} \boldsymbol{Q}_j(\boldsymbol{x}_1,t)[\sum_{k=1}^m e_{1,k}\boldsymbol{x}_k]_{s_j+1}^{s_j+k_j} \\ \vdots \\ \boldsymbol{Q}_j(\boldsymbol{x}_1,t)[\sum_{k=1}^m e_{m-1,k}\boldsymbol{x}_k]_{s_j+1}^{s_j+k_j} \end{pmatrix} + \boldsymbol{P}^T \begin{pmatrix} \tilde{\boldsymbol{E}}[\boldsymbol{r}_{s_j+1}(\boldsymbol{x}_l,\boldsymbol{x}_1,t)]_{l=2}^m \\ \vdots \\ \tilde{\boldsymbol{E}}[\boldsymbol{r}_{s_j+k_j}(\boldsymbol{x}_l,\boldsymbol{x}_1,t)]_{l=2}^m \end{pmatrix}$$

$$= (\boldsymbol{I}_{m-1} \otimes \boldsymbol{Q}_j(\boldsymbol{x}_1,t))\boldsymbol{P}^T \begin{pmatrix} \boldsymbol{E}\tilde{\boldsymbol{x}}_{s_j+1} \\ \vdots \\ \boldsymbol{E}\tilde{\boldsymbol{x}}_{s_j+k_j} \end{pmatrix} + \boldsymbol{P}^T(\boldsymbol{I}_{k_j} \otimes \tilde{\boldsymbol{E}}) \begin{pmatrix} [\boldsymbol{r}_{s_j+1}(\boldsymbol{x}_l,\boldsymbol{x}_1,t)]_{l=2}^m \\ \vdots \\ [\boldsymbol{r}_{s_j+k_j}(\boldsymbol{x}_l,\boldsymbol{x}_1,t)]_{l=2}^m \end{pmatrix}$$

$$= (\boldsymbol{I}_{m-1} \otimes \boldsymbol{Q}_j(\boldsymbol{x}_1,t))\boldsymbol{P}^T\bar{\boldsymbol{y}}_{uj} + \boldsymbol{P}^T(\boldsymbol{I}_{k_j} \otimes \tilde{\boldsymbol{E}})\boldsymbol{P} \begin{pmatrix} [\boldsymbol{r}(\boldsymbol{x}_2,\boldsymbol{x}_1,t)]_{s_j+1}^{s_j+k_j} \\ \vdots \\ [\boldsymbol{r}(\boldsymbol{x}_m,\boldsymbol{x}_1,t)]_{s_j+1}^{s_j+k_j} \end{pmatrix}.$$

Therefore,

$$\boldsymbol{U}_j(t) = \boldsymbol{P}(\boldsymbol{I}_{m-1} \otimes \boldsymbol{Q}_j(\boldsymbol{x}_1,t))\boldsymbol{P}^T, \tag{2.50a}$$

and

$$\boldsymbol{R}_{uj}(\bar{\boldsymbol{y}},t) = (\boldsymbol{I}_{k_j} \otimes \tilde{\boldsymbol{E}})\boldsymbol{P} \begin{pmatrix} [\boldsymbol{r}(\boldsymbol{x}_2,\boldsymbol{x}_1,t)]_{s_j+1}^{s_j+k_j} \\ \vdots \\ [\boldsymbol{r}(\boldsymbol{x}_m,\boldsymbol{x}_1,t)]_{s_j+1}^{s_j+k_j} \end{pmatrix}. \tag{2.50b}$$

The first assertion of the position now follows from (2.50a), $\mu_2(\boldsymbol{U}_j(t)) = \mu_2(\boldsymbol{Q}_j(\boldsymbol{x}_1,t)) \leq -\gamma$. Upon using the similar techniques as those in establishing the inequality in (2.47), we conclude that (2.48a)- (2.48c) hold as asserted. □

Now, we are in the position to impose the hypotheses for synchronization. We remark that although these conditions are quite like those given in (2.22) and (2.24), to be self-contained and clear, we list corresponding the hypotheses herein.

(H1) System (1.1a) is bounded dissipative with respect to α.

(H2) Functions $f_i(\cdot,t)$, $i=1,\ldots,k$ in (1.1a) are uniformly Lipschitz in region B given in (H1). That is, there is a constant $r>0$ such that $|f_i(\boldsymbol{u},t)-f_i(\boldsymbol{v},t)|\le r\|\boldsymbol{u}-\boldsymbol{v}\|$, whenever t is sufficiently large, and $\boldsymbol{u},\boldsymbol{v}$ in B.

(H3) The matrix $\boldsymbol{Q}(\boldsymbol{v},t)$, which is given as in (2.45), is of block diagonal form, i.e., $\boldsymbol{Q}(\boldsymbol{v},t)=\mathrm{diag}(\boldsymbol{Q}_1(\boldsymbol{v},t),\cdots,\boldsymbol{Q}_l(\boldsymbol{v},t))$. Here the sizes of $\boldsymbol{Q}_j(\boldsymbol{v},t)$, $j=1,\ldots,l$, are $k_j\times k_j$. Moreover, there is some $\gamma>0$ such that matrix measures $\mu_2(\boldsymbol{Q}_j(\boldsymbol{v},t))\le -\gamma$, for all j, whenever t is sufficiently large, and $\boldsymbol{v}$ in B.

(H4) Denoted by $s_1=k$ and $s_j=k+\sum_{i=1}^{j-1}k_i$, $j=2,\ldots,l$, where k_i and l are defined in (H4). Suppose, for any $1\le j\le l$, there is a $\delta>0$ such that

$$\|[\boldsymbol{r}(\boldsymbol{u},\boldsymbol{v},t)]_{s_j+1}^{s_j+k_j}\|\le\delta\|[\boldsymbol{u}-\boldsymbol{v}]_1^{s_j}\|,$$

for t sufficiently large, and $\boldsymbol{u},\boldsymbol{v}$ in B. Here $[\boldsymbol{u}]_i^j$ is defined to be $(u_i,\ldots,u_j)^T$.

Remark 2.3.2. *Using the similar techniques as developed in the proof of Propositions 2.3.4 and 2.3.5, we may also conclude that the global theorems obtained in [17] may still be valid by using the coordinate transformation developed here in this paper. Consequently, the size limit problem of their approach can be removed.*

The main criterion for synchronization in the time-varying coupled system is now stated in the following. The proof of the main theorem follows directly from Theorem 2.3.3 and Propositions 2.3.4 and 2.3.5.

Theorem 2.3.4. *Let the coupling matrices $\boldsymbol{G}(t)$ and $\boldsymbol{D}$ satisfy* (2.42). *Suppose hypotheses (H1), (H2), (H3), and (H4) hold true. Then coupled system* (2.26) *achieves global synchronization whenever*

$$d>\frac{r\sqrt{k}\,cond(\boldsymbol{E}_1\boldsymbol{E}^T)}{\lambda}\left(1+\frac{\delta^2\|\tilde{\boldsymbol{E}}\|^2\|\boldsymbol{E}_1\boldsymbol{E}^T\|^2}{\gamma^2}\right)^{\frac{l}{2}} \tag{2.51}$$

where $\boldsymbol{E}$, $\boldsymbol{E}_1$, and $\tilde{\boldsymbol{E}}$ are given as in Theorem 2.3.1, (2.30), *and* (2.48c), *respectively.*

Remark 2.3.3. *The small price to pay by introducing the coordinate transformation $\boldsymbol{E}$ is that the lower bound, given as in the right hand side of* (2.51), *on the coupling strength d, is size dependent.*

Chapter 3

Applications for Model I

3.1 Synchronization in coupled Lorenz and coupled Duffing systems

To see the effectiveness of our main results in Chapter 2, we consider two examples in this chapter. These are coupled Lorenz equations [8,63], and coupled Duffing oscillators [105].

Example 1: We shall begin with Lorenz equations. Let $\boldsymbol{x} = (x_1, x_2, x_3)^T$,

$$\begin{aligned}\boldsymbol{f}(\boldsymbol{x}, t) = \boldsymbol{f}(\boldsymbol{x}) &= (\sigma(x_2 - x_1),\ rx_1 - x_2 - x_1x_3,\ -bx_3 + x_1x_2)^T \\ &=: (f_1(\boldsymbol{x}),\ f_2(\boldsymbol{x}),\ f_3(\boldsymbol{x}))^T.\end{aligned}$$

Here $\sigma = 10$, $r = 28$ and $b = \frac{8}{3}$. In the following cases (a), (b), (c) and (d), $\boldsymbol{G}$ denotes the diffusive coupling with zero flux and $\boldsymbol{D}$ is, respectively, $\begin{pmatrix} 1 & 0 & 0 \\ 0 & 0 & 0 \\ 0 & 0 & 0 \end{pmatrix}$, $\begin{pmatrix} 0 & 0 & 0 \\ 0 & 1 & 0 \\ 0 & 0 & 0 \end{pmatrix}$, $\begin{pmatrix} 0 & 0 & 0 \\ 0 & 0 & 0 \\ 0 & 0 & 1 \end{pmatrix}$, and $\begin{pmatrix} 0 & 0 & 0 \\ 0 & 1 & 1 \\ 0 & 0 & 1 \end{pmatrix}$. For the first three cases, it was shown in [5] that such the coupled system (2.6) has the topological product of an absorbing domain

$$B_0 = \{x_1^2 + x_2^2 + (x_3 - r - \sigma)^2 < \frac{b^2(r+\sigma)^2}{4(b-1)} =: \beta\}. \tag{3.1}$$

Hence, in each case, we will concentrate on the illustration of how our main results may or may not be applied.

(a) Let $\boldsymbol{D} = \boldsymbol{D}_1 = \begin{pmatrix} 1 & 0 & 0 \\ 0 & 0 & 0 \\ 0 & 0 & 0 \end{pmatrix}$. For "coupled" nonlinearity f_1, we get that

$$|f_1(\boldsymbol{u}) - f_1(\boldsymbol{v})| = \sigma|(u_2 - v_2) - (u_1 - v_1)| \leq \sqrt{2}\sigma\|\boldsymbol{u} - \boldsymbol{v}\|.$$

Hence, condition (2.14a) is satisfied. For "uncoupled" nonlinearities f_2 and f_3, we see that

$$\begin{aligned} f_2(\boldsymbol{u}) - f_2(\boldsymbol{v}) &= (-u_2 - u_1u_3 + ru_1) - (-v_2 - v_1v_3 + rv_1) \\ &= [-(u_2 - v_2) - u_1(u_3 - v_3)] + (r - v_3)(u_1 - v_1) \end{aligned} \tag{3.2a}$$

and

$$\begin{aligned} f_3(\boldsymbol{u}) - f_3(\boldsymbol{v}) &= (u_1u_2 - bu_3) - (v_1v_2 - bv_3) \\ &= [u_1(u_2 - v_2) - b(u_3 - v_3)] + v_2(u_1 - v_1). \end{aligned} \tag{3.2b}$$

Writing (3.2a)-(3.2b) in the vector form, we get

$$\begin{aligned} \begin{pmatrix} f_2(\boldsymbol{u}) - f_2(\boldsymbol{v}) \\ f_3(\boldsymbol{u}) - f_3(\boldsymbol{v}) \end{pmatrix} &= \begin{pmatrix} -1 & -u_1(t) \\ u_1(t) & -b \end{pmatrix} \begin{pmatrix} u_2 - v_2 \\ u_3 - v_3 \end{pmatrix} + \begin{pmatrix} (r - v_3)(u_1 - v_1) \\ v_2(u_1 - v_1) \end{pmatrix} \\ &=: \boldsymbol{Q}_{\boldsymbol{u},\boldsymbol{v},1}(t) \begin{pmatrix} u_2 - v_2 \\ u_3 - v_3 \end{pmatrix} + \boldsymbol{r}_1. \end{aligned} \tag{3.2c}$$

Clearly, $\mu_2(\boldsymbol{Q}_{\boldsymbol{u},\boldsymbol{v},1}(t)) = \max\{-1, -b\} = -1 < 0$, and $\|\boldsymbol{r}_1\| \leq (\sigma + \sqrt{\beta}) \cdot |u_1 - v_1|$, where its estimate depends only on coupled space. Hence, conditions (2.24b), and (2.24c) are satisfied.

(b) Let $\boldsymbol{D} = \boldsymbol{D}_2 = \begin{pmatrix} 0 & 0 & 0 \\ 0 & 1 & 0 \\ 0 & 0 & 0 \end{pmatrix}$. As in the case (a), the "coupled" nonlinearity f_2 is clearly Lipschitz on the absorbing domain. The difference of "uncoupled" nonlinearities f_1 and f_3 are given as follows.

$$\begin{aligned} f_1(\boldsymbol{u}) - f_1(\boldsymbol{v}) &= [-\sigma(u_1 - v_1)] + \sigma(u_2 - v_2), \\ f_3(\boldsymbol{u}) - f_3(\boldsymbol{v}) &= [-b(u_3 - v_3)] + u_1(u_2 - v_2) + v_2(u_1 - v_1). \end{aligned}$$

If $l = 1$ is chosen, then (2.24c) is violated. For in the case, the norm estimate in the right hand side of (2.24c) can only depend on $u_2 - v_2$. Now, if we choose $l = 2$ and pick the space of the first diagonal block being the one associated with the nonlinearity f_1, then $\boldsymbol{Q}_{\boldsymbol{u},\boldsymbol{v},1} = (-\sigma)$ and $r_1 = \sigma(u_2 - v_2)$. Consequently, (2.24b) and (2.24c) are satisfied. Moreover, we have $\boldsymbol{Q}_{\boldsymbol{u},\boldsymbol{v},2} = (-b)$ and $r_2 = u_1(u_2 - v_2) + v_2(u_1 - v_1)$, which depends only on the coupled space and the first uncoupled space. Thus, r_2 satisfies (2.24c).

(c) For illustration, we also consider $\boldsymbol{D} = \boldsymbol{D}_3 = \begin{pmatrix} 0 & 0 & 0 \\ 0 & 0 & 0 \\ 0 & 0 & 1 \end{pmatrix}$. In this case, the uncoupled nonlinearities of f_1 and f_2 both contain the terms x_2 and x_1. The only feasible choice to break the uncoupled space is not to do any breaking. Consequently, $\boldsymbol{Q}_{\boldsymbol{u},\boldsymbol{v},1} = \begin{pmatrix} -\sigma & \sigma \\ r - u_3(t) & -1 \end{pmatrix}$. For such $\boldsymbol{Q}_{\boldsymbol{u},\boldsymbol{v},1}$, its matrix measure can not stay negative for all time. An indicated, see e.g., [63], synchronization fails for this type of partial coupling.

(d) Let $\boldsymbol{D} = \boldsymbol{D}_4 = \begin{pmatrix} 0 & 0 & 0 \\ 0 & 1 & 1 \\ 0 & 0 & 1 \end{pmatrix}$. To apply Theorem 2.2.3, we first note that for $\boldsymbol{D} = \boldsymbol{D}_5 = \begin{pmatrix} 0 & 0 & 0 \\ 0 & 1 & 0 \\ 0 & 0 & 1 \end{pmatrix}$, the corresponding coupled system is indeed globally synchronized, and hence, so is the coupled system with $\boldsymbol{D} = \boldsymbol{D}_4$. Note that bounded dissipation of the coupled system can be verified similarly as in [63].

(e) The work that are most related to ours are those in [4,8]. While their estimates for $d_{\min}$ seems to be sharper than ours, which we shall illustrate in case (f), their connectivity topology requires that off-diagonal entries be nonnegative. We only assume our connectivity topology satisfies (2.7). Consider for instant the following matrix:

$$\boldsymbol{G} = \begin{pmatrix} -1 & 2 & 0 & -1 \\ -1 & -1 & 0 & 2 \\ 2 & -1 & -3 & 2 \\ 0 & 0 & 3 & -3 \end{pmatrix}.$$

Such $\boldsymbol{G}$ has some negative off-diagonal entries and satisfy (2.7a) and (2.7b). In fact, the eigenvalues of $\boldsymbol{G}$ are 0, $-1 \pm \sqrt{5}i$, and -6. Clearly, applying our results, we see immediately that the coupled system (2.6) with $\boldsymbol{D} = \boldsymbol{D}_i$, $i = 1, 2, 4$, is globally synchronized. Numerical results (see Figure 3.1.) indeed confirm synchronization of such connectivity topology. We remark that by constructing the Lyapunov function as given in [63], one would be able to show bounded dissipation of the coupled system with this particular connectivity topology.

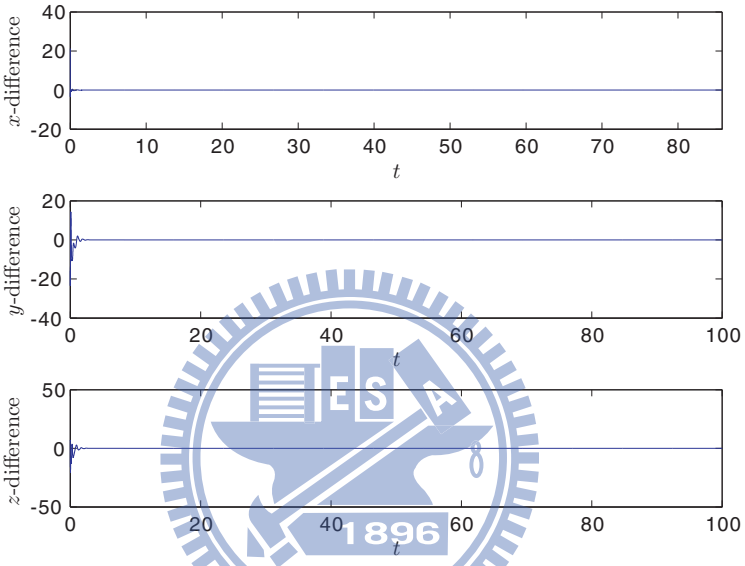

Figure 3.1: The difference of each component of two coupled oscillators in case (e).

(f) In this part, we shall compute the lower bound for global synchronization for case (a) by using our method, those obtained in [8] and MSF, respectively. To compute $d_{\min}$, given in (2.15), we note that $\bar{\boldsymbol{G}} = \boldsymbol{E}_2\boldsymbol{G}\boldsymbol{E}_2^T(\boldsymbol{E}_2\boldsymbol{E}_2^T)^{-1} = \boldsymbol{E}_2(\boldsymbol{E}_2^T\boldsymbol{E}_2)\boldsymbol{E}_2^T(\boldsymbol{E}_2\boldsymbol{E}_2^T)^{-1}$ $= \boldsymbol{E}_2\boldsymbol{E}_2^T$. Here $\boldsymbol{E}_2$ is given as in (2.30). Since $\bar{\boldsymbol{G}}$ is symmetric, c and ϵ, given as in (2.16c), can be chosen to be 1, and 0, respectively. Consequently,

$$d_{\min} = \frac{\sqrt{2}\sigma\sqrt{1+\beta+2\sigma\sqrt{\beta}+\sigma^2}}{4\sin^2(\frac{\pi}{2m})}. \tag{3.3}$$

Here $4\sin^2(\frac{\pi}{2m}) = |\lambda_1|$. Applying Theorem 2.2.3, we see that the coupled system is globally synchronized provided that the coupling strength d is greater than $d_{\min}$. For

$m = 4$, $d_{\min} \approx 1189$. In [8], the bound $\bar{d}_{\min}$ for threshold of global synchronization is

$$\bar{d}_{\min} = \begin{cases} \frac{a}{8}m^2 & \text{if } m \text{ is even} \\ \frac{a}{8}(m^2-1) & \text{if } m \text{ is odd} \end{cases}.$$

Here $a = \frac{b(b+1)(r+\sigma)^2}{16(b-1)} - \sigma$. For $m = 4$, $\bar{d}_{\min} \approx 1039$, which is slightly better than $d_{\min}$.

Using the MSF-criteria, we numerically (see Figure 3.2.) compute the maximum Lyapunov exponent of the variational equations with respect to the parameter α. We have in this example that if

$$\alpha = d\lambda_1 < -7.778, \tag{3.4}$$

then its maximum Lyapunov exponent is negative. Here $\lambda_1 = -4\sin^2\frac{\pi}{8}$ is the largest nonzero eigenvalues of $\boldsymbol{G}$. Hence if $d > \frac{-7.778}{\lambda_1} \approx 13.3$, then local synchronization of the coupled system (2.6) can be realized.

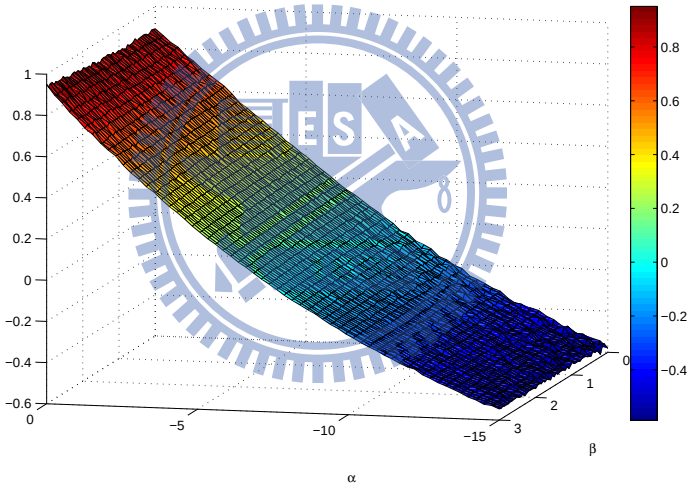

Figure 3.2: The vertical axis denotes the maximum Lyapunov exponent of the variational equations. While the horizontal axis represents $\alpha = d\lambda$.

(g) Let coupling matrix $\boldsymbol{G}(t)$ be time dependent as given in (2.33), (2.35), (2.37) or (2.39), and the coupling matrix $\boldsymbol{D} = \boldsymbol{D}_i$, $i = 1, 2$. Then by Theorem 2.3.4 and above arguments, we can also have coupled system is globally synchronized whenever the coupling strength d is sufficient large. Fig. 3.3 illustrates the phenomenon of synchronization with $\boldsymbol{G}(t)$ of the form (2.37), $d_1(t) = \frac{3}{2} - \sin(t)$, and $\boldsymbol{D} = \boldsymbol{D}_1$.

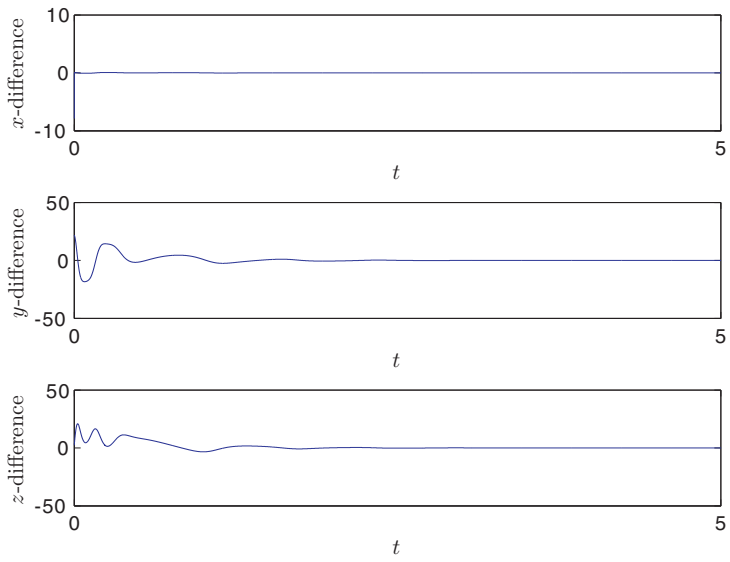

Figure 3.3: The difference of components of the first two coupled oscillators. Here the x-component partial-state coupling is considered. and the $\boldsymbol{G}(t)$ is given as in (2.37) with $d_1(t) = \frac{3}{2} - \sin(t)$ and $m = 8$.

Example 2: Now, we consider the coupled Duffing oscillators, where the individual system considered is defined by

$$\dot{x}_1 = -\alpha x_1 - x_2^3 + a\cos wt \tag{3.5a}$$

$$\dot{x}_2 = x_1, \tag{3.5b}$$

where α and a are positive constants. Letting $\boldsymbol{x} = (x_1, x_2)^T$, we have

$$\boldsymbol{f}(\boldsymbol{x}, t) = (f_1(\boldsymbol{x}, t), f_2(\boldsymbol{x})) = (-\alpha x_1 - x_2^3 + a\cos wt,\ x_1), \tag{3.6a}$$

Assume coupling matrices $\boldsymbol{D}$ and $\boldsymbol{G}$ are, respectively,

$$\boldsymbol{D}(c) = \begin{pmatrix} 1 & c \\ 0 & 0 \end{pmatrix} \tag{3.6b}$$

and

$$\boldsymbol{G}(\epsilon, r) = \begin{pmatrix} -2\epsilon & \epsilon - r & 0 & \cdots & 0 & \epsilon + r \\ \epsilon + r & -2\epsilon & \epsilon - r & \ddots & & 0 \\ 0 & \ddots & \ddots & \ddots & \ddots & \vdots \\ \vdots & \ddots & \ddots & \ddots & \ddots & 0 \\ 0 & & \ddots & \ddots & -2\epsilon & \epsilon - r \\ \epsilon - r & 0 & \cdots & 0 & \epsilon + r & -2\epsilon \end{pmatrix}, \tag{3.6c}$$

where $\epsilon > 0$ and r are scalar diffusive and gradient coupling parameters, respectively. In this way, the coupled Duffing systems can be written as

$$\dot{\tilde{\boldsymbol{x}}}_1 = -\alpha\tilde{\boldsymbol{x}}_1 - \tilde{\boldsymbol{x}}_2^3 + \boldsymbol{g}(t) + dc\boldsymbol{G}(\epsilon, r)\tilde{\boldsymbol{x}}_2 + d\boldsymbol{G}(\epsilon, r)\tilde{\boldsymbol{x}}_1 \tag{3.7a}$$

$$\dot{\tilde{\boldsymbol{x}}}_2 = \tilde{\boldsymbol{x}}_{1.} \tag{3.7b}$$

Here $\tilde{\boldsymbol{x}}_2^3 = (x_{1,2}^3, \ldots, x_{m,2}^3)^T$, and $\boldsymbol{g}(t) = a\cos(wt)\,(1, \cdots, 1)^T$. Note that

$$f_2(\boldsymbol{u}) - f_2(\boldsymbol{v}) = 0(u_2 - v_2) + (u_1 - v_1)$$

and so the matrix measure of the corresponding $\boldsymbol{Q}_{\boldsymbol{u},\boldsymbol{v},1}$ is zero. To apply our theorem, we need to make the following coordinate change.

Letting $y_2 = x_2$ and $y_1 = qx_1 + px_2$, we see that (3.5) becomes

$$\dot{y}_1 = (\frac{p}{q} - \alpha)y_1 + p(\alpha - \frac{p}{q})y_2 - qy_2^3 + qa\cos wt =: \bar{\boldsymbol{f}}_1(\boldsymbol{y}) \tag{3.8a}$$

$$\dot{y}_2 = \frac{-p}{q}y_2 + \frac{1}{q}y_1 =: \bar{\boldsymbol{f}}_2(\boldsymbol{y}), \tag{3.8b}$$

and the corresponding coupled system (3.7) becomes

$$\begin{aligned} \dot{\tilde{\boldsymbol{y}}}_1 = {} & (\frac{p}{q} - \alpha)\tilde{\boldsymbol{y}}_1 + p(\alpha - \frac{p}{q})\tilde{\boldsymbol{y}}_2 - q\tilde{\boldsymbol{y}}_2^3 + \boldsymbol{g}(t) \\ & + d(qc - p)\boldsymbol{G}(\epsilon, r)\tilde{\boldsymbol{y}}_2 + d\boldsymbol{G}(\epsilon, r)\tilde{\boldsymbol{y}}_1 \end{aligned} \tag{3.9a}$$

$$\dot{\tilde{\boldsymbol{y}}}_2 = -\frac{q}{p}\tilde{\boldsymbol{y}}_2 + \frac{1}{q}\tilde{\boldsymbol{y}}_{1,} \tag{3.9b}$$

where $\tilde{\boldsymbol{y}}_2^3 = (y_{1,2}^3, \ldots, y_{m,2}^3)^T$ and $\boldsymbol{g}(t) = a\cos(wt)\,(1, \cdots, 1)^T$. In the following, we choose (p, q) to be $(c - \frac{1}{d}, 1)$ as $c > 0$, and to be $(-1, -\frac{1}{d})$ as $c = 0$, respectively. Then

in the case of $c > 0$, (3.9) becomes

$$\begin{aligned}
\dot{\tilde{\boldsymbol{y}}}_1 &= d\boldsymbol{G}(\epsilon, r)\tilde{\boldsymbol{y}}_1 + (c - \alpha - \frac{1}{d})\tilde{\boldsymbol{y}}_1 + (\alpha - c + \frac{1}{d})\tilde{\boldsymbol{y}}_2 - \tilde{\boldsymbol{y}}_2^3 + \boldsymbol{g}(t) + \boldsymbol{G}(\epsilon, r)\tilde{\boldsymbol{y}}_2 \\
&=: d\boldsymbol{G}(\epsilon, r)\tilde{\boldsymbol{y}}_1 + \tilde{\boldsymbol{F}}_c(\tilde{\boldsymbol{y}}, t) \\
\dot{\tilde{\boldsymbol{y}}}_2 &= -\frac{1}{c - \frac{1}{d}}\tilde{\boldsymbol{y}}_2 + \tilde{\boldsymbol{y}}_1.
\end{aligned}$$

The purpose of the coordinate transformation is two-fold. First, to make the dynamics of the linear part on the uncoupled space stable. In this case, the coefficient of $\tilde{\boldsymbol{y}}_2$ becomes negative when $d > \frac{2}{c}$. Second, to make sure the parameters in the nonlinear part of coupled space contain no bad influence of d, coupling strength. Otherwise, we may not be able to control its corresponding dynamics by choosing d large.

It is then easy to check that assumptions for Theorem 2.2.1 are all satisfied, and similar arguments can be followed for the case of $c = 0$. What the remainder is the checking of the bounded disspation of the coupled system.

Consider the following scalar-valued function as the Lyapunov function of the coupled system (3.7)

$$U(\tilde{\boldsymbol{x}}_1, \tilde{\boldsymbol{x}}_2) = \frac{1}{2} < \tilde{\boldsymbol{x}}_1, \tilde{\boldsymbol{x}}_1 > + \sum_{i=1}^{m} \frac{x_{i,2}^4}{4} + c < \tilde{\boldsymbol{x}}_2, \tilde{\boldsymbol{x}}_1 >, \tag{3.10}$$

Taking the time derivative of U along solutions of the coupled system (3.7), we have

$$\begin{aligned}
\frac{dU}{dt} =& < \tilde{\boldsymbol{x}}_1, \dot{\tilde{\boldsymbol{x}}}_1 > + \sum_{i=1}^{m} x_{i,2}^3 x_{i,1} + c < \tilde{\boldsymbol{x}}_1, \tilde{\boldsymbol{x}}_1 > + c < \tilde{\boldsymbol{x}}_2, \dot{\tilde{\boldsymbol{x}}}_1 > \\
&= (c - \alpha) < \tilde{\boldsymbol{x}}_1, \tilde{\boldsymbol{x}}_1 > - c\alpha < \tilde{\boldsymbol{x}}_2, \tilde{\boldsymbol{x}}_1 > - c < \tilde{\boldsymbol{x}}_2, \tilde{\boldsymbol{x}}_2^3 > + < \tilde{\boldsymbol{x}}_1 + c\tilde{\boldsymbol{x}}_2, \boldsymbol{g}(t) > \\
&\quad + d < \tilde{\boldsymbol{x}}_1, \boldsymbol{G}(\epsilon, r)\tilde{\boldsymbol{x}}_1 > + 2dc < \tilde{\boldsymbol{x}}_1, \boldsymbol{G}(\epsilon, r)\tilde{\boldsymbol{x}}_2 > + dc^2 < \tilde{\boldsymbol{x}}_2, \boldsymbol{G}(\epsilon, r)\tilde{\boldsymbol{x}}_2 > \\
&= (c - \alpha) < \tilde{\boldsymbol{x}}_1, \tilde{\boldsymbol{x}}_1 > - c\alpha < \tilde{\boldsymbol{x}}_2, \tilde{\boldsymbol{x}}_1 > - c < \tilde{\boldsymbol{x}}_2, \tilde{\boldsymbol{x}}_2^3 > + < \tilde{\boldsymbol{x}}_1 + c\tilde{\boldsymbol{x}}_2, \boldsymbol{g}(t) > \\
&\quad + d\left(\tilde{\boldsymbol{x}}_1^T, \tilde{\boldsymbol{x}}_2^T\right)\left(\begin{pmatrix} 1 & c \\ c & c^2 \end{pmatrix} \otimes \boldsymbol{G}(\epsilon, r)\right)\begin{pmatrix} \tilde{\boldsymbol{x}}_1 \\ \tilde{\boldsymbol{x}}_2 \end{pmatrix} \\
&\leq (c - \alpha) < \tilde{\boldsymbol{x}}_1, \tilde{\boldsymbol{x}}_1 > - c\alpha < \tilde{\boldsymbol{x}}_2, \tilde{\boldsymbol{x}}_1 > - c < \tilde{\boldsymbol{x}}_2, \tilde{\boldsymbol{x}}_2^3 > + < \tilde{\boldsymbol{x}}_1 + c\tilde{\boldsymbol{x}}_2, \boldsymbol{g}(t) >
\end{aligned}$$

Note that the last inequality holds true since

$$\begin{aligned}&\left(\begin{pmatrix} 1 & c \\ c & c^2 \end{pmatrix} \otimes \boldsymbol{G}(\epsilon, r)\right) + \left(\begin{pmatrix} 1 & c \\ c & c^2 \end{pmatrix} \otimes \boldsymbol{G}(\epsilon, r)\right)^T \\ = &\begin{pmatrix} 1 & c \\ c & c^2 \end{pmatrix} \otimes (\boldsymbol{G}(\epsilon, r) + \boldsymbol{G}(\epsilon, r)^T),\end{aligned}$$

and $\boldsymbol{G}(\epsilon, r) + \boldsymbol{G}(\epsilon, r)^T$ is a nonpositive definite matrix. On the other hand, since

$$< \tilde{\boldsymbol{x}}_2, \tilde{\boldsymbol{x}}_2^3 >= \sum_{i=1}^{m} x_{2,i}^4 \geq \frac{1}{m}\left(\sum_{i=1}^{m} x_{i,2}^2\right)^2 \geq \frac{1}{m}\|\tilde{\boldsymbol{x}}_2\|_2^4,$$

we have

$$\begin{aligned}\frac{dU}{dt} &\leq (c-\alpha)\|\tilde{\boldsymbol{x}}_1\|_2^2 + c\alpha\|\tilde{\boldsymbol{x}}_2\|_2\|\tilde{\boldsymbol{x}}_1\|_2 - \frac{c}{m}\|\tilde{\boldsymbol{x}}_2\|_2^4 + \sqrt{m}a(\|\tilde{\boldsymbol{x}}_1\|_2 + c\|\tilde{\boldsymbol{x}}_2\|_2) \\ &=: u(\|\tilde{\boldsymbol{x}}_1\|_2, \|\tilde{\boldsymbol{x}}_2\|_2).\end{aligned}$$

We are now in a position to show bounded dissipation of the coupled system (3.7).

Proposition 3.1.1.

(i) If c satisfies the inequality

$$0 < c < \min\{\frac{4\alpha}{4+\alpha^2 m}, \alpha\} = \frac{4\alpha}{4+\alpha^2 m}. \tag{3.11}$$

Then there exists a constant c_0 so that $\frac{dU}{dt} < 0$ for $\|\tilde{\boldsymbol{x}}_2\|_1^2 + \|\tilde{\boldsymbol{x}}_2\|_2^2 \geq c_0$.

(ii) If $c = 0$, then the first assertion of the proposition still holds true.

Proof. Suppose $\|\tilde{\boldsymbol{x}}_2\|_2 \geq 1$. Then

$$\begin{aligned}u(\|\tilde{\boldsymbol{x}}_1\|_2, \|\tilde{\boldsymbol{x}}_2\|_2) &\leq (c-\alpha)\|\tilde{\boldsymbol{x}}_1\|_2^2 + c\alpha\|\tilde{\boldsymbol{x}}_2\|_2\|\tilde{\boldsymbol{x}}_1\|_2 - \frac{c}{m}\|\tilde{\boldsymbol{x}}_2\|_2^2 + \sqrt{m}a(\|\tilde{\boldsymbol{x}}_1\|_2 + c\|\tilde{\boldsymbol{x}}_2\|_2) \\ &=: \bar{u}(\|\tilde{\boldsymbol{x}}_1\|_2, \|\tilde{\boldsymbol{x}}_2\|_2).\end{aligned}$$

It then follows from (3.11) that the the level curve of $\bar{u}$ is a bounded closed curve. We shall call such curve ellipse-like is an elliptic in the plane. Thus, there exists a c_1 so that $\frac{dU}{dt} < 0$ whenever $\|\tilde{\boldsymbol{x}}_2\|_1^2 + \|\tilde{\boldsymbol{x}}_2\|_2^2 \geq c_1$ and $\|\tilde{\boldsymbol{x}}_2\|_2 \geq 1$. Let $\|\tilde{\boldsymbol{x}}_2\|_2 < 1$ and $\|\tilde{\boldsymbol{x}}_2\|_1^2 + \|\tilde{\boldsymbol{x}}_2\|_2^2 \geq c_2$. Here c_2 is a constant to be determined. Then

$$u(\|\tilde{\boldsymbol{x}}_1\|_2, \|\tilde{\boldsymbol{x}}_2\|_2) \leq (c-\alpha)\|\tilde{\boldsymbol{x}}_1\|_2^2 + (c\alpha + \sqrt{m}a)\|\tilde{\boldsymbol{x}}_1\|_2 + \sqrt{m}ac =: h(\|\tilde{\boldsymbol{x}}_1\|_2).$$

Since $h(\|\tilde{\boldsymbol{x}}_1\|_2)$ is a parabola-like curve which is open downward, there exists a $c_3 > 1$ such that $h(\|\tilde{\boldsymbol{x}}_1\|_2) < 0$ whenever $\|\tilde{\boldsymbol{x}}_1\|_2 \geq c_3$. Thus, if $c_2 \geq c_3^2+1$, then $u(\|\tilde{\boldsymbol{x}}_1\|_2, \|\tilde{\boldsymbol{x}}_2\|_2) < 0$ whenever $\|\tilde{\boldsymbol{x}}_2\|_2 < 1$ and $\|\tilde{\boldsymbol{x}}_1\|_2^2 + \|\tilde{\boldsymbol{x}}_2\|_2^2 \geq c_2$. Picking $c_0 = \max\{c_1, c_2\}$, we have that the assertion of the proposition holds true. □

Proposition 3.1.2. *Assume* (3.11) *holds true. Then* $\lim_{r\to\infty} U(\tilde{\boldsymbol{x}}_1, \tilde{\boldsymbol{x}}_2) = \infty$, *where* $r = \sqrt{\|\tilde{\boldsymbol{x}}_1\|^2 + \|\tilde{\boldsymbol{x}}_2\|^2}$.

Proof. From (3.10), we have that

$$\begin{aligned} U(\tilde{\boldsymbol{x}}_1, \tilde{\boldsymbol{x}}_2) &= \frac{1}{2}\|\tilde{\boldsymbol{x}}_1\|^2 + \sum_{i=1}^{m} \frac{x_{i,2}^4}{4} + c < \tilde{\boldsymbol{x}}_2, \tilde{\boldsymbol{x}}_1 > \\ &\geq \frac{1}{2}\|\tilde{\boldsymbol{x}}_1\|^2 + \frac{1}{4m}\|\tilde{\boldsymbol{x}}_2\|^4 - c\|\tilde{\boldsymbol{x}}_2\| \cdot \|\tilde{\boldsymbol{x}}_1\|, \end{aligned}$$

Let $\frac{1}{4m}b_1^2 > c^2$. Then suppose $\|\tilde{\boldsymbol{x}}_2\| > b_1$, we have

$$U(\tilde{\boldsymbol{x}}_1, \tilde{\boldsymbol{x}}_2) \geq \frac{1}{2}\|\tilde{\boldsymbol{x}}_1\|^2 + c^2\|\tilde{\boldsymbol{x}}_2\|^2 - c\|\tilde{\boldsymbol{x}}_2\|\|\tilde{\boldsymbol{x}}_1\| =: h_1(\|\tilde{\boldsymbol{x}}_1\|, \|\tilde{\boldsymbol{x}}_2\|).$$

Since the level curve of $h_1(\|\tilde{\boldsymbol{x}}_1\|, \|\tilde{\boldsymbol{x}}_2\|)$ is elliptic-like in the plane. Thus, for any given $M > 0$, there exists a $d_1 > 0$ such that $U(\tilde{\boldsymbol{x}}_1, \tilde{\boldsymbol{x}}_2) > M$ whenever $\|\tilde{\boldsymbol{x}}_1\|^2 + \|\tilde{\boldsymbol{x}}_2\|^2 \geq d_1^2$ and $\|\tilde{\boldsymbol{x}}_2\| > b_1$.
Let $\|\tilde{\boldsymbol{x}}_2\| \leq b_1$. Then

$$U(\tilde{\boldsymbol{x}}_1, \tilde{\boldsymbol{x}}_2) \geq \frac{1}{2}\|\tilde{\boldsymbol{x}}_1\|^2 - cb_1\|\tilde{\boldsymbol{x}}_1\| =: h_2(\|\tilde{\boldsymbol{x}}_1\|, \|\tilde{\boldsymbol{x}}_2\|),$$

since $h_2(\|\tilde{\boldsymbol{x}}_1\|, \|\tilde{\boldsymbol{x}}_2\|)$ is a parabola-like curve which is open upward in the plane. Thus, for any given $M > 0$, there exists a $d_2 > 0$ such that $U(\tilde{\boldsymbol{x}}_1, \tilde{\boldsymbol{x}}_2) > M$ whenever $\|\tilde{\boldsymbol{x}}_1\|^2 + \|\tilde{\boldsymbol{x}}_2\|^2 \geq d_2^2$ and $\|\tilde{\boldsymbol{x}}_2\| \leq b_1$. Picking $\delta = \max\{d_1, d_2\}$, we have that $U(\tilde{\boldsymbol{x}}_1, \tilde{\boldsymbol{x}}_2) > M$ for all $\|\tilde{\boldsymbol{x}}_1\|^2 + \|\tilde{\boldsymbol{x}}_2\|^2 \geq \delta^2$. Thus, the assertion of the proposition holds true. □

Theorem 3.1.1. *The coupled system* (3.7) *is bounded dissipative if condition* (3.11) *holds true.*

Proof. The proof is direct consequences of Propositions 3.1.1 and 3.1.2. □

Thus, summarizing above results and applying Theorem 2.2.1, we get the following conclusion.

Theorem 3.1.2. *Let* $\boldsymbol{f}$, $\boldsymbol{D}(c)$ *and* $\boldsymbol{G}(\epsilon, r)$ *be given as in* (3.6a), (3.6b) *and* (3.6c), *respectively. Let* $0 \leq c < \frac{4\alpha}{4+\alpha^2 m}$. *Then the coupled Duffing system* (3.7) *is globally synchronized provided that* d *is chosen sufficiently large.*

Proof. It remains only to verify that $\boldsymbol{G}(\epsilon, r)$ satisfies assumptions (2.7a) and (2.7b). Indeed $\boldsymbol{G}(\epsilon, r)$ is a circulant matrix (see e.g., [22]), the eigenvalues λ_k of $\boldsymbol{G}(\epsilon, r)$ are

$$\lambda_k = -2\epsilon(1 - \cos\frac{2k\pi}{m}) - i\, 2r \sin\frac{2k\pi}{m}, \quad k = 0, \ldots, m-1.$$

□

3.2 Synchronization in Hindmarsh-Rose Neurons with Chemical and Electrical Synapses

3.2.1 Introduction of the Hindmarsh-Rose Neurons

The fundamental building block of every nervous system is the neuron. There is an increasing trend [35,43,67] towards studying the dynamical behavior of relatively large networks of neurons, and modeling/emulating such networks is also on the rise. Neural synchronization has been suggested as particularly relevant for neuronal signal transmission and coding in the brain. Brain [14,24,33,34,73,84,86,90] oscillations that are ubiquitous phenomena in all brain areas eventually get into synchrony and consequently allow the brain to process various tasks from cognitive to motor tasks. Indeed, it is hypothesized that synchronous brain activity is the most likely mechanism for many cognitive functions such as attention, feature binding, learning, development and memory function.

In the last decades, many biological neuron models have been proposed for an accurate description and prediction of biological phenomena. The pioneering work in such direction is due to Hodgkin and Huxley. To simplify such a model, simpler approximations, namely, the second order systems such as the FitzHugh-Nagumo(FN) and

Morris-Lecar neuron models have been proposed. However, the second order models are not able to reproduce some interesting phenomena such as terminating themselves by triggering a set of stable firings. Hence, the Hindmarsh-Rose(HR) model was added a third dynamical component, whose role is to tune the above subsystem over the mono- and bistability regions in order to activate or terminate the neuronal response. The third order system of HR has turned out to be accurate in capturing both qualitative and quantitative aspects of experimental data [23,45,46,87]. Furthermore, major neuronal behaviors such as spiking, bursting, and chaotic regime have been produced by such HR model [23,39,44].

In a human brain, there are about 10^{10} neurons with an approximate 10^{14} links between them. Neurons are sparsely connected and their underlying network has small-world property [14] though they are within only a few synaptic steps from other neurons. Neurons in a population synchronize their activity using electrical and chemical synapses with other neurons in the same population as well as with neurons from other populations. Note that the electrical coupling via gap junctions is linear and directly depends on the difference of the membrane potentials. And the chemical coupling is pulsatile and often modeled as a static sigmoidal nonlinear input-output function with a threshold and saturation.

In this section, we study the multi-state and multi-stage synchronization in ensembles of electrically and chemically coupled HR neurons whose connection topology with respect to the electrical coupling is allowed to be complex including, e.g., Newman-Wattts networks, and whose coupling through chemical synapse is unidirectional from presynaptic cell to the postsynaptic cell. By *multi-state synchronization*, we mean that given a fixed set of parameters, the corresponding system is capable of producing the coexistence of stable regular bursting and periodic/steady-state synchronization, depending on the choice of initial conditions. By varying certain parameters, if the associated system is capable of yielding different types of synchronization such as chaotic, periodic or steady-state synchronization, then the system is said to exhibit the *multi-stage synchronization*.

More closely related work can be refereed to the articles by Jalili [48], Kopell and

Ermentrout [58], Belykh, Lange and Hasler [6], Checco, Righero, Biey and Kocarev [16], and Wang etc., [94–96]. In [58], the single neuron model is a quadratic integrate and fire. They obtained that the chemical and electrical couplings play complementary roles in the coherence of rhythms in inhibitory networks. In [6], densely coupled HR system with only chemical coupling was studied. They demonstrated the bound of the minimum chemical strength for obtaining the steady-state synchronization only depends on the number of signals each neuron receives, independent of all other details of the network topology. These two works used both numerical and analytical techniques to address local synchronization. Coupled HR system with only chemical coupling was also investigated in [16]. They have found multi-stage synchronization. However, the presence of multi-state synchronization has not been addressed there. Furthermore, their results are based on the Master Stability Equation, which is numerical in nature. Whereas the results in [48], though the same model as ours were studied, was numerical. The work done in [94–96] dealt with only electrical coupling. However, effects of delay on synchronization were investigated there, where some interesting results are obtained when delays are varied.

3.2.2 Synchronization of the Hindmarsh-Rose Neurons

The HR model was obtained by biological consideration over the response to stimuli of a real neuronal cell. The motion of the model reads as follows:

$$\begin{aligned} \dot{x} &= f(x) + y - z + q, \\ \dot{y} &= -y - 5x^2 + 1, \\ \dot{z} &= \mu(b(x - x_0) - z). \end{aligned} \tag{3.12}$$

Here $f(x) = ax^2 - x^3$, x is the membrane potential, y and z are the recovery(fast) and the adaptation(slow) current, respectively. The roles played by the system parameters are roughly the following. q mimics the membrane input current for biological neurons; a allows one to switch between bursting and spiking behaviors and to control the spiking frequency; μ controls the speed of variation of the slow variable z, and in the presence of spiking behaviors, it governs the spiking frequency, whereas in the case of bursting,

it affects the number of spikes per burst; b governs adaptation; a unitary value of b determines spiking behavior without accommodation and subthreshold adaptation, whereas around $b = 4$ give strong accommodation and subthreshold overshoot, or even oscillations; x_0 sets the resting potential of the system. Hereafter, the parameters are chosen and fixed as follows: $x_0 = -1.6$, $\mu = 0.01$, $b = 4$, $q = 4$, and $a = 2.6$. The dynamics of the neuron with such set of parameters is regular bursting (see, e.g., [87]). Moreover, the dynamics on the corresponding synchronous manifold of the coupled HR neurons may generate multistability region (see equation (3.16) and Table 3.1) containing a stable regular bursting, a stable periodic solution and a stable fixed point.

Neuronal synaptic connections are either chemical or electrical, and chemical connections might be excitatory or inhibitory. Moreover, the electrical coupling through gap junctions is bidirectional, whereas the chemical synapse is unidirectional from the presynaptic cell to the postsynaptic cell. In fact, the current q_{ij} injected from the presynaptic cell j to the postsynaptic cell i, is a nonlinear function of the membrane potential x_j of the presynaptic cell and a linear function of the membrane potential x_i of the postsynaptic cell. The current q_{ij} has the following form

$$q_{ij} = g_s(v - x_i)p(x_j), \tag{3.13a}$$

where g_s is the strength of chemical coupling and v is the synaptic reversal potential. If $x_i < v$, the current injected to the cell is positive and depolarizes it, thus the coupling is excitatory. On the other hand, for $x_i > v$, the injected current to the cell is negative and consequently hyperpolarizes it, thus introducing inhibitory coupling. In this thesis, we numerically choose $v = 2$ so that $x_i(t) < v$ for all t, thus the synapse is depolarizing (excitatory). It is certainly interesting to justify that such choice of v is always possible.

The chemically synaptic coupling function is modeled by the sigmoidal function

$$p(x_j) = \frac{1}{1 + \exp\{-\lambda(x_j - \theta_s)\}}, \tag{3.13b}$$

where $\theta_s = -0.25$ is the threshold and $\lambda = 10$. The threshold is chosen so that every spike in the single neuron burst can reach the threshold. In the limit $\lambda \to \infty$, the above sigmoid function reduces to a Heaviside step function.

We are now in a position to consider a network of m excitatory HR neurons with bidirectional electrical coupling and unidirectional excitatory chemical coupling. The equations of motion are the following. For, $i = 1, \ldots, m$,

$$\begin{aligned}
\dot{x}_i &= f(x_i) + y_i - z_i + q + d\sum_{j=1}^{m} g_{ij}x_j - g_s(x_i - v)\sum_{j=1}^{m} c_{ij}p(x_j), \\
&= f(x_i) + y_i - z_i + q + d\sum_{j=1}^{m} g_{ij}x_j - g_s k(x_i - v)p(x_i) - g_s(x_i - v)\sum_{j=1}^{m} d_{ij}p(x_j), \\
\dot{y}_i &= -y_i - 5x_i^2 + 1, \\
\dot{z}_i &= \mu(b(x_i - x_0) - z_i),
\end{aligned} \tag{3.14}$$

where

$$\boldsymbol{G} =: (g_{ij}),\ \sum_{j=1}^{m} g_{ij} = 0 \text{ for all } i, \tag{3.15a}$$

$$\boldsymbol{C} =: (c_{ij}),\ c_{ij} = 0 \text{ or } 1,\ c_{ii} = 0,\ \sum_{j=1}^{m} c_{ij} = k \text{ for all } i, \tag{3.15b}$$

and

$$\boldsymbol{S} =: (d_{ij}), \text{ and } d_{ij} = \begin{cases} -k & \text{if } i = j, \\ c_{ij} & \text{if } i \neq j. \end{cases} \tag{3.15c}$$

Here k represents the number of chemical signals each neuron receives. Moreover, d is the coupling strength for electrical synapses via gap junctions, and coupling matrix $\boldsymbol{G}$ is a symmetric matrix with vanishing row sums and nonnegative off-diagonal entries. It should be noted that the symmetry of $\boldsymbol{G}$ is a biological assumption. From the mathematical side, our analysis here is capable of treating unsymmetrical matrices with both positive and negative off-diagonal entries. $\boldsymbol{C}$ is the connection matrix of the chemical coupling which is not necessarily symmetric; $c_{ij} = 1$ if neuron i receives synaptic current(via chemical synapses) from neuron j, otherwise $c_{ij} = 0$. The matrix $\boldsymbol{S}$ has all row sums being zero and nonnegative off-diagonal entries.

We next describe the synchronous equation of HR network (3.14). On the syn-

chronous manifold, its dynamics is governed by the following equations

$$\begin{aligned}
\dot{x} &= f(x) + y - z + q - kg_s(x - v)p(x), \\
\dot{y} &= -y - 5x^2 + 1, \\
\dot{z} &= \mu(b(x - x_0) - z).
\end{aligned} \tag{3.16}$$

To study local synchronization, we begin with the derivation of the variational equation of (3.14) along the synchronous manifold $\mathfrak{M}$. The equation is

$$\begin{aligned}
\dot{u}_i = f'(x(t))u_i + v_i - w_i + \left[d\sum_{j=1}^{m} g_{ij}u_j \right] - kg_s p(x(t))u_i \\
- \left[g_s(x(t) - v)p'(x(t)) \sum_{j=1}^{m} c_{ij}u_j \right], \\
\dot{v}_i = -v_i - 10x(t)u_i, \\
\dot{w}_i = \mu(bu_i - w_i),
\end{aligned} \tag{3.17}$$

where $x(t)$ lies on the synchronous manifold of (3.14) and satisfies equation (3.16).

In vector-matrix form, (3.17) becomes

$$\begin{aligned}
\dot{\boldsymbol{u}} &= \{[f'(x(t)) - kg_s p(x(t))]\,\boldsymbol{I} + d\boldsymbol{G} \\
&\quad - g_s(x(t) - v)p'(x(t))\boldsymbol{C}\}\boldsymbol{u} + \boldsymbol{v} - \boldsymbol{w}, \\
&= \{[f'(x(t)) - kg_s p(x(t)) - kg_s(x(t) - v)p'(x(t))]\,\boldsymbol{I} \\
&\quad + d\boldsymbol{G} - g_s(x(t) - v)p'(x(t))\boldsymbol{S}\}\boldsymbol{u} + \boldsymbol{v} - \boldsymbol{w}, \qquad (3.18a) \\
\dot{\boldsymbol{v}} &= -10x(t)\boldsymbol{u} - \boldsymbol{v}, \qquad (3.18b) \\
\dot{\boldsymbol{w}} &= \mu b\boldsymbol{u} - \mu\boldsymbol{w}. \qquad (3.18c)
\end{aligned}$$

To study synchronized HR neurons (3.14), we first apply a coordinate transformation, developing in Subsection 2.3.1, on $\boldsymbol{G}$ so that the resulting matrix has a negative matrix measure as possible. The structure of linear system (3.18) is then explored so that the theory of some monotone dynamics and time averaging estimates described in Section 2.1 can be applied to make the linear system asymptotically stable.

Let $\boldsymbol{E}$ be chosen from $\mathfrak{O}$ given in Definition 2.3.1 and define $\boldsymbol{A}$ as in it. Let

$$\tilde{\boldsymbol{x}} = \boldsymbol{A}\begin{pmatrix} u_1 \\ \vdots \\ u_m \end{pmatrix},\ \tilde{\boldsymbol{y}} = \boldsymbol{A}\begin{pmatrix} v_1 \\ \vdots \\ v_m \end{pmatrix},\ \tilde{\boldsymbol{z}} = \boldsymbol{A}\begin{pmatrix} w_1 \\ \vdots \\ w_m \end{pmatrix},$$

and $\bar{\boldsymbol{x}} = (\overline{x}_1, \ldots, \overline{x}_{m-1})^T$. As well, $\bar{\boldsymbol{y}}$, $\bar{\boldsymbol{z}}$ be similarly defined, and for any given matrix $\boldsymbol{B}$, we define

$$\overline{\boldsymbol{B}} = \boldsymbol{E}\boldsymbol{B}\boldsymbol{E}^{\dagger}. \tag{3.19}$$

Then their motions of dynamics read

$$\begin{aligned}
\dot{\bar{\boldsymbol{x}}} &= \{[f'(x(t)) - kg_s p(x(t)) - kg_s(x(t) - v)p'(x(t))]\,\boldsymbol{I} \\
&\quad + d\overline{\boldsymbol{G}} + g_s(v - x(t))p'(x(t))\overline{\boldsymbol{S}}\}\bar{\boldsymbol{x}} + \bar{\boldsymbol{y}} - \bar{\boldsymbol{z}}, \\
&:= \widetilde{\boldsymbol{H}}(t)\bar{\boldsymbol{x}} + \bar{\boldsymbol{y}} - \bar{\boldsymbol{z}}. && \text{(3.20a)} \\
\dot{\bar{\boldsymbol{y}}} &= -10x(t)\bar{\boldsymbol{x}} - \bar{\boldsymbol{y}}, && \text{(3.20b)} \\
\dot{\bar{\boldsymbol{z}}} &= \mu b\bar{\boldsymbol{x}} - \mu\bar{\boldsymbol{z}}. && \text{(3.20c)}
\end{aligned}$$

Instead of calculating the transverse Lyapunov exponents of the corresponding variational equation (3.17) of equation (3.14), we would prove directly that the origin of (3.20) is asymptotically, exponentially stable. As a consequence, all transverse Lyapunov exponents of (3.14) are negative.

Sufficient conditions to obtain the synchronization of coupled HR system (3.14) are stated precisely in the following.

Theorem 3.2.1. *(i) Assume $x(t)$ satisfies synchronous equation (3.16). Let λ_2 be the second largest eigenvalue of coupling matrix $\boldsymbol{G}$. Let $r_2 = \mu_2(\overline{\boldsymbol{S}})$, the matrix measure of $\overline{\boldsymbol{S}}$ with respect to 2-norm. Here $\overline{\boldsymbol{S}}$ is defined in (3.19). Set $\alpha =: -1 - \frac{r_2}{k}$ and*

$$h_{kg_s,\alpha}(x) = f'(x) + kg_s\left[-p(x) - (v - x)p'(x)\alpha\right]. \tag{3.21a}$$

Define

$$\sup_x h_{kg_s,\alpha}(x) =: \begin{cases} (h_\alpha)kg_s & \text{if } kg_s \neq 0, \\ d_1 & \text{if } kg_s = 0, \end{cases} \tag{3.21b}$$

where h_α *is a constant and* $d_1 = \max_{x\in\mathbb{R}} f'(x) \approx 2.253$. *Let* $d_0 = \sup_{x(t)} 10|x(t)| \le 20$. *Then coupled HR system* (3.14) *is locally synchronized provided that*

$$(-\lambda_2)d + (-h_\alpha)kg_s > 24 > d_0 + b, \text{ for } kg_s > 0, \text{ and}$$
$$-\lambda_2 d > 26.253 > d_0 + b + d_1, \text{ for } kg_s = 0. \tag{3.21c}$$

(ii) Assume that $\lim_{t\to\infty} x(t) = x_c$. *Let* $\lim_{t\to\infty} \widetilde{\boldsymbol{H}}(t) := \widetilde{\boldsymbol{H}}_c$. *Here* $\widetilde{\boldsymbol{H}}(t)$ *is defined in* (3.20a). *Then system* (3.14) *is locally synchronized if all real parts of eigenvalues of*

$$\begin{pmatrix} \widetilde{\boldsymbol{H}}_c & \boldsymbol{I} & -\boldsymbol{I} \\ -10x_c\boldsymbol{I} & -\boldsymbol{I} & \boldsymbol{0} \\ \mu b\boldsymbol{I} & \boldsymbol{0} & -\mu\boldsymbol{I} \end{pmatrix} =: \overline{\boldsymbol{H}}_c$$

are negative.

Proof. To obtain local synchronization of (3.14), we study equations (3.20). Note that for excitatory HR neurons, $x(t) < v = 2$ for all t. Clearly, $\mu_2(\widetilde{\boldsymbol{H}}(t)) \le \lambda_2 d + h_\alpha k g_s =: \lambda$. Here h_α is defined in (3.21b). Then by equation (3.20), we have

$$D_l\|\bar{\boldsymbol{x}}(t)\| \le \lambda\|\bar{\boldsymbol{x}}(t)\| + \|\bar{\boldsymbol{y}}(t)\| + \|\bar{\boldsymbol{z}}(t)\|, \tag{3.22a}$$
$$D_l\|\bar{\boldsymbol{y}}(t)\| \le d_0\|\bar{\boldsymbol{x}}(t)\| - \|\bar{\boldsymbol{y}}(t)\|, \tag{3.22b}$$
$$D_l\|\bar{\boldsymbol{z}}(t)\| \le \mu b\|\bar{\boldsymbol{x}}(t)\| - \mu\|\bar{\boldsymbol{z}}(t)\|. \tag{3.22c}$$

Applying Proposition 2.1.1-(ii), we see that the first part of the assertion of the theorem holds true provided the real parts of the eigenvalues of

$$\boldsymbol{B} = \begin{pmatrix} \lambda & 1 & 1 \\ d_0 & -1 & 0 \\ \mu b & 0 & -\mu \end{pmatrix} \tag{3.23}$$

are negative. Indeed, the Routh-Hurwitz Criterion asserts that it occurs whenever $-\lambda > d_0 + b$. So the first assertion of the Theorem holds true.

The last assertion of the Theorem is a direct consequence of Proposition 2.1.2. □

If the steady-state synchronization is considered, then some easier verifiable conditions than those stated in Theorem 3.2.1-(ii) can be obtained.

Corollary 3.2.1. *Let $d = 0$. Assume $\lim_{t\to\infty} x(t) = x_c$. Then system (3.14) without electrical coupling is locally synchronized if the real parts of the eigenvalues of $\overline{\boldsymbol{A}}$ are negative, where*

$$\overline{\boldsymbol{A}} = \begin{pmatrix} h_{kg_s,-1}(x_c) & 1 & -1 \\ -10x_c & -1 & 0 \\ \mu b & 0 & -\mu \end{pmatrix}. \tag{3.24}$$

Proof. Note that $\overline{\boldsymbol{H}}_c$ with $d = 0$ has the following form.

$$\begin{pmatrix} f'(x_c) + kg_s\left[-p(x_c) + (v - x_c)p'(x_c)\right] & 1 & -1 \\ -10x_c & -1 & 0 \\ \mu b & 0 & -\mu \end{pmatrix}$$
$$\otimes \boldsymbol{I}_{m-1} + \begin{pmatrix} \boldsymbol{I}_1 & \boldsymbol{0} \\ \boldsymbol{0} & \boldsymbol{0} \end{pmatrix} \otimes (g_s(v - x_c)p'(x_c)\overline{\boldsymbol{S}}).$$

Applying Proposition 2.1.3, we have that system (3.14) is locally synchronized provided that

$$\begin{pmatrix} \gamma & 1 & -1 \\ -10x_c & -1 & 0 \\ \mu b & 0 & -\mu \end{pmatrix},$$

where $\gamma = f'(x_c) + kg_s\left[-p(x_c) + (v - x_c)p'(x_c)\right] + g_s(v - x_c)p'(x_c)\bar{\lambda}_i$ and $\bar{\lambda}_i \in \sigma(\overline{\boldsymbol{S}})$, have all its eigenvalues with negative real parts.

Define matrix $\boldsymbol{A}(x)$ as

$$\boldsymbol{A}(x) = \begin{pmatrix} f'(x_c) + x & 1 & -1 \\ -10x_c & -1 & 0 \\ \mu b & 0 & -\mu \end{pmatrix}.$$

Then it can be proved by applying the Routh-Hurwitz Criterion that for any $y < x \leq 0$, if all eigenvalues of $\boldsymbol{A}(x)$ have positive real parts, then so do those of $\boldsymbol{A}(y)$.

Upon using the above observation and the fact that $\bar{\lambda}_i$, the real parts of eigenvalues of $\overline{\boldsymbol{S}}$, are negative, we conclude that the assertion of the Corollary holds true. □

Corollary 3.2.2. *Let $\boldsymbol{C}$ be a node-balancing matrix, i.e., its row sums and column sums are equal. Assume $\lim_{t\to\infty} x(t) = x_c$. Then system (3.14) is locally synchronized if all real parts of the eigenvalues of $\overline{\boldsymbol{A}}$, as given in (3.24), are negative.*

Proof. As in the proof of Corollary 3.2.1, it suffices to show that all real parts of the eigenvalues of $d\overline{\boldsymbol{G}} + g_s(v - x_c)p'(x_c)\overline{\boldsymbol{S}}$ are negative. However, by Theorem 2.1.1, we have $\lambda_{\max}(d\overline{\boldsymbol{G}} + g_s(v - x_c)p'(x_c)\overline{\boldsymbol{S}}) \leq \mu_2(d\overline{\boldsymbol{G}} + g_s(v - x_c)p'(x_c)\overline{\boldsymbol{S}}) \leq d\mu_2(\overline{\boldsymbol{G}}) + g_s(v - x_c)p'(x_c)\mu_2(\overline{\boldsymbol{S}}) \leq 0$. Thus, the proof of the Corollary is completed. □

Remark 3.2.1. *(i) To acquire synchronization of coupled networks, the second largest eigenvalue of the coupling matrix plays an inescapable and decisive role. Indeed, in certain cases, such as the system is fully coupled, the necessary and sufficient condition [83] with $k = 0$ for local synchronization is*

$$h_{\max} + d\lambda_2 < 0.$$

Here $h_{\max}$ is the largest Lyapunov exponent of the individual oscillator. In most of interesting networks, λ_2 becomes closer to the origin from the left as the number of oscillators grows. Hence, it takes greater coupling strengths to synchronize the larger system. In other cases, such as the coupled map lattices (1.2)*, the system exhibits the size instability phenomena, that is, the system with the number of nodes greater than a certain critical value loses its synchrony regardless how strong the coupling strength is. Such size instability is induced by the competition between a certain eigenvalues, including λ_2, of the coupling matrix, we will study it in the next chapter.*

(ii) If the connection $\boldsymbol{C}$ is symmetric, then r_2 is the second largest eigenvalue of $\boldsymbol{S}$. It is easy to see that if the connection network is all-to-all coupled, then $k = m - 1$, $r_2 = -m$, and so $\alpha = \frac{1}{m-1} \leq 1$. It can be computed that the denser the network is coupled, the larger α is. Hence, α is an indicator of how densely coupled the system is. Note also that $-1 < \alpha \leq 1$. We shall call α the density *of the coupling network.*

We also mention that the computation cost to verify the synchronous conditions (3.21c) or (3.24) is very little as compared to that of computing second Lyapunov exponent of the network. Specifically, if HR system (3.14) is both electrically and chemically coupled, one needs to check the inequality (3.21c) to see if the system is synchronized. To check the steady-state synchronization, one only needs to verify the sign of the largest real part of eigenvalues of a 3×3 matrix, $\overline{\boldsymbol{A}}$, see (3.24), regardless of the number of neurons.

3.2.3 Further Discussions and Numerical results

In the subsection, we shall focus on applying Theorem 3.2.1 and Corollaries 3.2.1, 3.2.2 to coupled HR neurons (3.14) to extract more detailed synchronization phenomena. To this end, we need to know, firstly, the dynamics on synchronous manifold.

(I) **Dynamics on synchronous manifold**

We begin with the study of the dynamics of synchronous equation (3.16). Its dynamics is to be provided numerically. For $q = 4$, $a = 2.6$, $x_0 = -1.6$, $\mu = 0.01$, $b = 4$ and $v = 2$, the single HR neuron model, i.e., $g_s = 0$, is capable of producing major neuronal behavior, bursting. (see e.g., [44]). Furthermore, such neuron is excitatory, i.e., $x(t) < v = 2$ for all $t \geq 0$. We shall treat kg_s as a bifurcation parameter. The corresponding dynamical behavior of equation (3.16) is summarized in Table 3.1. A similar result to Table 3.1 was also reported in Fig. 2 of [16]. On the synchronous manifold, the solution trajectory $x(t)$ of (3.16), depending on initial conditions and kg_s, may settle into various stable states. Figure 3.4 provides the maximum Lyapunov exponent (MLE) of synchronous equation (3.16) versus kg_s. For $0 \leq kg_s \leq 0.85$, there is a set of initial conditions with positive measure for which their corresponding MLE is positive. However, for $0.809 \leq kg_s \leq 0.85$, there is also a set of initial conditions with positive measure for which its corresponding MLE is negative. For instance, if $0.809 \leq kg_s \leq 0.813$, then there are sets of initial conditions with positive measure so that the solution trajectories of (3.16) converge to a stable periodic solution (see Fig. 3.5) and stable regular bursting (see Fig. 3.6), respectively. Specifically, let (x_c, y_c, z_c) be the steady state of (3.16) (see, Fig. 3.7), and let

$$C_r = \{(x, y, z) : |x - x_c| < r, |y - y_c| < r, \text{ and } |z - z_c| < r\}, \tag{3.25a}$$

and

$$I_r = \{(x, y, z) : |x - x_c| > r, |y - y_c| > r, \text{ and } |z - z_c| > r\}. \tag{3.25b}$$

In fact, our numerical results suggest that the following hold. Pick, for instance, $kg_s = 0.812$. If the initial condition (x_0, y_0, z_0) is randomly chosen from $C_{0.02}$ (resp.,

I_1), then its trajectory converges to a periodic orbit (resp., a stable regular bursting) (see Figs. 3.5, 3.6). Similarly, for $kg_s \in [0.814, 0.85]$, synchronous equation (3.16) also exhibits rich dynamics showing the coexistence of stable multi states. Moreover, if $kg_s \geq 0.814$, the numerical results suggest that the corresponding steady state is locally stable. In fact, a direct calculation shows that a Hopf bifurcation occurs near 0.813. Furthermore, if one performs the linearized stability at the steady-state (x_c, y_c, z_c), then one sees that (x_c, y_c, z_c) is stable whenever $kg_s \geq 0.814$ (see Fig. 3.8). Such analysis of linearized stability provided some supportive evidence for the validity of Table 3.1.

Table 3.1: The dynamics of synchronous equation (3.16) with various range of kg_s. The multi-stability of (3.16) is observed with $kg_s \in [0.809, 0.85]$.

kg_s	$kg_s < 0.808$	$0.809 \leq kg_s \leq 0.813$	$0.814 \leq kg_s \leq 0.85$	$kg_s \geq 0.87$
Types	Stable regular bursting	Stable regular bursting Stable periodic solution	Stable regular bursting Stable steady state	Stable steady state

In summary, the numerical results suggest that on the synchronous manifold, for kg_s small, the regular bursting behavior of single HR persists. For kg_s in an intermediate range, the multistability of equation (3.16) occurs. Depending on initial conditions, the coexistence of multi stability states including a stable regular bursting and a stable periodic solution/a stable fixed point could be observed. When kg_s becomes large, equation (3.16) has a globally asymptotically stable fixed point. Such complex dynamical behavior of synchronous equation (3.16) leads to the possibility of stable multi-state synchronization of coupled HR neurons (3.14). If the initial conditions and the range of kg_s are so chosen that the corresponding synchronous equation leads to a regular bursting solution, then the associated coupled HR neurons (3.14) achieves stable regular bursting synchronization. Likewise, we define stable periodic synchronization and stable steady-state synchronization accordingly. As we can see, via Table 3.1, that for $0.809 \leq kg_s \leq 0.85$, the coexistence of stable multi-state synchronization of coupled HR neurons (3.14) could be observed. It should also be mention that the theory of weakly coupled oscillators has often been used to analyze networks of neuron coupled by small chemical synapses g_s, see e.g. [60], and the many related

work cited therein. Using this theory enables one to obtain some extensive analytical insight. Furthermore, the ups and downs of synaptic strength can be controlled. For instant, N-methyl-aspartate receptors can both boost and dampen synaptic efficiency in the brain [10]. Such observations give the justification for the consideration of small chemical synapses g_s.

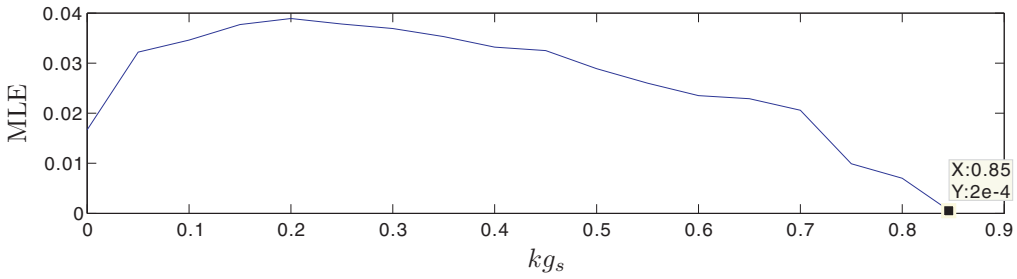

Figure 3.4: The maximum Lyapunov exponent (MLE) of synchronous equation (3.16) is computed for various kg_s. For $0 \leq kg_s \leq 0.85$, MLE> 0 for a set of initial conditions with positive measure. For $kg_s \in [0.809, 0.85]$, there is also a set of initial conditions for which its corresponding MLE< 0.

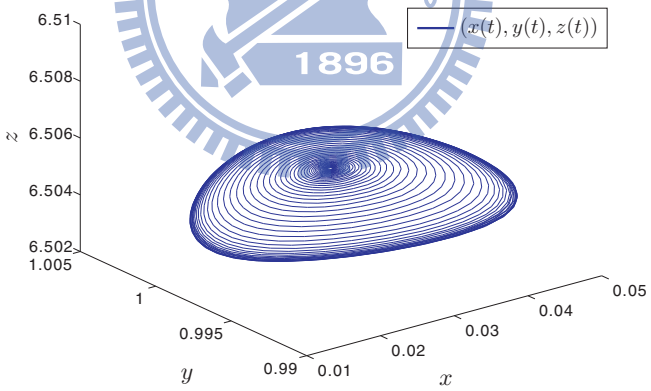

Figure 3.5: The solution trajectory with randomly chosen initial conditions from $C_{0.02}$ converges to a stable periodic orbit. Here $kg_s = 0.812$.

(II) **Neurons with only chemical synapse**

In [6], a local steady-state synchronization of bursting neurons with no electrical

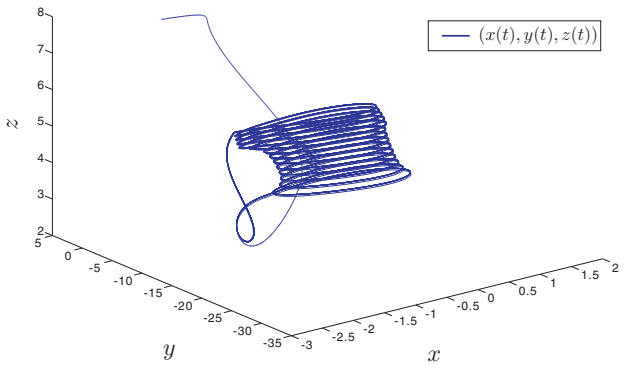

Figure 3.6: The solution trajectory with randomly chosen initial conditions from I_1 converges to a stable regular bursting. Here $kg_s = 0.812$.

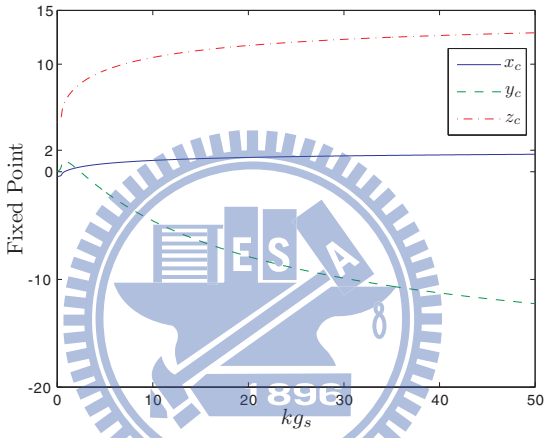

Figure 3.7: Fixed points (x_c, y_c, z_c) for different values kg_s. The fixed point (x_c, y_c, z_c) tends to $(2, -19, 14.4)$ as kg_s tends to infinity.

coupling is studied without providing mathematical details. Moreover, their approach fails to see if synchronization of neurons can be achieved when the networks are intermediately and sparsely coupled. Their major contribution was to prove that the bound for achieving synchronization of HR neurons depends only on the number k of chemical signals each neuron receives, and is independent of all other details of the network topology. From (3.21a) and (3.21c), it is clear that the larger the density α of the network is, the greater chance coupled HR neurons (3.14) gets synchronized. In the following, we shall prove that the system of coupled HR neurons (3.14) achieves

steady-state synchronization regardless how sparsely the network is coupled provided that $kg_s \geq 0.87$.

By Corollary 3.2.1, it suffices to show that the maximum real part $\lambda_{\max}(\overline{\boldsymbol{A}})$ of eigenvalue of matrix $\overline{\boldsymbol{A}}$ defined in (3.24) is negative. From Fig. 3.8, we see that $\lambda_{\max}(\overline{\boldsymbol{A}}) < 0$ whenever $kg_s \geq 0.814$. Upon taking into consideration of the dynamics on synchronous manifold as provided in Table 3.1, we have the following conclusion.

Coupled HR neurons (3.14) *with* $d = 0$ *achieves the steady-state synchronization for a set of initial conditions with positive measure whenever* $kg_s \geq 0.814$ *regardless how sparsely the network is coupled, which improves the result obtained in [6]. Moreover, the system acquires the steady-state local synchronization for all initial conditions sufficiently close to each other whenever* $kg_s \geq 0.87$.

Numerically, the following scenarios are also observed. Coupled two HR neurons achieves synchronization only when $kg_s \geq 0.809$. Stable regular bursting and steady-state synchronization is found on a set of initial conditions with positive measure, respectively, whenever $kg_s \approx 0.85$. Such numerical results are illustrated in Figs. 3.9 and 3.10.

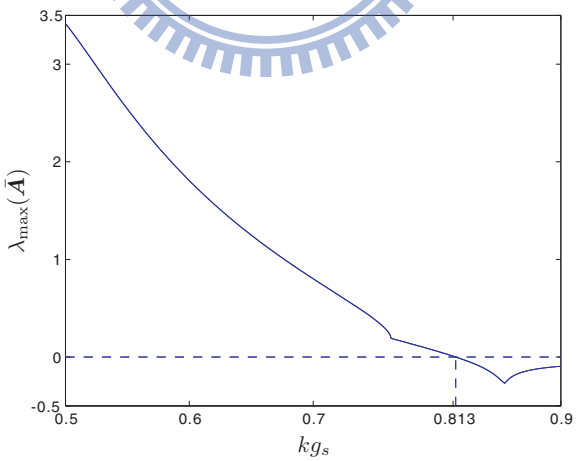

Figure 3.8: The maximum eigenvalue of the linearized operator with respect to the synchronous equation (3.16) is computed for various kg_s.

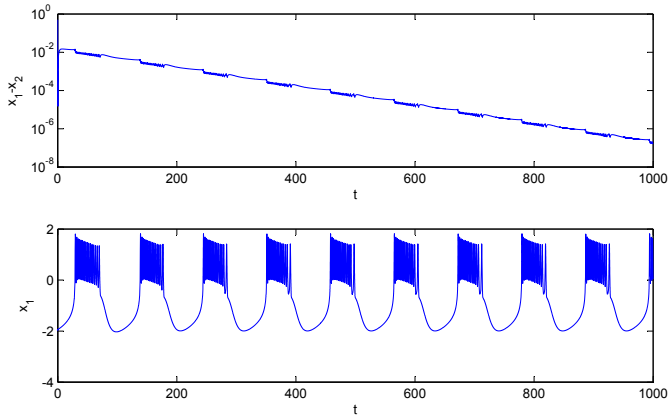

Figure 3.9: The time series of $x_1(t) - x_2(t)$ and $x_1(t)$. The graphs demonstrate the stable regular bursting synchronization. Here $g_s = 0.85$, initial $= [-2, -18, 3, -2.5, -18.5, 2.5]$.

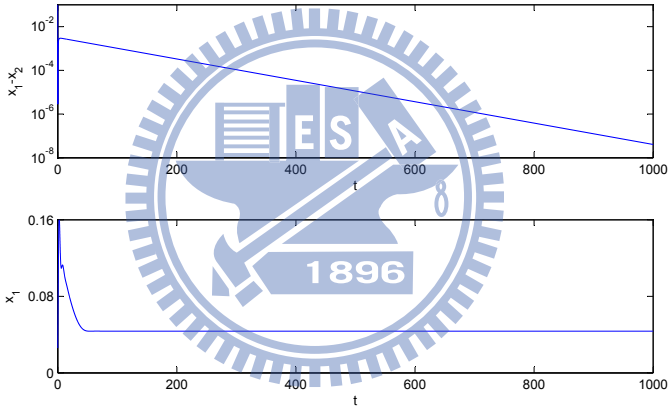

Figure 3.10: The time series of $x_1(t) - x_2(t)$ and $x_1(t)$. The graphs demonstrate the stable steady-state synchronization. Here $g_s = 0.85$, initial $= [0.026, 1, 6.5, 0.126, 1.1, 6.6]$.

(III) **Neural synchronization with only electrical synapse**

For $g_s = 0$, by Theorem 3.2.1, we obtain stable regular bursting synchronization whenever $d > \frac{d_0+b+d_1}{-\lambda_2} =: d_{\min}$. Consider, for instance, a ring of $2K$-nearest-neighbor mutually coupled networks, the predicted minimum electrical coupling strength $d_{\min}$ is

computed with the number m of neurons and K being given. Note that in such case

$$\lambda_2 = -4\sum_{i=1}^{K}\sin^2\frac{i\pi}{m} = \frac{\sin\left((K+\frac{1}{2})\frac{2\pi}{m}\right) - \sin\frac{\pi}{m}}{\sin\frac{\pi}{m}} - 2K. \tag{3.26a}$$

The results are listed in Table 3.2. For instance, given a number of (10^4+1) neurons, it takes the electrical coupling strength 6.66×10^7 or greater to reach synchrony for a network with the nearest-neighbor coupling. It only takes 2.7×10^{-3} or greater to do so for an all-to-all network. If the coupling matrix $\boldsymbol{G}$ is of high dimension and without fine structure for computers to be able to calculate its second largest eigenvalue effectively, one may use some known estimates to find the upper bound of λ_2. For instance, we have that (see e.g., [70])

$$\lambda_2 \le \frac{-2}{(m-1)\bar{\rho}(\boldsymbol{G}) - \frac{m-2}{2}}, \tag{3.26b}$$

where $\bar{\rho}(\boldsymbol{G})$ is the mean distance of the graph associated with $\boldsymbol{G}$. Upper bounds for $d_{\min}$ by using (3.26b) are listed in the Table 3.2, too. For $m = 10^4+1$, the upper bounds of $d_{\min}$ are 3.29×10^8 and 65640, respectively, for a network with the nearest-neighbor coupling and all-to-all coupling. In a nutshell, connecting each neuron to more neighbors is an effective way for large-size networks to lower the synchronization threshold.

The upper bound for λ_2 in (3.26b) is quite good for the sparsely coupled networks. Indeed, in the case of the nearest-neighbor coupling, the exact value of λ_2 and its estimated upper are both $O(\frac{1}{m^2})$. On the other hand, if the network is densely coupled, the upper bound in (3.26b) gives a poor estimate for λ_2. Nevertheless, if one picks other type of upper bound for λ_2, better estimates could be expected. For example, it is also known, see e.g. [103], that

$$\lambda_2 \le -\frac{m}{\beta}, \tag{3.26c}$$

where $\beta > 0$ is such that $\beta\boldsymbol{G} + \boldsymbol{L}$ is negative semidefinite. Here $\boldsymbol{L}$ is the Laplacian matrix of the complete graph, i.e., $\boldsymbol{L} = m(\boldsymbol{I} - \boldsymbol{e}\boldsymbol{e}^T)$, where $\boldsymbol{e}$ is given as in (2.7a). For the all-to-all coupling, it is readily verified that $\beta\boldsymbol{G} + \boldsymbol{L}$ with $\beta = 1$ is negative

Table 3.2: The first component of the pair in the table gives the predicted minimum electrical coupling strength $d_{\min}$ by using the exact value of λ_2. For instance, with $m = 10^2 + 1$, $K = \left[\frac{m-1}{4}\right] = 25$, the predicted minimum electrical coupling strength is $d_{\min} = 1.4$. The second component of the pair in the table is the upper bound of $d_{\min}$ by using (3.26b).

m	21	$10^2 + 1$	$10^4 + 1$
$K = 1$ (the nearest-neighbor coupling)	$(296, 1320)$	$(6786, 32824)$	$(6.66 \times 10^7, 3.29 \times 10^8)$
$K = [\frac{m-1}{4}]$	$(6.10, 269)$	$(1.40, 1320)$	$(0.0145, 1.32 \times 10^5)$
$K = \frac{m-1}{2}$ (the all-to-all coupling)	$(1.26, 138)$	$(0.27, 663)$	$(0.0027, 65640)$

semidefinite. Consequently, the equality in (3.26c) can be achieved, which yields the best possible estimate.

(IV) **Neural synchronization with both excitatory chemical and electrical synapses**

Herein, networks with both excitatory electrical and chemical connections are considered. To extract more information on synchronization of the system, we further assume $\boldsymbol{C}$ to be a node-balancing matrix. We first observe that $x(t) < v$ and $p'(x(t)) \geq 0$ for all t. So h_α, defined in (3.21b), is decreasing in α. If

$$(-\lambda_2)d + (-h_{-1})kg_s > 24, \tag{3.27}$$

then (3.21c) is also satisfied. The synchronization region satisfying (3.27) and $kg_s \geq 0.87$ is demonstrated in Fig. 3.11. That is to say, if $(-\lambda_2 d, kg_s)$ is chosen from the shaded region in Fig. 3.11, then multi-state or single-state synchronization can be realized depending on the range of kg_s. Consider, for instance, coupled two HR neurons. Let $kg_s = 0.812$ and $d = 30$. If $(x_i(0), y_i(0), z_i(0)) \in C_{0.02}$ (resp., I_1), $i = 1, 2$, as given in (3.25a) (resp., (3.25b)), and are distinct, then the stable periodic (resp., stable regular bursting) synchronization occurs (see Figs. 3.12, 3.13).

We further observe that there exists a t_1 such that $h_{-1} < 0$ (resp., $h_{-1} > 0$) whenever $kg_s \in [0, t_1) =: J_1$ (resp., $kg_s \in (t_1, 0.87] =: J_2$) (see Fig. 3.11). Here $t_1 \approx 0.6044$. Hence, both chemical and electrical synapses enforce the synchronization

phenomena whenever $kg_s \in J_1$. For $kg_s \in J_2$, the chemical synapses play dragging roles for system to reach synchrony. To synchronize, the electrical synapses have to be strong enough to suppress the dragging force created by chemical synapses. Such t_1 is called a *turning point* for h_{-1}.

We are then led to compute turning points for h_α (see Fig. 3.14). For $\alpha \geq -0.67$ the corresponding turning points are $kg_s = 0.87$. Hence, for $0 \leq kg_s < 0.87$, if the density α of the coupling network is at least -0.67, then chemical synapses can also enforce the synchrony of the system.

To summarize, a synchronization region is obtained in Fig. 3.11. Particularly, multi-state synchronization of coupled HR neurons can be realized whenever $kg_s \in [0.809, 0.85]$ *and* $(-\lambda_2 d, kg_s)$ *lies in the synchronization region. Furthermore, for* $0 \leq kg_s < 0.87$*, if the density* α *of the coupling network is at least* -0.67*, then chemical synapses can enforce the synchrony of the system.*

To conclude this section, we will elaborate more on some crucial points.

(i) As evidence in Table 3.1, the multi-stable state, which depends on the choice of the initial conditions exist in excitatory HR neuron. In fact, other choice of parameters, such as $a = 3$, $\mu = 0.006$, $q = 3$, $x_0 = 1.56$, $b = 4$, would result the neurons burst irregularly (chaotically). Under such circumstance, the presence of both stable chaotic attractor and stable periodic state can be detected. And our approach can be applied to the above described scenario as well.

(ii) From inequality (3.21c), we see that the denser the coupling network is, or equivalently, the larger the density α is, the easier the system gets synchronized.

(iii) We mention that free packages SLEPc developed by V. Hernández, J. E. Román, A. Tomás, and V. Vidal [38] can be used to compute λ_2 efficiently.

(iv) In vivo experiments, the strength of an excitatory mono-synaptic connection has a biologically realistic value $g_s = 0.66 \times 10^{-3}$ (see e.g., [9]). Using such g_s and our theory, we may conclude that if the number of presynaptic neurons that connect to a single cortical neuron is greater than 1319 and in between 1226 and 1288, then the system may reach steady-state synchronization and multistate synchronization,

respectively. It should be mentioned that the quantitative description of the circuit of cat area 17 is given in [9]. Depending on the cell type and its layer location, the presynaptic synapses could range from 0 to 3500. For instance, it seems that excitatory cell types ss4(L4), p5(L2/3), p6(L4) and p6(L5/6) are the most likely candidates to generate multistate synchronization.

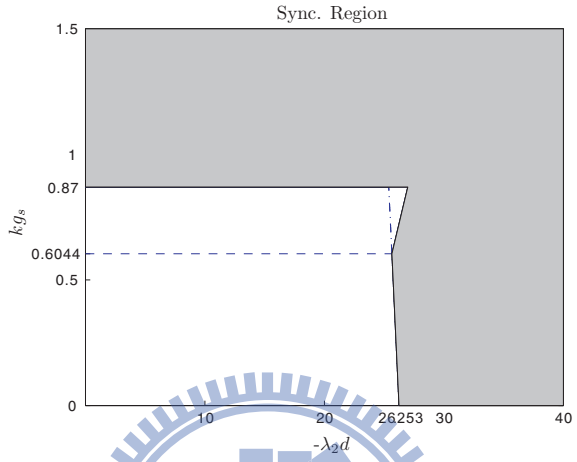

Figure 3.11: The shaded area is the synchronization region satisfied by (3.27) and $kg_s \geq 0.87$.

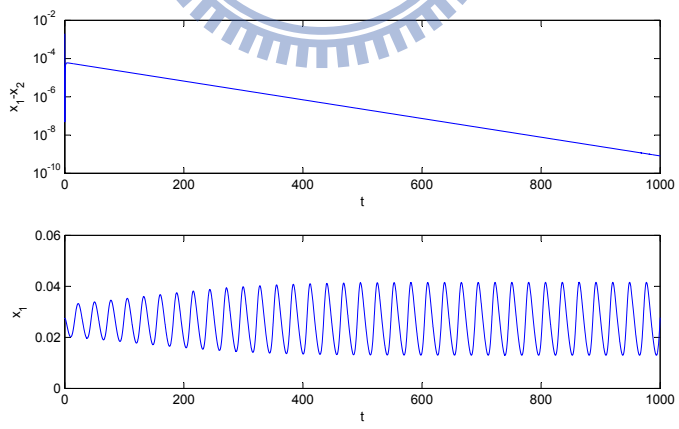

Figure 3.12: The time series of $x_1(t) - x_2(t)$ and $x_1(t)$. The graphs demonstrate the stable periodic synchronization. Here $d = 30$, $g_s = 0.812$, initial $= [0.26459e-1+r, 0.996499+r, 6.5058+r, 0.26459e-1-r, 0.996499-r, 6.5058-r]$ and $r = 0.001$.

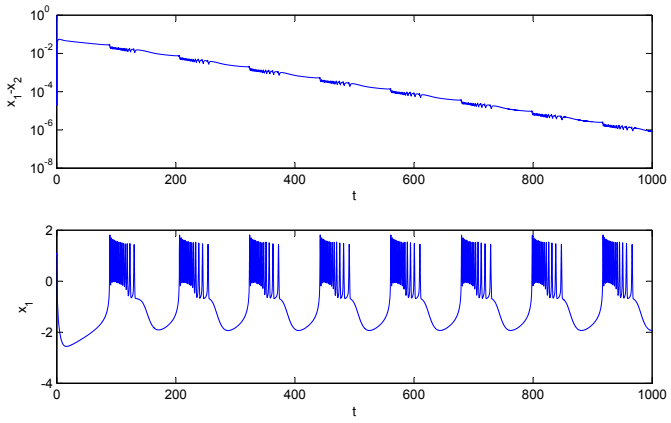

Figure 3.13: The time series of $x_1(t) - x_2(t)$ and $x_1(t)$. The graphs demonstrate the stable regular bursting synchronization. Here $d = 30$, $g_s = 0.812$, initial= $[0.26459e - 1 + r, 0.996499 + r, 6.5058 + r, 0.26459e - 1 - r, 0.996499 - r, 6.5058 - r]$ and $r = 1$.

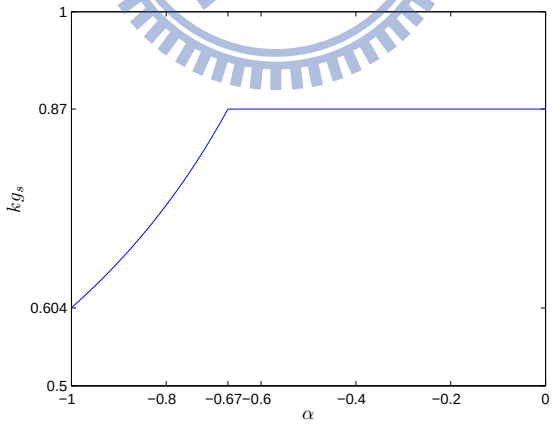

Figure 3.14: Turning points of h_α.

Chapter 4

Synchronization in Model II

In this chapter, we consider the synchronization in CMLs (1.2). Throughout the chapter, we, as usual, assume coupling matrix $\boldsymbol{G}$ satisfies

$$\begin{aligned} &\text{(i) } \lambda = 0 \text{ is a simple eigenvalue of } \boldsymbol{G} \text{ and} \\ &\quad \boldsymbol{e} = \tfrac{1}{\sqrt{m}}(1, 1, \ldots, 1)^T_{1\times m} \text{ is its corresponding eigenvector.} \end{aligned} \tag{4.1}$$

4.1 Local Synchronization Criteria

To study the stability of the synchronous manifold $\mathfrak{M} = \{\boldsymbol{x}_i = \boldsymbol{s}, \forall i\}$ of CMLs (1.2), we consider the variational equation of (1.2):

$$\begin{aligned} \boldsymbol{\xi}(k+1) &= D\boldsymbol{F}(\boldsymbol{s}(k))\boldsymbol{\xi}(k) + d(\boldsymbol{G}\otimes\boldsymbol{I})D\boldsymbol{F}(\boldsymbol{s}(k))\boldsymbol{\xi}(k) \\ &= \left[\boldsymbol{I}\otimes D\boldsymbol{f}(\boldsymbol{s}(k)) + d\left(\boldsymbol{G}\otimes\boldsymbol{I}\right)\left(\boldsymbol{I}\otimes D\boldsymbol{f}\left(\boldsymbol{s}(k)\right)\right)\right]\boldsymbol{\xi}(k), \end{aligned} \tag{4.2a}$$

where $\boldsymbol{\xi} = (\boldsymbol{\xi}_1, \ldots, \boldsymbol{\xi}_m)$ and each $\boldsymbol{\xi}_i$ is the perturbation to the ith oscillator. Let $\boldsymbol{J} = \boldsymbol{P}^{-1}\boldsymbol{G}\boldsymbol{P}$, where $\boldsymbol{J} = [0]\oplus\boldsymbol{J}_1\oplus\cdots\oplus\boldsymbol{J}_p$ is the real Jordan Canonical form of $\boldsymbol{G}$. Applying the change of variables $\boldsymbol{\eta} = (\boldsymbol{P}^{-1}\otimes\boldsymbol{I})\boldsymbol{\xi}$, we get

$$\boldsymbol{\eta}(k+1) = \left[(\boldsymbol{I}+d\boldsymbol{J})\otimes D\boldsymbol{f}(\boldsymbol{s}(k))\right]\boldsymbol{\eta}(k),$$

or, equivalently, in block diagonal form,

$$\begin{aligned} \boldsymbol{\eta}_i(k+1) &= \left[(\boldsymbol{I}+d\boldsymbol{J}_i)^k\otimes D\boldsymbol{f}^k(\boldsymbol{s}(1))\right]\boldsymbol{\eta}_i(1) \\ &=: \boldsymbol{A}_i(k)\boldsymbol{\eta}_i(1). \end{aligned} \tag{4.2b}$$

Let $\sigma(\boldsymbol{A})$ denotes the spectrum of $\boldsymbol{A}$. Then $\sigma(\boldsymbol{A}_i(k)\boldsymbol{A}_i^*(k))$ equals to

$$\begin{aligned}
&\sigma([(\boldsymbol{I}+d\boldsymbol{J}_i)^k \otimes D\boldsymbol{f}^k(\boldsymbol{s}(1))]\,[(\boldsymbol{I}+d\boldsymbol{J}_i^*)^k \otimes (D\boldsymbol{f}^k(\boldsymbol{s}(1)))^*]) \\
&= \sigma([(\boldsymbol{I}+d\boldsymbol{J}_i)^k\,(\boldsymbol{I}+d\boldsymbol{J}_i^*)^k] \otimes [D\boldsymbol{f}^k(\boldsymbol{s}(1)) \cdot (D\boldsymbol{f}^k(\boldsymbol{s}(1)))^*]) \\
&= \sigma((\boldsymbol{I}+d\boldsymbol{J}_i)^k\,(\boldsymbol{I}+d\boldsymbol{J}_i^*)^k) \cdot \sigma(D\boldsymbol{f}^k(\boldsymbol{s}(1)) \cdot (D\boldsymbol{f}^k(\boldsymbol{s}(1)))^*) \\
&= \sigma((\boldsymbol{I}+d\bar{\boldsymbol{J}}_i)^k\,(\boldsymbol{I}+d\bar{\boldsymbol{J}}_i^*)^k) \cdot \sigma(D\boldsymbol{f}^k(\boldsymbol{s}(1)) \cdot (D\boldsymbol{f}^k(\boldsymbol{s}(1)))^*),
\end{aligned}$$

where $\bar{\boldsymbol{J}} = [0] \oplus \bar{\boldsymbol{J}}_1 \oplus \cdots \oplus \bar{\boldsymbol{J}}_p$ is the Jordan Canonical form of $\boldsymbol{G}$. Consequently, the Lyapunov exponents of (1.2) are

$$h_j + \lim_{k\to\infty} \frac{\ln \sqrt{\lambda_{w,i}}}{k}.$$

Here h_j are the Lyapunov exponents of the individual system $\boldsymbol{f}$ and $\lambda_{w,i}$ are the eigenvalues of $(\boldsymbol{I}+d\boldsymbol{J}_{\lambda_i})^k(\boldsymbol{I}+d\boldsymbol{J}_{\lambda_i}^*)^k$ where $\boldsymbol{J}_{\lambda_i}$ is a Jordan block of matrix $\boldsymbol{G}$ and λ_i is an eigenvalue of $\boldsymbol{G}$. Let the size of matrix $\boldsymbol{J}_{\lambda_i}$ be $k_i \times k_i$, and let $\boldsymbol{N} = \boldsymbol{J}_{\lambda_i} - \lambda_i \boldsymbol{I}$. It should be noted that for sufficiently large k,

$$\begin{aligned}
(\boldsymbol{I}+d\boldsymbol{J}_{\lambda_i})^k &= ((1+d\lambda_i)\boldsymbol{I}+d\boldsymbol{N})^k = (1+d\lambda_i)^k(\boldsymbol{I}+\alpha\boldsymbol{N})^k \\
&= (1+d\lambda_i)^k(\boldsymbol{I}+\sum_{j=1}^{k_i-1}\binom{k}{j}\alpha^j\boldsymbol{N}^j) \\
&=: (1+d\lambda_i)^k\boldsymbol{T}_i,
\end{aligned}$$

where $\alpha = d/(1+d\lambda_i)$. Clearly, the order of the magnitude of each entry of $\boldsymbol{T}_i\boldsymbol{T}_i^*$ is at most $\mathrm{O}(k^{2k_i-2})$. We conclude, via the Gershgörn disk theorem, that all eigenvalues of $\boldsymbol{T}_i\boldsymbol{T}_i^*$ are of the order $\mathrm{O}(k^{2k_i-2})$. Consequently, the Lyapunov exponents of (1.2) are

$$h_j + \ln|1+d\lambda_i|. \tag{4.3}$$

We summarize the above as follows.

Theorem 4.1.1. *Let coupling matrix $\boldsymbol{G}$ satisfy* (4.1)*. Then CMLs* (1.2) *achieves local synchronization provided that*

$$h_{max} + \ln|1+d\lambda_i| < 0,\ \ i = 2,\ldots,m, \tag{4.4}$$

where $h_{\max}$ is the largest Lyapunov exponent of the individual map $\boldsymbol{f}$ and $\lambda_i \in \sigma(\boldsymbol{G}) - \{0\}$, $i = 2,\ldots,m$. Otherwise, CMLs (1.2) *will not acquire local synchronization.*

Remark 4.1.1. *The decoupling form* (4.2b) *of variational equation* (4.2a) *was first observed and proposed by Pecora and Carroll [75].*

We shall assume from here on that the real parts of the eigenvalues of $\mathbf{G}$ are nonpositive. To find the range of the coupling d so that (4.4) is fulfilled, we need to solve the following min max problem.

$$\begin{aligned}\min_{d\in\mathbb{R}} \max_{2\le i\le m} |1+d\lambda_i| &= \min_{d>0} \max_{2\le i\le m_1} |1+d\lambda_i| \\ &=: \min_{d>0} \max_{2\le i\le m_1} r_i(d) =: \min_{d>0} r(d). \end{aligned} \tag{4.5}$$

Here m_1 is the number of eigenvalues lying in upper complex plane or on the real axis. The curves $r_i(d)$ are termed the ith-mode of the transverse Lyapunov exponent curves. The equalities above are due to the facts that $|1+d\lambda_i| = |1+d\bar{\lambda}_i|$, the real parts of the eigenvalues of $\mathbf{G}$ are nonpositive and (4.4) is violated whenever $d \le 0$. Without lose of generality, we may assume those distinct nonzero eigenvalues are λ_i, $i = 2, \ldots, m_1$, with $0 < |\lambda_2| \le \cdots \le |\lambda_{m_1}|$. The coupling value $d := d_c$ solving the min max problem (4.5) is the optimal choice of the coupling in the sense that it gives the fastest convergent rate of the initial values toward the synchronous state. To understand how $r(d)$ is formed, we need to know the ordering of $r_i(d)$. For $d > 0$, direct computations yield

$$\begin{aligned} r_i(d) &= \left[|\lambda_i|^2 d^2 + 2\mathrm{Re}(\lambda_i) d + 1\right]^{\frac{1}{2}} \\ &= \left[|\lambda_i|^2 \left(d - \frac{\mathrm{Re}(-\lambda_i)}{|\lambda_i|^2}\right)^2 + \frac{|\lambda_i|^2 - \mathrm{Re}^2(\lambda_i)}{|\lambda_i|^2}\right]^{\frac{1}{2}} \\ &=: \left[|\lambda_i|^2 (d - c_i)^2 + \tan^2\theta_i\right]^{\frac{1}{2}}. \end{aligned} \tag{4.6a}$$

Moreover, $r_i(d) \ge r_j(d)$ if and only if

$$\mathrm{Re}(\lambda_i) \ge \mathrm{Re}(\lambda_j) \qquad \text{if } |\lambda_i| = |\lambda_j|, \tag{4.6b}$$

and

$$(|\lambda_i|^2 - |\lambda_j|^2)(d - d_{ij}) \ge 0 \quad \text{if } |\lambda_i| \ne |\lambda_j|, \tag{4.6c}$$

where

$$d_{ij} = \frac{2(\mathrm{Re}(-\lambda_i) - \mathrm{Re}(-\lambda_j))}{|\lambda_i|^2 - |\lambda_j|^2}. \tag{4.6d}$$

Let $A_i = \{j : 2 \le j \le m_1 \text{ and } |\lambda_i| = |\lambda_j|\}$. Then $\max_{j \in A_i} |1+d\lambda_j| = |1+d\lambda_w|$, where w is so chosen that $\mathrm{Re}(\lambda_w) \ge \mathrm{Re}(\lambda_j)$ for all $j \in A_i$. This gives that within each of the index set A_i, their corresponding quantities $|1+d\lambda_i|$ are well ordered for any $d > 0$. Consequently, to solve (4.5), we may assume, without loss of generality, that $0 < |\lambda_2| < \cdots < |\lambda_{m_1}|$ from here on. Using the terminology in [37], we see that the numbers 2 and m_1 correspond to the longest and shortest wavelength modes, respectively. The numbers in between 2 and m_1 are to be called intermediate wavelength modes. Since $d_{ij} = d_{ji}$, for any i and j, we consider only d_{ij} with $i > j$. Our reduction process is now complete.

The following procedures are proposed to determine the "actual" node points of $r(d)$ from the candidate set $\{d_{ij} : i > j\}$.

(A) Set $k_0 = 0$, and $k_1 = \max\{l | \mathrm{Re}(\lambda_i) \le \mathrm{Re}(\lambda_l), \forall i = 2 \ldots, m_1\}$. Let k_2 be the largest index so that $0 < d_{k_2 k_1} \le d_{w k_1}$ for all $k_1 < w \le m_1$.

(B) Let k_3 be the largest index so that $d_{k_2 k_1} < d_{k_3 k_2} \le d_{w k_2}$ for all $k_2 < w$. The process can be continued until $k_p = m_1$ for some $p \le m_1$.

The next result shows that $\{k_i\}_{i=1}^{p}$ is the set of "actual" node points of $r(d)$.

Theorem 4.1.2. *Let coupling matrix $\boldsymbol{G}$ satisfy* (4.1). *Assume that the real parts of the eigenvalues of $\boldsymbol{G}$ are nonpositive. Then $r(d) = r_{k_i}(d)$ whenever $d_{k_i k_{i-1}} \le d \le d_{k_{i+1} k_i}$, $i = 1, \ldots, p$. Here $d_{k_1, k_0} = 0$ and $d_{k_{p+1} k_p} = \infty$.*

Proof. Denote by $I_j = [d_{k_j k_{j-1}}, d_{k_{j+1} k_j}]$. It then follows from (4.6c) that if $i > j$ and $d_{ij} > 0$, then $r_i(d) > r_j(d)$ whenever $d > d_{ij}$ and $r_i(d) < r_j(d)$ whenever $0 < d < d_{ij}$. We then conclude that

$$(i) \text{ the ordering of } r_i(d) \text{ and } r_j(d) \text{ remains the same until both curves meet;} \quad (4.7a)$$

$$(ii) \text{ if } r_i(d^*) > r_j(d^*) \text{ for some } d^* > 0 \text{ with } i > j, \text{ then } r_i(d) > r_j(d) \text{ for all } d \ge d^*. \quad (4.7b)$$

Using the first inequality in (4.6a), we have that $r(d) = r_{k_1}(d)$ for $\epsilon_1 > d \ge 0$. Here ϵ_1 is sufficiently small. It then follows from (4.7a), (4.7b) and procedure **(A)** that $r(d) = r_{k_1}(d)$ on I_1. Upon using (4.7a), we conclude that $r(d) = r_{k_2}(d)$ for $d \in (d_{k_2 k_1}, d_{k_2 k_1} + \epsilon_2)$.

Here ϵ_2 is sufficiently small. Similarly, $r(d) = r_{k_2}(d)$ on I_2. We omit the proof of the remaining assertions of the theorem due to the similarity. □

Note that not all c_{k_i} given in (4.6a) could be critical points of $r(d)$. In fact, the critical points of $r(d)$ may not even come from the set $\{c_{k_i}\}$. We next identify the "actual" critical points of $r(d)$. Our next main result shows that $r(d)$ has exactly one critical point.

Theorem 4.1.3. *The curve $r(d)$ has a unique critical point d_c that solves the min max problem* (4.5). *Moreover, the optimal range of coupling d to sustain stably synchronous chaos of* (1.2b) *is (d_l, d_r). Here d_l and d_r, $d_l < d_r$, are the intersection points (if exist) of the straight line $y = e^{-h_{\max}}$ and the curve $y = r(d)$. Consequently, CMLs* (1.2b) *acquires local synchronization if and only if $d \in (d_l, d_r)$.*

Proof. We break up the proof of the theorem into the following three steps.

(Step I) We first claim that the number of c_{k_i} lying in the interior $\overset{\circ}{I}_i$ of I_i is at most one. Indeed, suppose there exist $c_{k_a} \in \overset{\circ}{I}_a$ and $c_{k_b} \in \overset{\circ}{I}_b$ with $c_{k_a} < c_{k_b}$. Then the following hold true. (i) $r_{k_a}(c_{k_b}) > r_{k_a}(c_{k_a})$. (ii) $r_{k_a}(c_{k_a}) > r_{k_b}(c_{k_a})$. (iii) $r_{k_b}(c_{k_a}) > r_{k_b}(c_{k_b})$. Inequalities (i) and (iii) hold true since c_{k_a} and c_{k_b} are, respectively, the minimum points of $r_{k_a}(d)$ and $r_{k_b}(d)$. The fact that $r_{k_a}(d)$ lies above all other curves on I_a leads to inequality (ii). Combining these inequalities, we have that $r_{k_a}(c_{k_b}) > r_{k_b}(c_{k_b})$, a contradiction to the fact that r_{k_b} is the maximum curve on I_{k_b}.

(Step II) We next show that if $c_{k_i} \in \overset{\circ}{I}_i$, then $r(d)$ is decreasing on $(0, c_{k_i})$ and increasing on (c_{k_i}, ∞). Indeed, for $d \in I_{i+1}$, $r(d) = r_{k_{i+1}}(d) > r_{k_i}(d) > r_{k_i}(d_{k_{i+1}k_i}) = r_{k_{i+1}}(d_{k_{i+1}k_i})$. Using the conclusion in Step I and the fact that $r^2_{k_i}(d)$ is parabolic, we conclude that $r_{k_{i+1}}(d)$ must be increasing on I_{i+1}. On the other hand, $r_{k_{i-1}}(d)$ must be decreasing on I_{i-1} since $r_{k_{i-1}}(d) > r_k(d) > r_{k_i}(d_{k_ik_{i-1}}) = r_{k_{i-1}}(d_{k_ik_{i-1}})$. The monotonicity of $r(d)$ on each interval I_j, $1 \le j \le m_1$, can be similarly determined.

(Step III) Since $r(d)$ is decreasing initially on I_1 and increasing eventually on I_p, there must have at least one critical point. If such points do not lie in the set of node points, then $r(d)$ has a unique critical point. Suppose $c_{k_i} \notin \overset{\circ}{I}_i$ for all $i = 1, \ldots, p$. Then $r(d)$ is monotonic on each interval I_i. Suppose $r(d)$ first changes its monotonicity at

$d_{k_{l+1}k_l}$ for some l. Then a similar argument as given in the Step II shows that once $r(d)$ becomes increasing on I_{l+1} it will stay increasing the rest of the way. We have just completed the proof of the theorem. □

Now, we define some terminologies occurring in Theorem 4.1.3. The curve $r(d)$ given in is to be called the *synchronization curve* of CMLs (1.2), and the interval $N_{m,f} := (d_l, d_r)$ is termed the *synchronization interval*. (1.2), if exists. The value d_c is called the *optimal coupling strength* of CMLs. The value $r(d_c)$ is called the *synchronization index* of CMLs since local synchronization occurs iff it is less than $e^{-h_{\max}}$. The value $h_{max} + \ln r(d_c)$ is called the *Lyapunov index* of CMLs.

Remark 4.1.2. *(i) The optimal coupling strength $d_c \in (d_l, d_r)$ and depends only on the connectivity topology. (ii) If the straight line $y = e^{-h_{\max}}$ and the curve $y = r(d)$ do not intersect, then CMLs* (1.2) *will not achieve synchronization for any coupling strength. Suppose d_r and d_l exist. Then as soon as d exceeds d_r, a certain wavelength mode is excited, which, in turn, causes the instability of the synchronous state. The illustration in Examples 2 and 3 shows that the excited wavelength mode could be either the shortest wavelength mode, the intermediate wavelength mode or the longest wavelength mode. In any event, d_r is the exact critical value where wavelength bifurcation (WB), as the terminology using in [37], occurs. On the other hand, d_l is the exact critical value where all wavelength modes become deexcited enough to induce the stability of the synchronous state.*

Theorem 4.1.4. *Suppose the coupling matrix $\mathbf{G} \in \mathbb{R}^{m\times m}$ has nonpositive real eigenvalues. Denote by $\{\lambda_i\}_{i=2}^{m_1}$ the distinct nonzero eigenvalues of $\mathbf{G}$. Then*

(i) The synchronization curve is

$$r(d) = \begin{cases} \lambda_2(d), & d \in [0, d_{m_1 2}] = I_1 \\ \lambda_{m_1}(d), & d \in (d_{m_1 2}, \infty) = I_2 \end{cases} . \tag{4.8a}$$

(ii) The optimal coupling strength is

$$d_c = d_{m_1 2} = \frac{-2}{\lambda_2 + \lambda_{m_1}}. \tag{4.8b}$$

(iii) The synchronization interval is, if exists,

$$N_{m,f} := \left(\frac{1 - e^{-h_{\max}}}{-\lambda_2}, \frac{1 + e^{-h_{\max}}}{-\lambda_{m_1}} \right). \tag{4.8c}$$

(iv) The synchronization index is

$$t_{2,m} := \left| \frac{\lambda_2 - \lambda_{m_1}}{\lambda_2 + \lambda_{m_1}} \right|. \tag{4.8d}$$

(v) The Lyapunov index is

$$\delta_{m,f} := h_{\max} + \ln |t_{2,m}|. \tag{4.8e}$$

Consequently, depending on the quantity of $h_{\max}$, either CMLs (1.2) achieves no synchronization or short wavelength bifurcation occurs as d varies.

Proof. It is easily seen that $k_1 = 2$ and $k_2 = m_1$ since $d_{ij} = \frac{-2}{\lambda_i + \lambda_j}$. Thus, $r(d)$ is as asserted. It then follows from the facts that $c_{m_1} = -\frac{1}{\lambda_{m_1}} < \frac{-2}{\lambda_2 + \lambda_{m_1}} < -\frac{1}{\lambda_2} = c_2$, $d_c = d_{m_1 2}$. Solving equations $y = r(d)$ and $y = e^{-h_{\max}}$, we have that d_l and d_r are as claimed. □

4.2 Application: Local Synchronization in coupled logistic maps

We illustrate our theorems with the following examples.

Example 1: Let the oscillators be diffusively coupled with periodic boundary conditions. It means coupling matrix $\boldsymbol{G}$ is given in the form of (2.31). Then for such $\mathbf{G}$, $m_1 = m$, $-\lambda_{m_1} = 4 \sin^2 \frac{\left[\frac{m}{2}\right]\pi}{m}$ and $-\lambda_2 = 4 \sin^2 \frac{\pi}{m}$.

Let $f(x) = 4x(1 - x)$, $0 \le x \le 1$. Then $h_{\max} = \ln 2$, and the corresponding candidates for d_l and d_r are, respectively, $\frac{1}{8} \sin^{-2} \frac{\pi}{m}$ and $\frac{3}{8} \sin^{-2} \frac{\left[\frac{m}{2}\right]\pi}{m}$. However, $d_l \le d_r$ only if $m \le 5$. Hence, we conclude that the maximum size of the number of oscillators to sustain synchronous chaos is 5.

We next compare our results with those obtained in [19,79]. Their sufficient conditions on the coupling strength for obtaining stable synchronization are, respectively, given as follows. $\frac{1-e^{-h_{\max}}}{m} < d\,g_{ij} < \frac{1+e^{-h_{max}}}{m}$, and $\left(\sum_{k=1,k\neq i}^{m}|g_{ki}-g_{ji}|\right) + \left|\frac{1}{d}+g_{ii}-g_{ji}\right| < \frac{1}{d}e^{-h_{\max}}$, for all i,j with $i \neq j$. However, the first inequality above fails to find any suitable coupling strength provided that $\boldsymbol{G}$ has zero off-diagonal elements. If $\boldsymbol{G}$ is given as above with $m \geq 4$ and $f(x) = 4x(1-x)$, then the second inequality also fails to find any suitable coupling strength.

Example 2: Consider synchronization in a directed ring of $2K$ nearest neighbors coupled oscillators [1] with $K = 2$ and $m = 9$. Specifically, the coupling matrix $\boldsymbol{G}$ under consideration is a circulant matrix of the form

$$\boldsymbol{G} = \text{circ}(-30,\ 13,\ 2,\ 0,\ \ldots,\ 0,\ 5.4,\ 9.6).$$

The spectrum of $\boldsymbol{G}$ is $\{-30+13e^{\frac{2(j-1)\pi}{9}i}+2e^{\frac{4(j-1)\pi}{9}i}+5.4e^{\frac{14(j-1)\pi}{9}i}+9.6e^{\frac{16(j-1)\pi}{9}i} : j = 1,\ldots,9\}$. Here $\lambda_2 \approx -11.4024+1.1629i$, $\lambda_3 \approx -33.0293+2.1855i$, $\lambda_4 \approx -45+5.8890i$ and $\lambda_5 \approx -45.5683+3.3483i$. Direct computations yield that $d_{42} \approx 0.0348 < d_{52} < d_{32}$, $d_{54} \approx 0.0406$, and $c_5 < c_4 < d_{42} < d_{54} < c_2$ (see Fig. 4.1). Consequently,

$$r(d) = \begin{cases} r_2(d), & d \in I_1 = [0, d_{42}] \\ r_4(d), & d \in I_2 = [d_{42}, d_{54}] \\ r_5(d), & d \in I_3 = [d_{54}, \infty] \end{cases},$$

the node points of $r(d)$ are d_{42} and d_{54}, and the critical point of $r(d)$ occurs at d_{42}. Let $f_\mu(x) = \mu x(1-x)$. For $\mu = 4$, since $e^{-h_{max}} = e^{-\ln 2} = 0.5 < r(d_{42})$, *synchronization interval* does not exist. As μ varies from $\mu_\infty \approx 3.57$ to $\mu = 4$, scenarios (i) no synchronization, (ii) short wavelength bifurcation(SWB) and (iii) immediate wavelength bifurcation(IWB) can be clearly observed from the figure.

On the other hand, the maximum size of the number of oscillators on such connectivity topology to sustain stably synchronous chaos is 7. The claim above is done by checking the intersection of the equations $y = \frac{1}{2}$ and $y = r(d)$ for all $m \leq 8$.

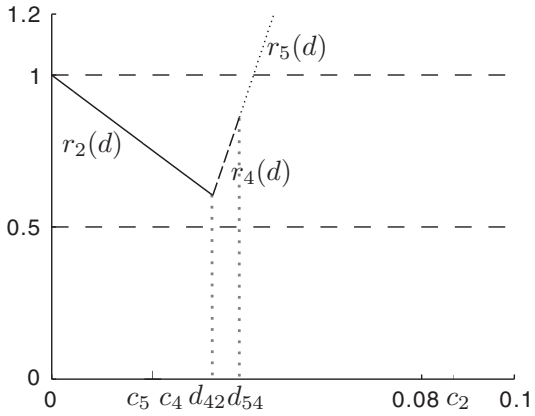

Figure 4.1: Graph of $r(d)$ in Example 2. Here $d_{42} \approx 0.0348$, $d_{54} \approx 0.0406$, $r(d_{42}) \approx 0.6040$, $r(d_{54}) \approx 0.8604$, $c_5 \approx 0.02182$, $c_4 \approx 0.02185$ and $c_2 \approx 0.0868$. The critical point of $r(d)$ is d_{42}.

Example 3: The following example shows that long wavelength bifurcation(LWB) is also possible. Let $\boldsymbol{G}$ be given as follows:

$$\begin{pmatrix} -30 & 3 & 12 & 5 & 10 \\ 10 & -30 & 3 & 12 & 5 \\ 5 & 10 & -30 & 3 & 12 \\ 12 & 5 & 10 & -30 & 3 \\ 3 & 12 & 5 & 10 & -30 \end{pmatrix}.$$

The spectrum of $\boldsymbol{G}$ is $\{0, -35.2639 + 10.7719i =: \lambda_2, -39.7361 + 2.5429i =: \lambda_3, \bar{\lambda}_2, \bar{\lambda}_3\}$. Then the graph of $r(d)$ is demonstrated in Fig. 4.2. Consider $f(x) = 4x(1-x)$. Then the longest wavelength mode becomes excited to induce instability as d is increased beyond d_r.

Example 4: To illustrate the accuracy of our theorems, *synchronization intervals* established in Theorem 4.1.4 are compared with those obtained by the computer simulation. In particular, theoretically and numerically predicted *synchronization intervals* for three examples above are almost identical. Such comparisons are recorded in Fig. 4.3. They are "almost" identical. This simulation is so setup that the differences between the initial values $\boldsymbol{x}_i$ are within 10^{-5}. Synchronization is achieved when their differences are within 10^{-15}.

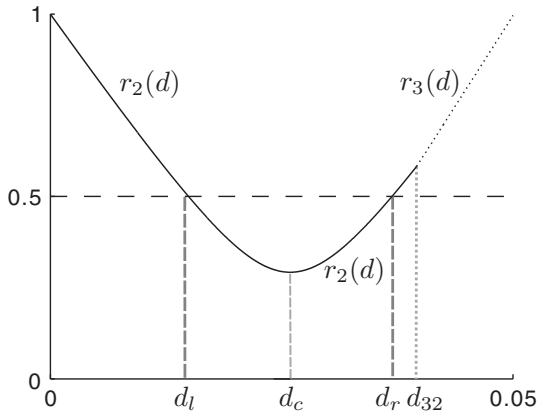

Figure 4.2: Graph of $r(d)$ in Example 3. Here $d_{32} \approx 0.0396$, $c_2 \approx 0.0259$, $c_3 \approx 0.0251$, $d_l \approx 0.0149$ and $d_r \approx 0.0369$. The critical point of $r(d)$ is c_2.

4.3 Wavelet Transform Method for Coupled Map Lattices

In this section, we consider how the wavelet transform method [98] affects the stability of synchronous manifold of (1.2). As required hypothesis in [98], we as well assume coupling matrix $\boldsymbol{G}$ being symmetric and satisfies (4.1), and the number m of nodes being equal to $\tilde{m}2^i$.

Write $\boldsymbol{G}$ as

$$\boldsymbol{G} = \begin{pmatrix} \boldsymbol{G}_{11} & \cdots & \boldsymbol{G}_{1\tilde{m}} \\ \vdots & \ddots & \vdots \\ \boldsymbol{G}_{\tilde{m}1} & \cdots & \boldsymbol{G}_{\tilde{m}\tilde{m}} \end{pmatrix}_{m\times m}.$$

Here, the dimension of each small block matrices is $2^i \times 2^i$. By the i-scale wavelet operator W [21,98], the matrix $\boldsymbol{G}$ is transformed into $W(\boldsymbol{G})$ of the form

$$W(\boldsymbol{G}) = \begin{pmatrix} \boldsymbol{W}_{11} & \cdots & \boldsymbol{W}_{1\tilde{m}} \\ \vdots & \ddots & \vdots \\ \boldsymbol{W}_{\tilde{m}1} & \cdots & \boldsymbol{W}_{\tilde{m}\tilde{m}} \end{pmatrix}_{m\times m}.$$

where each entry of $\boldsymbol{W}_{pq}$ $(1 \le p, q \le \tilde{m})$ is the average of entries of $\boldsymbol{G}_{pq}$. After

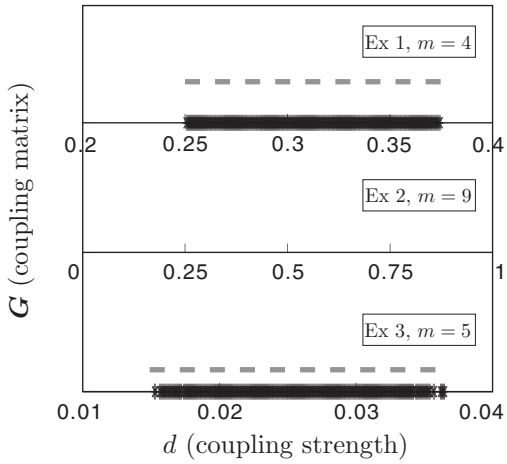

Figure 4.3: Three typical *synchronization intervals* (SIs) for coupled logistic map with various coupling matrices are shown. Solid (bold) lines are SIs obtained by computer simulation. Dotted (fine) line lines are SIs predicted by our theorems. All scaled for clear visualization.

reconstruction [98], the coupling matrix $\boldsymbol{G}$ becomes

$$\boldsymbol{G} + K \cdot W(\boldsymbol{G}) = \begin{pmatrix} \tilde{G}_{11} & \cdots & \tilde{G}_{1\tilde{m}} \\ \vdots & \ddots & \vdots \\ \tilde{G}_{\tilde{m}1} & \cdots & \tilde{G}_{\tilde{m}\tilde{m}} \end{pmatrix}_{m \times m} .$$

where K is a wavelet parameter. In summary, the effects of the wavelet transform method can be viewed as the changes of eigenvalues of the coupling matrix and vary dramatically for different m's. The eigenvalues of $\boldsymbol{G} + K\, W(\boldsymbol{G})$ are denoted by $\lambda_i(K)$, with $0 = \lambda_1(K) > \lambda_2(K) \geq \cdots \geq \lambda_m(K)$. Clearly, Theorem 4.1.4 is still valid for such new coupling matrix. Note that the corresponding $\delta_{m,f}$, d_c, $N_{m,f}$ and $t_{2,m}$ defined in Theorem 4.1.4 now depend on the wavelet parameter K as well. To emphasize such dependence, we shall write them as $\delta_{m,f}(K)$, $d_c(K)$, $N_{m,f}(K)$ and $t_{2,m}(K)$, respectively.

In the following, we consider the applications of the wavelet transformation method in the case that $\boldsymbol{f}$ in CMLs (1.2) is the logistic map, i.e., $\boldsymbol{f} = f_\mu(x) = \mu x(1-x)$, and the coupling matrix $\boldsymbol{G} \in \mathbb{R}^{m \times m}$ is the diffusive matrix with periodic boundary conditions as given in (2.31).

Example A. $m = 4$ (No improvement)

Fig. 4.4(a) shows the calculated eigenvalues $\lambda_i(K)$ of the coupling matrix as a function of wavelet parameter K. The coupling matrices before and after reconstruction are denoted by $\boldsymbol{G} + KW(\boldsymbol{G}) = [\tilde{\boldsymbol{G}}_{pq}]$, with $K = 0$ and $K > 0$, respectively, where

$$\tilde{\boldsymbol{G}}_{11} = \tilde{\boldsymbol{G}}_{22} = \begin{pmatrix} \frac{-(4+K)}{2} & \frac{2-K}{2} \\ \frac{2-K}{2} & \frac{-(4+K)}{2} \end{pmatrix},$$
$$\tilde{\boldsymbol{G}}_{12} = \tilde{\boldsymbol{G}}_{21} = \begin{pmatrix} \frac{K}{2} & \frac{2+K}{2} \\ \frac{2+K}{2} & \frac{K}{2} \end{pmatrix}.$$

The solid line is $\lambda_2(K)$, while the dotted line is $\lambda_4(K)$. Note that as K is increased, a crossing appears at $K = 1$. This crossing makes the analytical identification of $\lambda_i(K)$ a difficult task. Thus, the optimal K is numerically determined from Fig. 4.4(b), where $t_{2,m}$, the synchronization index, is obtained from Fig. 4.4(a). We set $K = K_{m,\min}$ is the number for which $t_{2,m}(K_{m,\min})$ is a minimum. Fig. 4.4(b) shows that $K_{m,\min} \in [0, 1]$. Thus, it is clear that no enhancement of synchronization is expected.

Example B. $m = 8$ (Significantly improved)

For $m = 8$, the enhancement of synchronization is shown. Fig. 4.5(a) shows the eigenvalues $\lambda_i(K)$ of the coupling matrix as a function of the wavelet parameter K. In this case,

$$\tilde{\boldsymbol{G}}_{pq} = \begin{pmatrix} \frac{-(4+K)}{2} & \frac{2-K}{2} \\ \frac{2-K}{2} & \frac{-(4+K)}{2} \end{pmatrix}, \quad \text{if } p = q,$$
$$\tilde{\boldsymbol{G}}_{pq} = \begin{pmatrix} \frac{K}{4} & \frac{K}{2} \\ \frac{4+K}{2} & \frac{K}{4} \end{pmatrix} = \tilde{\boldsymbol{G}}_{qp}^T = \tilde{\boldsymbol{G}}_{41} = \tilde{\boldsymbol{G}}_{14}^T, \quad \text{if } q - p = 1,$$
$$\tilde{\boldsymbol{G}}_{pq} = \begin{pmatrix} 0 & 0 \\ 0 & 0 \end{pmatrix}, \quad \text{otherwise.}$$

Note that two crossing points appear. Similarly, the synchronization index, $t_{2,8}(K)$ is shown in Fig. 4.5(b). It is observed that $K_{8,\min} \in (1.13, 1.204)$. Thus, using an optimal K (in the min region), it is expected to have a significant improvement over $K = 0$.

Given the optimal K, the effects of the wavelet transform method on synchronization with different growth rates and coupling strength are further investigated. Fig. 4.5(c) shows the Lyapunov index of coupled system (1.2) with $K = 0$ and $K = 1.15$. These two graphs are identical with a vertical shift. It is seen, via Fig. 4.5(c), that if $\mu > \mu_8 \approx 3.67$, so as $\delta_{8,\mu} > 0$, then the local synchronization is lost without the wavelet transform method. However, with wavelet transform method ($K = 1.15$), $\delta_{8,\mu}(1.15) < 0$ for all μ's, and so the local synchronization of (1.2) is preserved. Fig. 4.5(d) and Fig. 4.5(e) shows the optimal length of the coupling strength as a function of growth rate without the transform ($K = 0$) and with the optimal transform ($K = 1.15$), respectively.

The numerical simulation for obtaining the interval of synchronization recorded in Fig. 4.5(f) and Fig. 4.5(g) again confirms our theoretical prediction above. Without the transform ($K = 0$), there is a narrow region for the complete synchronization. In dark areas around $\mu = 3.64$ and 3.85, each cell shows a periodic window-type of behavior. In gray areas, different initial conditions give rise to different scenarios of partial synchronization (for example, even/odd cells are synchronized). With the wavelet transform method, there is a very significant increase in dark areas as compared to those in Fig. 4.5(f). The applicable ranges of the coupling strength and the growth rate are significantly improved. The numerically produced Fig. 4.5(f) and Fig. 4.5(g) are in agreement with our theoretically predicted Fig. 4.5(d) and Fig. 4.5(e).

Example C. $m = 40$ (Effects on large m)

The wavelet transform method is most dramatic for a large number of oscillators. Fig. 4.6(a) shows the maximum number of oscillators for which the local synchronization of the system with or without the wavelet transform method can still be sustained. The numbers are obtained by Theorem 4.1.4. It is seen, via Fig. 4.6(a), that the good improvement on the maximum number of oscillators allowed is that even without choosing the optimal K. The graphs in Fig. 4.6(a) are decreasing with respect to the growth rate μ of the map, except at those μ's yielding the window behavior. As m increases, the

dominant eigenvalue approaches zero. Hence, local synchronization becomes unobservable. Furthermore, the change of the dominant eigenvalue due to the wavelet transform method is very significant. Fig. 4.6(b) shows that if $\mu_0 = 3.5699456 < \mu < \mu_1 = 3.5708$, then coupled system (1.2) acquires synchronization with $m = 40$ and $K = 1$. However, it is easily verified from Theorem 4.1.4 that if $\mu = \mu_1$, then the maximum number of oscillators allowed for synchronization without the wavelet transform method is $m = 24$. It should be noted that in producing Fig. 4.6(a) only the end points of synchronization intervals are recorded. For those μ's, where $\mu > 3.571$, exhibiting the window behavior, the end points of synchronization intervals lie outside the interval $(0.1, 0.5)$.

With the wavelet transform method, global synchronization can be achieved for $m = 40$. In the case of $m = 8$, the transform enhances the synchronization effect. In this case, there is a very significant region, as shown in the dark areas in Fig. 4.6(c). Without the transform, synchronization for such a large number of oscillators would not be possible. This demonstrates the dramatic effects of the transform with relatively large m.

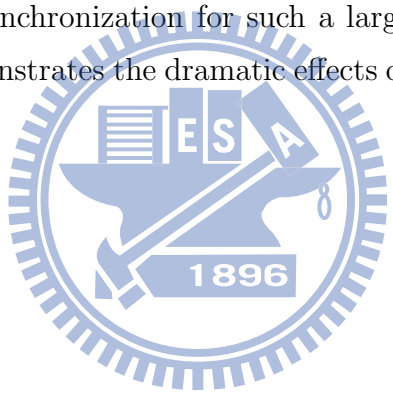

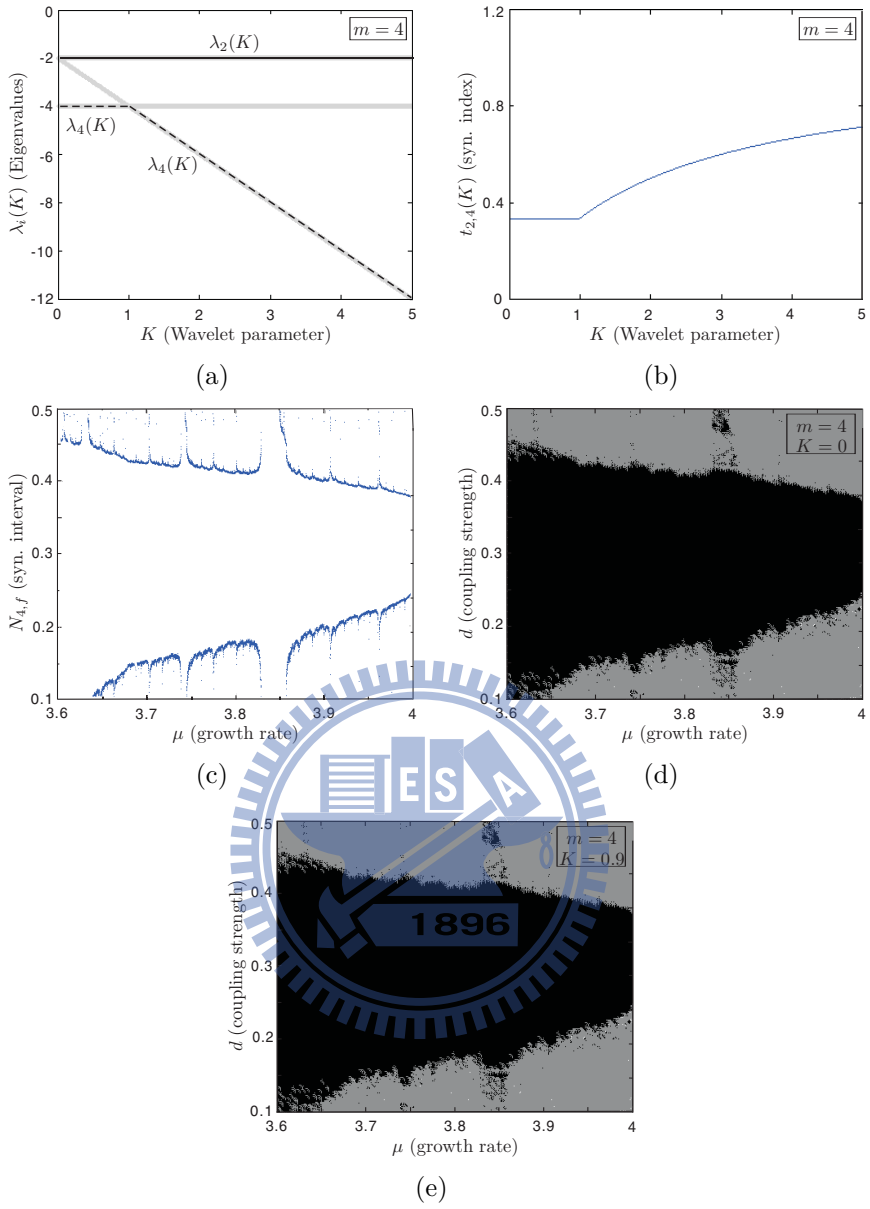

Figure 4.4: (a) Eigenvalues $\lambda_i(K)$ of the coupling matrix as a function of wavelet parameter K for $m = 4$. The solid line is $\lambda_2(K)$, while the dotted line is $\lambda_4(K)$. (b) Synchronization index of the coupling matrix as a function of wavelet parameter K. (c) Theoretical predicted synchronization intervals which are in agreement with Fig.4.4 (d) and (e). (d) Numerically produced synchronization intervals without the wavelet transform method. (e) Numerically produced synchronization intervals with ($K = 0.9$) the wavelet transform method. The dark, gray, and white regions represent in complete synchronization, partial synchronization, and out of synchronization, respectively. The dark areas around $\mu = 3.64$ and $\mu = 3.85$ are caused by periodic windows. They are consistent with the results of Fig. (a)-(c), where $K_{m,\min} \in [0, 1]$.

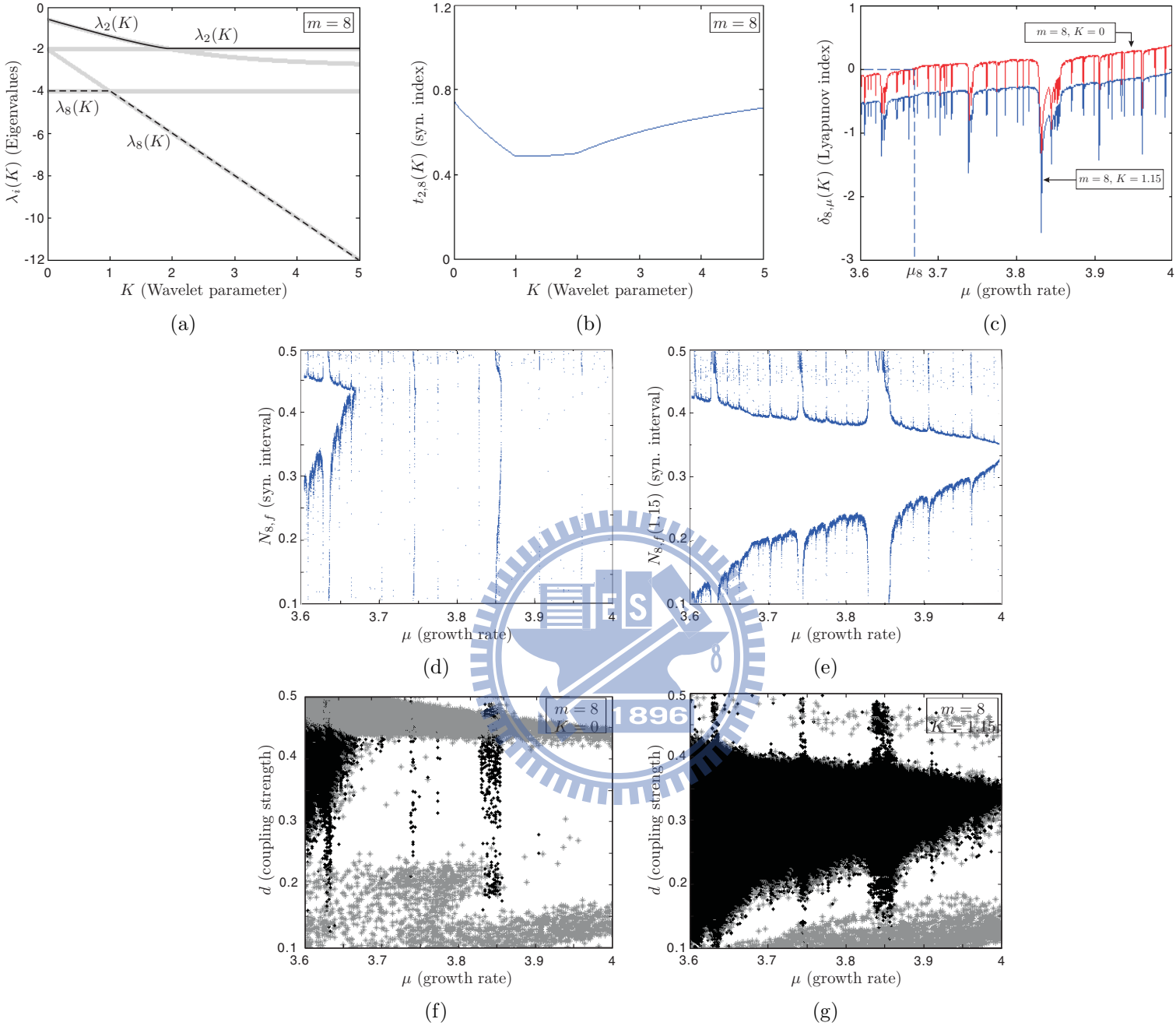

Figure 4.5: (a) Eigenvalues $\lambda_i(K)$ of the coupling matrix as a function of wavelet parameter K for $m = 8$. (b) Synchronization index of the coupling matrix as a function of wavelet parameter K. (c) Lyapunov index versus growth rate μ. (d) White region gives the synchronization intervals for $K = 0$. (e) White region gives the synchronization intervals with $K = 1.15$. (f) Numerically produced synchronization intervals without the wavelet transform method. (g) Numerically produced synchronization intervals with ($K = 1.15$) the wavelet transform method.

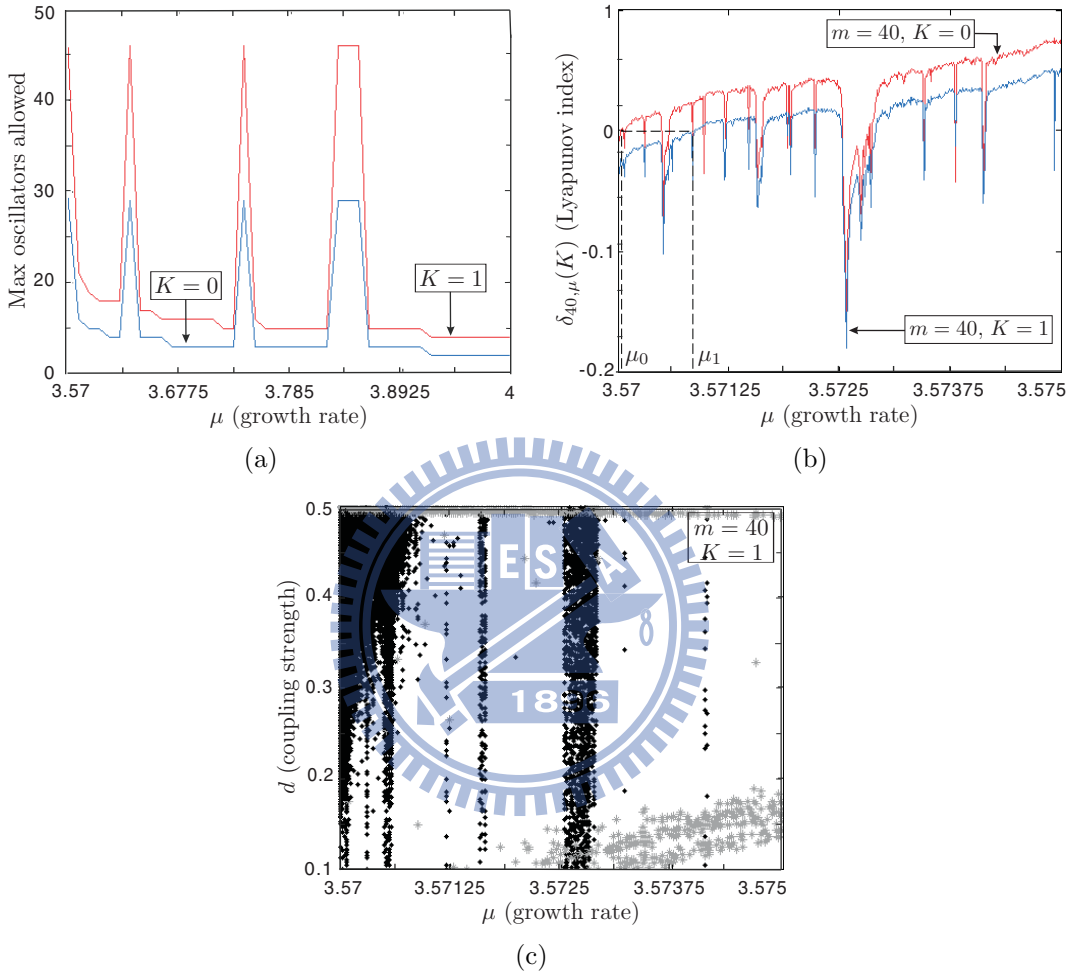

Figure 4.6: (a) Maximum number of oscillators allowed for which (1.2) acquires synchronization. (b) Lyapunov index versus growth rate μ. Here $\mu_0 = 3,5704$ and $\mu_1 = 3.57085$. (c) Numerically produced synchronization intervals with $K = 1$ and $m = 40$.

Chapter 5

Conclusion

In this thesis, we consider the synchronization problems in the lattices of the coupled systems (1.1) and (1.2). Some criteria and applications are drawn.

First, for the coupled system (1.1), we have developed theories (see Theorems 2.2.2, 2.2.1, 2.3.4) to prove the occurring of global synchronization, and a rigorous lower bound on the coupling strength to acquire global synchronization is obtained. The results can be applied to quite general connectivity topology including the time-varying coupling. Moreover, by merely checking the structure of the vector field of single oscillator and verifying bounded dissipation of the coupled system, we shall be able to determine if the coupled system is synchronized or not.

In Chapter 3, to see the applicability of the developed theorems, the coupled Lorentz and coupled Duffing oscillators are considered as examples. Moreover, synchronization of coupled Hindmarsh-Rose neurons with excitatory chemical and electrical synapses is analytical studied. Particularly, multi-state and multi-stage synchronization are observed with the presence of both chemical and electrical synapses. A measurement for the density of the network is introduced to ensure that chemical synapses play positive effects on the synchronization of the system of coupled neurons.

Secondly, the necessary and sufficient condition for the local synchronization in the CMLs (1.2), as a version of the MSF criterion proposed by Pecora and Carroll [75] in (1.1), is supplied for arbitrary coupling matrix $\boldsymbol{G}$, see, for examples, Theorems 4.1.1, 4.1.3, 4.1.4. We also show analytically and numerically that the wavelet transformation

method applied well in the CMLs. The result is illustrated in Fig. 4.5, for instance.

Before concluding the thesis, we mention some possible future work. First, it is of great interest to show how bounded dissipation of the coupled system is related to the uncoupled dynamics and its connectivity topology. Second, the analysis of the local (global) synchronization in the CMLs with the partial-state coupling is also worth studying.

Bibliography

[1] M. Barahona and L. M. Pecora, *Synchronization in small-world systems*, Phys. Rev. Lett., 89 (2002), p. 054101.

[2] I. V. Belykh, V. N. Belykh, and M. Hasler, *Blinking model and synchronization in small-world networks with a time-varying coupling*, Phys. D, 195 (2004), pp. 188–206.

[3] ——, *Generalized connection graph method for synchronization in asymmetrical networks*, Phys. D, 224 (2006), pp. 42–51.

[4] ——, *Synchronization in asymmetrically coupled networks with node balance*, Chaos, 16 (2006), p. 015102.

[5] I. V. Belykh, V. N. Belykh, K. V. Nevidin, and M. Hasler, *Persistent clusters in lattices of coupled nonidentical chaotic systems*, Chaos, 13 (2003), pp. 165–178.

[6] I. V. Belykh, E. de Lange, and M. Hasler, *Synchronization of bursting neurons: What matters in the network topology*, Phys. Rev. Lett., 94 (2005), p. 188101.

[7] V. N. Belykh, I. V. Belykh, and M. Hasler, *Hierarchy and stability of partially synchronous oscillations of diffusively coupled dynamical systems*, Phys. Rev. E, 62 (2000), pp. 6332–6345.

[8] V. N. Belykh, I. V. Belykh, and M. Hasler, *Connection graph stability method for synchronized coupled chaotic systems*, Phys. D, 195 (2004), pp. 159–187.

[9] T. Binzegger, R. J. Douglas, and K. A. C. Martin, *Topology and dynamics of the canonical circuit of cat V1*, Neural Networks, 22 (2009), pp. 1071–1078.

[10] T. Bliss and R. Schoepfer, *Controlling the ups and downs of synaptic strength*, Science, 304 (2004), pp. 973–974.

[11] S. Bottani, *Pulse-coupled relaxation oscillators: From biological synchronization to self-organized criticality*, Phys. Rev. Lett., 74 (1995), pp. 4189–4192.

[12] A. A. Brailove, *The dynamics of two pulse-coupled relaxation oscillators*, Int. J. Bifurcation Chaos, 2 (1992), pp. 341–352.

[13] J. Buck, *Synchronous rhythmic flashing of fireflies. II.*, Quart. Rev. Biol., 63 (1988), pp. 265–289.

[14] G. Buzsaki, *Rhythms of the Brain*, Oxford University Press, New York, 2006.

[15] Y.-C. Chang and J. Juang, *Stable synchrony in globally coupled integrate-and-fire oscillators*, SIAM J. Appl. Dyn. Syst., 7 (2008), pp. 1445–1476.

[16] P. Checco, M. Righero, M. Biey, and L. Kocarev, *Synchronization in networks of Hindmarsh-Rose neurons*, IEEE Trans. Circuits Syst. II, Exp. Briefs, 55 (2008), pp. 1274–1278.

[17] M. Chen, *Chaos synchronization in complex networks*, IEEE Trans. Circuits Syst. I, Reg. Papers, 55 (2008), pp. 1335–1346.

[18] M. Y. Chen, *Some simple synchronization criteria for complex dynamical networks*, IEEE Trans. Circuits Syst. II, Exp. Briefs, 53 (2006), pp. 1185–1189.

[19] Y. Chen, G. Rangarajan, and M. Ding, *General stability analysis of synchronized dynamics in coupled systems*, Phys. Rev. E, 67 (2003), p. 026209.

[20] J. P. Crutchfield, *Space-time dynamics in video feedback*, Phys. D, 10 (1984), pp. 229–245.

[21] I. Daubechies, *Ten Lectures on Wavelets*, Society for Industrial and Applied, Philadelphia, Pa., 1992.

[22] P. J. Davis, *Circulant Matrices*, Pure and applied mathematics, Wiley, New York, 1979.

[23] E. de Lange and M. Hasler, *Predicting single spikes and spike patterns with the Hindmarsh-Rose model*, Biol. Cybern., 99 (2008), pp. 349–360.

[24] R. Dzakpasu and M. Żochowski, *Discriminating differing types of synchrony in neural systems*, Phys. D, 208 (2005), pp. 115–122.

[25] E. Ermentrout, *An adaptive model for synchrony in the firefly Pteroptyx malaccae*, J. Math. Biol., 29 (1991), pp. 571–585.

[26] L. Fabiny, P. Colet, R. Roy, and D. Lenstra, *Coherence and phase dynamics of spatially coupled solid-state lasers*, Phys. Rev. A, 47 (1993), pp. 4287–4296.

[27] J. Fan and X. F. Wang, *On synchronization in scale-free dynamical networks*, Phys. A, 349 (2005), pp. 443–451.

[28] K. S. Fink, G. Johnson, T. Carroll, D. Mar, and L. Pecora, *Three coupled oscillators as a universal probe of synchronization stability in coupled oscillator arrays*, Phys. Rev. E, 61 (2000), pp. 5080–5090.

[29] P. M. Gade and R. E. Amritkar, *Spatially periodic orbits in coupled-map lattices*, Phys. Rev. E, 47 (1993), pp. 143–154.

[30] P. M. Gade, H. A. Cerdeira, and R. Ramaswamy, *Coupled maps on trees*, Phys. Rev. E, 52 (1995), pp. 2478–2485.

[31] W. Gerstner and W. M. Kistler, *Spiking neuron models: single neurons, populations, plasticity*, Cambridge University Press, New York, 2002.

[32] Z. Gills, C. Iwata, R. Roy, I. B. Schwartz, and I. Triandaf, *Tracking unstable steady states: Extending the stability regime of a multimode laser system*, Phys. Rev. Lett., 69 (1992), pp. 3169–3172.

[33] L. Glass, *Synchronization and rhythmic processes in physiology*, Nature, 410 (2001), pp. 277–284.

[34] C. M. Gray, P. Konig, A. K. Engel, and W. Singer, *Oscillatory responses in cat visual cortex exhibit inter-columnar synchronization which reflects global stimulus properties*, Nature, 338 (1989), pp. 334–337.

[35] S. Hashimoto and H. Torikai, *A novel hybrid spiking neuron: Bifurcations, responses, and on-chip learning*, IEEE Trans. Circuits Syst. I, Reg. Papers, 57 (2010), pp. 2168–2181.

[36] M. Hasler, *Engineering chaos for encryption and broadband communication*, Phil. Trans. R. Soc. Lond. A, 353 (1995), pp. 115–126.

[37] J. F. Heagy, L. M. Pecora, and T. L. Carroll, *Short wavelength bifurcations and size instabilities in coupled oscillator systems*, Phys. Rev. Lett., 74 (1995), pp. 4185–4188.

[38] V. Hernández, J. E. Román, A. Tomás, and V. Vidal, *Krylov-schur methods in slepc*. `http://www.grycap.upv.es/slepc`, 2007.

[39] J. L. Hindmarsh and R. M. Rose, *A model of neuronal bursting using three coupled first order differential equations*, Proc. R. Soc. Lond. B, 221 (1984), pp. 87–102.

[40] R. A. Horn and C. R. Johnson, *Matrix analysis*, Cambridge University Press, New York, 1990.

[41] S. B. Hsu, *Ordinary differential equations with applications*, Series on applied mathematics, World Scientific, Hackensack, NJ, 2006.

[42] G. Hu, J. Yang, and W. Liu, *Instability and controllability of linearly coupled oscillators: Eigenvalue analysis*, Phys. Rev. E, 58 (1998), pp. 4440–4453.

[43] Z. Huang, Q. Song, and C. Feng, *Multistability in networks with self-excitation and high-order synaptic connectivity*, IEEE Trans. Circuits Syst. I, Reg. Papers, 57 (2010), pp. 2144–2155.

[44] G. Innocenti and R. Genesio, *On the dynamics of chaotic spiking-bursting transition in the Hindmarsh-Rose neuron*, Chaos, 19 (2009), p. 023124.

[45] G. Innocenti, A. Morelli, R. Genesio, and A. Torcini, *Dynamical phases of the Hindmarsh-Rose neuronal model: Studies of the transition from bursting to spiking chaos*, Chaos, 17 (2007), p. 043128.

[46] E. M. Izhikevich, *Which model to use for cortical spiking neurons?*, IEEE Trans. Neural Netw., 15 (2004), pp. 1063–1070.

[47] J. Jalife, *Mutual entrainment and electrical coupling as mechanisms for synchronous firing of rabbit sinoatrial pacemaker cells*, J Physiol., 356 (1984), pp. 221–243.

[48] M. Jalili, *Synchronizing Hindmarsh-Rose neurons over Newman-Watts networks*, Chaos, 19 (2009), p. 033103.

[49] F.-J. Jhou, J. Juang, and Y.-H. Liang, *Multi-state and multi-stage synchronization of Hindmarsh-Rose neurons with excitatory chemical and electrical synapses*. Submitted, 2011.

[50] C. Juang, C.-L. Li, Y.-H. Liang, and J. Juang, *Wavelet transform method for coupled map lattices*, IEEE Trans. Circuits Syst. I, Reg. Papers, 56 (2009), pp. 840–845.

[51] J. Juang and C.-L. Li, *Eigenvalue problems and their application to the wavelet method of chaotic control*, J. Math. Phys., 47 (2006), p. 072704.

[52] J. Juang, C.-L. Li, and J.-W. Chang, *Perturbed block circulant matrices and their application to the wavelet method of chaotic control*, J. Math. Phys., 47 (2006), p. 122702.

[53] J. Juang, C.-L. Li, and Y.-H. Liang, *Global synchronization in lattices of coupled chaotic systems*, Chaos, 17 (2007), p. 033111.

[54] J. Juang and Y.-H. Liang, *Synchronous chaos in coupled map lattices with general connectivity topology*, SIAM J. Appl. Dyn. Syst., 7 (2008), pp. 755–765.

[55] ——, *Coordinate transformation and matrix measure approach for synchronization of complex networks*, Chaos, 19 (2009), p. 033131.

[56] K. Kaneko, *Period-doubling of kink-antikink patterns, quasi-periodicity in antiferro-like structures and spatial intermittency in coupled map lattices*, Prog. Theor. Phys., 72 (1984), pp. 480–486.

[57] ——, *Overview of coupled map lattices*, Chaos, 2 (1992), pp. 279–282.

[58] N. Kopell and B. Ermentrout, *Chemical and electrical synapses perform complementary roles in the synchronization of interneuronal networks*, PNAS, 101 (2004), pp. 15482–15487.

[59] Y. Kuramot, *Chemical oscillations, Waves, and Turbulence*, Springer-Verlag, Berlin, 1984.

[60] T. J. Lewis and J. Rinzel, *Dynamics of spiking neurons connected by both inhibitory and electrical coupling*, J. Comp. Neurosci, 14 (2003), pp. 283–309.

[61] P. Li, M. Chen, Y. Wu, and J. Kurths, *Matrix-measure criterion for synchronization in coupled-map networks*, Phys. Rev. E, 79 (2009), p. 067102.

[62] X. Li and G. Chen, *Synchronization and desynchronization of complex dynamical networks: an engineering viewpoint*, IEEE Trans. Circuits Syst. I, Fundam. Theory Appl., 50 (2003), pp. 1381–1390.

[63] W.-W. Lin and C.-C. Peng, *Chaotic synchronization in lattice of partial-state coupled Lorenz equations*, Phys. D, 166 (2002), pp. 29–42.

[64] W.-W. Lin and Y.-Q. Wang, *Chaotic synchronization in coupled map lattices with periodic boundary conditions*, SIAM J. Appl. Dyn. Syst., 1 (2002), pp. 175–189.

[65] ——, *Proof of synchronized chaotic behaviors in coupled map lattices*, Int. J. Bifurcation Chaos, 21 (2011), pp. 1493–1500.

[66] J. Lü, X. Yu, G. Chen, and D. Cheng, *Characterizing the synchronizability of small-world dynamical networks*, IEEE Trans. Circuits Syst. I, Reg. Papers, 51 (2004), pp. 787–796.

[67] T. M. Massoud and T. K. Horiuchi, *A neuromorphic VLSI head direction cell system*, IEEE Trans. Circuits Syst. I, Reg. Papers, 58 (2011), pp. 150–163.

[68] D. C. Michaels, E. P. Matyas, and J. Jalife, *Mechanisms of sinoatrial pacemaker synchronization: A new hypothesis*, Circulation Res., 61 (1987), pp. 704–714.

[69] R. E. Mirollo and S. H. Strogatz, *Synchronization of pulse-coupled biological oscillators*, SIAM J. Appl. Math., 50 (1990), pp. 1645–1662.

[70] B. Mohar, *Eigenvalues, diameter, and mean distance in graphs*, Graphs and Combinatorics, 7 (1991), pp. 53–64.

[71] E. Mosekilde, Y. Maistrenko, and D. Postnov, *Chaotic synchronization: applications to living systems*, World Scientific series on nonlinear science: Monographs and treatises, World Scientific, River Edge, NJ, 2002.

[72] A. E. Motter, C. Zhou, and J. Kurths, *Network synchronization, diffusion, and the paradox of heterogeneity*, Phys. Rev. E, 71 (2005), p. 016116.

[73] S. Neuenschwander and W. Singer, *Long-range synchronization of oscillatory light responses in the cat retina and lateral geniculate nucleus*, Nature, 379 (1996), pp. 728–732.

[74] T. Nishikawa, A. E. Motter, Y.-C. Lai, and F. C. Hoppensteadt, *Heterogeneity in oscillator networks: Are smaller worlds easier to synchronize?*, Phys. Rev. Lett., 91 (2003), p. 014101.

[75] L. M. Pecora and T. L. Carroll, *Master stability functions for synchronized coupled systems*, Phys. Rev. Lett., 80 (1998), pp. 2109–2112.

[76] C. S. Peskin, *Mathematical aspects of heart physiology*, Courant Institute of Mathematical Sciences, New York University, New York, 1975.

[77] A. Pikovsky, M. Rosenblum, and J. Kurths, *Synchronization: a universal concept in nonlinear sciences*, Cambridge nonlinear science series, Cambridge University Press, Cambridge, 2003.

[78] A. Pogromsky and H. Nijmeijer, *Cooperative oscillatory behavior of mutually coupled dynamical systems*, IEEE Trans. Circuits Syst. I, Fundam. Theory Appl., 48 (2001), pp. 152–162.

[79] G. Rangarajan and M. Ding, *Stability of synchronized chaos in coupled dynamical systems*, Phys. Rev. A, 296 (2002), pp. 204–209.

[80] J. Rubin and D. Terman, *Geometric analysis of population rhythms in synaptically coupled neuronal networks*, Neural Computation, 12 (2000), pp. 597–645.

[81] G. Russo and M. di Bernardo, *Contraction theory and master stability function: Linking two approaches to study synchronization of complex networks*, IEEE Trans. Circuits Syst. II, Exp. Briefs, 56 (2009), pp. 177–181.

[82] A. Sherman, J. Rinzel, and J. Keizer, *Emergence of organized bursting in clusters of pancreatic beta-cells by channel sharing*, Biophys. J., 54 (1988), pp. 411–425.

[83] S.-F. Shieh, Y. Wang, G.-W. Wei, and C.-H. Lai, *Mathematical proof for wavelet method of chaos control*, J. Math. Phys., 47 (2006), p. 082701.

[84] W. Singer, *Neuronal synchrony: a versatile code for the definition of relations?*, Neuron, 24 (1999), pp. 49–65.

[85] J. D. Skufca and E. M. Bollt, *Communication and synchronization in disconnected networks with dynamic topology: Moving neighborhood networks*, Math. Biosci., 1 (2004), pp. 347–359.

[86] C. J. Stam, B. F. Jones, G. Nolte, B. M., and S. Ph., *Small-world networks and functional connectivity in Alzheimer's disease*, Cereb. Cortex, 17 (2006), pp. 92–99.

[87] M. Storace, D. Linaro, and E. de Lange, *The Hindmarsh-Rose neuron model: Bifurcation analysis and piecewise-linear approximations*, Chaos, 18 (2008), p. 033128.

[88] S. H. Strogatz, *Norbert Wiener's brain waves*, in Frontiers in Mathematical Biology, S. Levin, ed., Lecture Notes in Biomathematics 100, Springer, Berlin, 1994, pp. 122–138.

[89] V. Torre, *A theory of synchronization of heart pacemaker cells*, J. Theoret. Biol., 61 (1976), pp. 55–71.

[90] P. J. Uhlhaas and W. Singer, *Neural synchrony in brain disorders: Relevance for cognitive dysfunctions and pathophysiology*, Neuron, 52 (2006), pp. 155–168.

[91] R. Urbanczik and W. Senn, *Similar nonleaky integrate-and-fire neurons with instantaneous couplings always synchronize*, SIAM J. Appl. Math., 61 (2000), pp. 1143–1155.

[92] M. Vidyasagar, *Nonlinear systems analysis*, Prentice-Hall, Englewood Cliffs, NJ, 1978.

[93] I. Waller and R. Kapral, *Spatial and temporal structure in systems of coupled nonlinear oscillators*, Phys. Rev. A, 30 (1984), pp. 2047–2055.

[94] Q. Wang, G. Chen, and M. Perc, *Synchronous bursts on scale-free neuronal networks with attractive and repulsive coupling*, PLoS ONE, 6 (2011), p. 15851.

[95] Q. Wang, M. Perc, Z. Duan, and G. Chen, *Synchronization transitions on scale-free neuronal networks due to finite information transmission delays*, Phys. Rev. E, 80 (2009), p. 026206.

[96] Q. Y. Wang, Q. S. Lu, G. R. Chen, and D. H. Guo, *Chaos synchronization of coupled neurons with gap junctions*, Physics Letters A, 356 (2006), pp. 17–25.

[97] D. J. Watts and S. H. Strogatz, *Collective dynamics of small world networks*, Nature, 393 (2002), pp. 440–442.

[98] G. W. Wei, M. Zhan, and C.-H. Lai, *Tailoring wavelets for chaos control*, Phys. Rev. Lett., 89 (2002), p. 284103.

[99] C. W. Wu, *Synchronization in coupled chaotic circuits and systems*, World Scientific series on nonlinear science: Monographs and treatises, World Scientific, River Edge, NJ, 2002.

[100] C. W. Wu, *Perturbation of coupling matrices and its effect on the synchronizability in arrays of coupled chaotic systems*, Phys. Lett. A, 319 (2003), pp. 495–503.

[101] ——, *Synchronization in coupled arrays of chaotic oscillators with nonreciprocal coupling*, IEEE Trans. Circuits Syst. I, Fundam. Theory Appl., 50 (2003), pp. 294–297.

[102] ——, *Synchronization in networks of nonlinear dynamical systems coupled via a directed graph*, Nonlinearity, 18 (2005), pp. 1057–1064.

[103] ——, *Synchronization in Complex Networks of Nonlinear Dynamical Systems*, World Scientific, Hackensack, NJ, 2007.

[104] C. W. Wu and L. Chua, *Synchronization in an array of linearly coupled dynamical systems*, IEEE Trans. Circuits Syst. I, Fundam. Theory Appl., 42 (1995), pp. 430–447.

[105] J. Yang, G. Hu, and J. Xiao, *Chaos synchronization in coupled chaotic oscillators with multiple positive Lyapunov exponents*, Phys. Rev. Lett., 80 (1998), pp. 496–499.

[106] M. Zhan, G. Hu, and J. Yang, *Synchronization of chaos in coupled systems*, Phys. Rev. E, 62 (2000), pp. 2963–2966.